Dissertation

zur Erlangung des Grades

Dr. rer. nat. im Fach Physik

Searches for New Physics with Neutrino Oscillations in the High Precision Era

Philipp Sicking

Dortmund, 12. Februar 2019

Fakultät Physik

technische universität
dortmund

Gutachter der Dissertation:
Prof. Dr. Heinrich Päs und Prof. Dr. Gudrun Hiller,

“Nature isn’t always what you like – It’s what I like”

Prof. H. Päs

Zusammenfassung

Die vorliegende Dissertation behandelt den Einfluss neuer Physik auf die Messungen aktueller Neutrino-Oszillations-Experimente. Insbesondere wird eine neue modellunabhängige Methode zur Analyse der CP-Verletzung in Neutrino Oszillationen entwickelt, die auf Unitaritäts-Argumenten beruht. Es wird gezeigt, dass aktuelle Experimente wie T2K oder NOvA in der Lage sind, den Parameter-Bereich für viele Modelle stark einzuschränken. Durch Einbeziehen der Materie-Effekte in diese neue Methode ergeben sich zahlreiche Herausforderungen, die tiefgehender behandelt werden. Außerdem wird der Einfluss eines leichten sterilen Neutrinos auf die Bestimmung der Massen-Hierarchie beim JUNO Experiment untersucht. Zusätzlich wird das erste stringente Modell entwickelt, das alle aktuellen Anomalien im Neutrino Bereich erklären kann und gleichzeitig konsistent ist mit Messungen von atmosphärischen Neutrinos und Neutrinos aus Beschleuniger-Experimenten.

Abstract

In this thesis we explore several new physics models and their implications on current neutrino oscillation experiments. In particular we develop a novel model-independent method to analyze the CP violation in neutrino oscillations, based on the unitarity constraints for the leptonic mixing matrix. We can show that current experiments like T2K or NOvA have sufficient sensitivity to restrict new physics models significantly. The inclusion of matter effects into this new approach leads to new challenges, that are studied in more detail. Additionally we analyzes the impact of a light sterile neutrino on the determination of the mass hierarchy at the JUNO experiment. We also propose the first stringent model that can explain all current neutrino oscillation anomalies and is consistent with atmospheric and accelerator based neutrino experiments.

Danksagungen

Diese Dissertation wäre ohne die Unterstützung von Arbeitskollegen, Familie und Freunden niemals möglich gewesen. Vielen Dank an alle, die mir auch in harten Zeiten gut zugesprochen haben und mir die Kraft geschenkt haben nicht aufzugeben. Ein paar besondere Menschen möchte ich hier herausstellen.

Allen voran gilt der größte Dank meinem Betreuer Prof. Dr. Heinrich Päs. Vielen Dank für die Möglichkeit an Ihrem Lehrstuhl zu promovieren. Sie haben mich stets unterstützt und mir die Gelegenheit zu großartigen Erfahrungen gegeben. Ihnen hab ich den Auslandsaufenthalt in den USA zu verdanken, der mich substantiell auch außerhalb der Physik geprägt hat. Vielen Dank für die Selbstverständlichkeit mit der Sie mich zu Sommerschulen, Konferenzen und Vorträgen geschickt haben. In Phasen, in denen ich bei meiner Forschung in Sackgassen steckte, konnte ich darauf vertrauen, dass Sie mir mit einer Idee oder mit einem neuen Blickwinkel einen Ausweg schaffen. Vielen Dank für die große Freiheit, die Sie mir in meiner Forschung gegeben haben.

Allen Kollegen von den Lehrstühlen TIII und TIV danke ich mit vollem Herzen. Ich habe es sehr genossen mit euch zu Arbeiten, in Kaffeepausen mit euch zu diskutieren und regelmäßig die neusten High- und Lowlights der Filmbranche zu begutachten. Die Hilfsbereitschaft und gute Stimmung auf dem Flur vermisse ich schon jetzt. Besonders herausstellen möchte ich Maggi, Peter, Dennis, Dominik und Mathias: Danke für eure fachliche, technische und moralische Unterstützung. Vielen Dank, Susanne, für all deine Arbeit im Hintergrund, ohne die unser Lehrstuhl zusammenbrechen würde.

Ein großer Dank gilt auch meiner Familie. Die Gewissheit, dass ihr immer hinter mir steht und ihr meinen Weg unterstützt, hat mir in vielen schwierigen Momenten geholfen. Danke, dass ich immer zu euch kommen kann, und ihr so viel Verständnis zeigt. Ohne eure Unterstützung in dieser privat oft nicht ganz einfachen Zeit, wäre diese Arbeit nicht in dieser Form möglich gewesen.

Ein riesen großes Dankeschön geht an Angelina. Trotz der großen räumlichen Entfernung, weiß ich, dass ich mich auf dich verlassen kann. Ein Wendepunkt während meiner Dissertation war der Besuch bei dir in Hamburg im Sommer 2016 ohne den ich diese Dissertation niemals zu Ende gebracht hätte.

Vielen Dank an Andreas, Arne, Bene, Felix, Jens, Lana, Laura, Leslie, Nora, Philip, Sören, Stephan und Timon für die Zerstreuung und die allgemeinen physikalischen Diskussionen. Großen Dank an Christoph, Maike, Lukas, Laura und Louis, dass ich Teil eurer Familie sein darf und ihr mir jeden Tag zeigt, dass es auch noch wichtigere Sachen im Leben gibt. Danke Alex, Carsten und Kajo, für jedes einzelne Bier bei Kurt.

Publications

This thesis is based on the following publications by the author:

- Heinrich Päs and Philipp Sicking. "Discriminating sterile neutrinos and unitarity violation with CP invariants". In: *Phys. Rev.* D95.7 (2017), p. 075004. DOI: 10.1103/PhysRevD.95.075004. arXiv: 1611.08450 [hep-ph]
- Dominik Döring et al. "Sterile Neutrinos with Altered Dispersion Relations as an Explanation for the MiniBooNE, LSND, Gallium and Reactor Anomalies". In: (2018). arXiv: 1808.07460 [hep-ph]

Contents

Part I.

Introduction

1. Overview

This thesis is structured as follows. In part I we give an introduction to the current status in neutrino physics including a brief historical overview and a conclusive introduction to the Standard Model of particle physics (SM) with a focus on neutrino physics.

Part II is based on the work done in [1] and deals with a new proposed method to analyze neutrino oscillations. We introduce a model independent method to describe neutrino oscillations, followed by analytic predictions for the newly introduced CP violating amplitudes and a numerical analysis in Chapter including an analysis for different experimental setups based on the GLoBES package. We also includes matter effects into the new approach and a point out the arising challenges.

In Part III the method of the JUNO experiment to determine the mass ordering is presented, and we show the impact of a light sterile neutrino on this determination.

Part IV of this thesis is based on [2] and introduces a specific model with additional sterile neutrinos and altered dispersion relations which can consequently explain all current experimental neutrino anomalies.

In Part V we conclude with a short summary and an outlook for possible further studies.

2. Historical Introduction

The history of neutrino physics begins with the measurement of the electron energy spectrum in nuclear β-decay. The energy spectrum turned out to be continuous in contrast to the discrete spectrum of α and γ decays. In a simple $1 \rightarrow 2$ reaction, where the neutron decays into a proton and an electron, a discrete spectrum is expected due to energy conservation and the huge mass difference of proton and electron. The measurement of a continuous β decay spectrum could not be explained in that framework and resulted in two different theoretical approaches. Niels Bohr stated the assumption that energy conservation does not hold in the β decay processes, while Wolfgang Pauli introduced a neutral yet undiscovered particle.

In his famous letter from 1930 to the "Gruppe der Radioaktiven" in Tübingen Pauli first suggested this light and weakly interacting particle (then called neutron). From today's perspective the prediction of a new particle seems rather straightforward compared to abolishing energy conservation, but in 1930 Pauli was still very cautious about his claim, did not even publish his idea but wrote in the aforementioned letter:

"Ich gebe zu, dass mein Ausweg vielleicht von vornherein wenig wahrscheinlich erscheinen mag, weil man die Neutronen, wenn sie existieren, wohl längst gesehen hätte. Aber nur wer wagt, gewinnt [...] Darum soll man jeden Weg zur Rettung ernstlich diskutieren." [3]

Pauli was aware that his newly introduced particle was not the most appealing due to the lack of any experimental evidence. Since the neutrino had to be light compared to the electron, electrically neutral and had to have a tiny interaction rate with normal matter, a direct detection was experimentally challenging [4].

The experimental solution came up by using a fission reactor power plant instead of simple radioactive materials. Due to the enormous number of decays in the power plant, the tiny interaction rate is compensated by the number of produced antineutrinos. Those antineutrinos were detected directly via an inverse β- decay in 1956 [5] and therefore provided evidence for Pauli's claim of a new neutral particle. The Nobel Prize was awarded to Frederick Reines for this discovery almost 40 years later in 1995.

Using the Alternating Gradient Synchrotron in Brookhaven, it was possible to prove the existence of a second flavor of neutrino. The synchrotron accelerated protons, which were dumped into a target to produce pions, which in turn decayed into muons and neutrinos. It was shown in [6], that these neutrinos did in turn produce only muons in the detector but no electrons. Leon M. Lederman, Melvin Schwartz and Jack Steinberger won the Nobel prize for the discovery of the muon neutrino in 1988.

Since the doublet structure of the leptons was established with the discovery of muon and electron neutrino, it was expected that the tau lepton, also called tauon, has a corresponding

partner - the tau neutrino - which was eventually discovered in 2000 by the DONUT collaboration [7]. The collaboration also used a proton beam dump experiment like in the discovery of the muon neutrino, but used a much higher proton energy of 600 GeV to produce D_s-mesons instead of pions, which also decay into tauon and tau neutrino.

Apart from direct detection, the discovery of neutrino oscillations is a major breakthrough in neutrino physics. This conversion from one neutrino flavor to another is evidence of non zero masses of neutrinos and will be discussed in detail in chapter 3.2. The starting point for discovering neutrino oscillations is the significant deficit of electron neutrinos coming from the sun known as the solar neutrino problem: The Homestake experiment [8] was the first to measure the neutrino flux from the sun with an extremely low background in the Homestake Gold Mine. Due to the chemical detection process of the transition from $^{37}\mathrm{Cl}$ to $^{37}\mathrm{Ar}$ induced by the inverse beta decay, the experiment was only able to measure electron neutrinos. They reported a deficit of around a third with respect to the standard solar model during the runtime of 24 years of measuring. A mistake in the solar model as well as experimental failures were discussed as the source of this deficit, but eventually both turned out to be correct and the deficit of electron neutrinos could be explained by the MSW-effect [9] based on non zero neutrino masses so that oscillations can occur [10]. This theoretical explanation was eventually confirmed by the SNO experiment[11] which was able to measure all three neutrino flavors. Together with the Super-Kamiokande experiment measuring solar and atmospheric neutrinos, the hypothesis of neutrino oscillations has been verified, resulting in the Nobel Prize 2015 for the heads of SNO and Super-Kamiokande, Arthur B. McDonald and Takaaki Kajita.

Neutrino oscillations were confirmed by several other experiments with different sources, like nuclear reactors, accelerators or cosmic rays leading to atmospheric neutrinos and established a picture of at least two non vanishing neutrino masses and large leptonic mixing angles compared to the quark sector.

Apart from oscillation experiments, neutrinos and their properties are studied in experiments searching for the absolute neutrino mass scale or neutrinoless double beta decay (see also Section 3.3.1). Since neutrinos play a significant role in the early universe, some properties can also be deduced from cosmological observations e.g. of the cosmic microwave background (CMB).

The history of neutrino physics shows a fruitful interplay among theorists and experimentalists. The combination of having tiny mass, being electrically neutral and interacting only weakly with other particle makes it challenging to experimentally test theoretical hypotheses. Nevertheless, as the past shows, growing experiments and technological progress made it possible to discover all SM predictions so far.

Currently, apart from the CP violating Dirac phase and the two Majorana phases, the mass ordering and absolute mass scale, and the octant of θ_{23}, all parameters are well determined and a lot of experiments are running, under construction or in planning to close these gaps. Nevertheless, there are some open questions and several theoretical predictions from new physics models concerning neutrino physics. In the tradition of Pauli, the founder of neutrino physics,

it is the perfect field of research to consider new ideas, brave predictions and experimental challenges, since *"nur wer wagt, gewinnt."*

3. Neutrino Oscillations as an Open Window to Physics Beyond the Standard Model

3.1. The Standard Model of Particle Physics

3.1.1. Definition of Fields and Forces

The SM of particle physics is a renormalizable quantum field theory that explains the fundamental particles as excitations of quantum fields and the interactions, governed by the local gauge group $\mathrm{SU}(3)_\mathrm{C} \times \mathrm{SU}(2)_\mathrm{L} \times \mathrm{U}(1)_Y$, which is broken down to the gauge group $\mathrm{SU}(3)_\mathrm{C} \times \mathrm{U}(1)_\mathrm{EM}$ after electroweak (EW) symmetry breaking. While $\mathrm{SU}(3)_\mathrm{C}$ describes the strong interaction or Quantum chromodynamics (QCD), $\mathrm{SU}(2)_\mathrm{L} \times \mathrm{U}(1)_Y$ corresponds to the EW interaction, which is broken spontaneously via the Higgs mechanism to $\mathrm{U}(1)_\mathrm{EM}$ corresponding to electromagnetic interaction, or Quantum electrodynamics (QED).

The fundamental constituents of matter are fermionic with spin $\frac{1}{2}$ and are divided into the two subgroups of quarks (Q, u_R and d_R) and leptons (L and ℓ_R), which each appear in three so-called families:

$$Q^i = \left(\begin{pmatrix} u_L \\ d_\mathrm{L} \end{pmatrix}, \begin{pmatrix} c_\mathrm{L} \\ s_\mathrm{L} \end{pmatrix}, \begin{pmatrix} t_\mathrm{L} \\ b_\mathrm{L} \end{pmatrix} \right), \tag{3.1}$$

$$L^i = \left(\begin{pmatrix} \nu_{e\mathrm{L}} \\ e_\mathrm{L} \end{pmatrix}, \begin{pmatrix} \nu_{\mu\mathrm{L}} \\ \mu_\mathrm{L} \end{pmatrix}, \begin{pmatrix} \nu_{\tau\mathrm{L}} \\ \tau_\mathrm{L} \end{pmatrix} \right), \tag{3.2}$$

$$u^i_\mathrm{R} = (u_\mathrm{R}, c_\mathrm{R}, t_\mathrm{R}), \tag{3.3}$$

$$d^i_\mathrm{R} = (d_\mathrm{R}, s_\mathrm{R}, b_\mathrm{R}), \tag{3.4}$$

$$\ell^i_\mathrm{R} = (e_\mathrm{R}, \mu_\mathrm{R}, \tau_\mathrm{R}). \tag{3.5}$$

The left handed fields are combined in $\mathrm{SU}(2)$-doublets. The representations and hypercharges of the fermion fields are shown in Table 3.1. We use Dirac spinors for the fermion fields and the subscripts L and R indicate the chirality with $\gamma_5 \Psi_\mathrm{L} = -\Psi_\mathrm{L}$ and $\gamma_5 \Psi_\mathrm{R} = \Psi_\mathrm{R}$. While the quarks are accommodated in triplets under $\mathrm{SU}(3)_\mathrm{C}$ and therefore interact via QCD, leptons are uncharged under $\mathrm{SU}(3)_\mathrm{C}$ and do not participate in QCD.

In addition to the fermionic fields, the bosonic spin-1 gauge fields B_μ, W^a_μ and G^A_μ arise from the gauge groups $\mathrm{U}(1)_Y$, $\mathrm{SU}(2)_\mathrm{L}$ and $\mathrm{SU}(3)_\mathrm{C}$, respectively. The superscript a runs over the 3

Field	$\mathrm{SU}(3)_\mathrm{C}$	$\mathrm{SU}(2)_\mathrm{L}$	Y
$Q = \begin{pmatrix} u_\mathrm{L} \\ d_\mathrm{L} \end{pmatrix}$	**3**	**2**	$\frac{1}{6}$
u_R	**3**	**1**	$\frac{2}{3}$
d_R	**3**	**1**	$-\frac{1}{3}$
$L = \begin{pmatrix} \nu_\mathrm{L} \\ \ell_\mathrm{L} \end{pmatrix}$	**1**	**2**	$-\frac{1}{2}$
ℓ_R	**1**	**1**	-1

Table 3.1.: Particle Content and their representations under the gauge groups $\mathrm{SU}(3)_\mathrm{C}$ and $\mathrm{SU}(2)_\mathrm{L}$, as well as the hypercharge Y.

generators of $\mathrm{SU}(2)_\mathrm{L}$ and A runs over the 8 generators of $\mathrm{SU}(3)_\mathrm{C}$. The field strength tensors are defined as

$$B_{\mu\nu} = \partial_\mu B^\nu - \partial_\nu B^\mu \tag{3.6}$$

$$W^a_{\mu\nu} = \partial_\mu W^a_\nu - \partial_\nu W^a_\mu + g\, f^{abc}_{\mathrm{SU}(2)} W^b_\mu W^c_\nu, \tag{3.7}$$

$$G^A_{\mu\nu} = \partial_\mu G^A_\nu - \partial_\nu G^A_\mu + g_s\, f^{ABC}_{\mathrm{SU}(3)} G^B_\mu G^C_\nu, \tag{3.8}$$

with the coupling constants g and g_s, and the structure constants f^{abc} defined via the commutator

$$[t_a, t_b] = \mathrm{i} f^{abc} t_c, \tag{3.9}$$

with the generators t^a of the corresponding group.

The complete SM Lagrangian can be written as

$$\mathcal{L}_\mathrm{SM} = \mathcal{L}_\mathrm{kin} + \mathcal{L}_\mathrm{EW} + \mathcal{L}_\mathrm{QCD} + \mathcal{L}_\mathrm{Higgs} + \mathcal{L}_\mathrm{Yukawa}, \tag{3.10}$$

where $\mathcal{L}_\mathrm{kin}$ describes the kinetic part for the fermionic fields, $\mathcal{L}_\mathrm{EW}$ the EW interaction, $\mathcal{L}_\mathrm{QCD}$ the strong interaction, $\mathcal{L}_\mathrm{Higgs}$ the self interaction of the Higgs field and the interaction with the gauge bosons and $\mathcal{L}_\mathrm{Yukawa}$ includes the Higgs-fermion interaction resulting in the mass terms after spontaneous symmetry breaking.

The QCD-Lagrangian reads

$$\mathcal{L}_\mathrm{QCD} = \sum_{\Psi=\{Q,u,d\}} -\mathrm{i}\bar{\Psi} g_s G^a_\mu T^a \gamma^\mu \Psi - \frac{1}{2}\mathrm{tr} G_{\mu\nu} G^{\mu\nu}, \tag{3.11}$$

and will not be considered further in this work.

The kinetic and the EW Lagrangian can be written as

$$\mathcal{L}_{\text{kin}} + \mathcal{L}_{\text{EW}} = \sum_{\Psi=\{Q,u,d,L,\ell\}} \mathrm{i}\bar{\Psi}\not{D}\Psi - \frac{1}{4}B_{\mu\nu}B^{\mu\nu} - \frac{1}{2}\mathrm{tr}W_{\mu\nu}W^{\mu\nu}, \tag{3.12}$$

with the trace in the last term over the intrinsic indices a of $W^a_{\mu\nu}$. The covariant derivative is defined via

$$D_\mu = \partial_\mu - \mathrm{i}gW^a_\mu\tau^a - \mathrm{i}g'YB_\mu, \tag{3.13}$$

with g' being the coupling constant of $\mathrm{U}(1)_Y$, and Y being the hypercharge of the corresponding field (see Tables 3.1) and $\tau^a = \frac{\sigma^a}{2}$ as the generators of the $\mathrm{SU}(2)_\mathrm{L}$ and the Pauli matrices σ^a.

Apart from masses, all interactions and the propagation of all fields are covered within $\mathcal{L}_{\text{EW}}$ and $\mathcal{L}_{\text{QCD}}$. Dirac mass terms like

$$\mathcal{L}_{\text{mass},e} = m_e\bar{e}_\mathrm{L}e_\mathrm{R} \tag{3.14}$$

are not $\mathrm{SU}(2)_\mathrm{L}$ gauge invariant and therefore forbidden. The Higgs field H and the corresponding Higgs sector $\mathcal{L}_{\text{Higgs}}$ is needed to generate mass terms via the $\mathcal{L}_{\text{Yukawa}}$ terms. This Higgs mechanism and the generation of masses and flavor is presented in the following section.

3.1.2. Mass Generation via Higgs Mechanism and Flavor Physics

The Higgs field H is a complex scalar $\mathrm{SU}(2)_\mathrm{L}$ doublet. The kinetic term for the Higgs boson and its self-coupling is described via

$$\mathcal{L}_{\text{Higgs}} = (D_\mu H)^\dagger (D_\mu H) + \underbrace{\mu^2 H^\dagger H - \lambda\left(H^\dagger H\right)^2}_{V_{\text{Higgs}}(H)}. \tag{3.15}$$

Since the Higgs field is an $\mathrm{SU}(2)_\mathrm{L}$ doublet and has a hypercharge $Y_H = \frac{1}{2}$, the covariant derivative reads

$$D_\mu H = \partial_\mu H - \mathrm{i}gW^a_\mu\tau^a H - \frac{1}{2}\mathrm{i}g'B_\mu H. \tag{3.16}$$

Due to the Higgs potential $V_{\text{Higgs}}(H)$, the Higgs field acquires a vacuum expectation value (VEV) $v = \frac{\mu}{\sqrt{\lambda}}$ which breaks the EW symmetry. By expanding the Higgs field around the VEV as

$$H = \begin{pmatrix} 0 \\ \frac{v}{\sqrt{2}} + \frac{h}{\sqrt{2}} \end{pmatrix}, \tag{3.17}$$

the mass terms for the gauge bosons are generated via the covariant derivative

$$|D_\mu H|^2 = g^2 \frac{v^2}{8} \left[\left(W_\mu^1\right)^2 + \left(W_\mu^2\right)^2 + \left(\frac{g'}{g} B_\mu - W_\mu^3 \right)^2 \right]. \tag{3.18}$$

We do not discuss the Higgs interactions with the real scalar h in this case, since we focus only on the mass terms.

The first two terms in Equation (3.18) represent the masses for the charged bosons of weak interaction $W^\pm = \frac{1}{\sqrt{2}} \left(W_\mu^1 \mp \mathrm{i} W_\mu^2\right)$ with masses $m_W = \frac{vg}{2}$.

Diagonalizing the third term via a rotation with the Weinberg-angle $\tan\theta_\mathrm{W} = \frac{g'}{g}$ yields the mass eigenstates, the photon A_μ and the neutral boson of weak interaction Z_μ:

$$A_\mu = \sin\theta_\mathrm{W} W_\mu^3 + \cos\theta_\mathrm{W} B_\mu \tag{3.19}$$

$$Z_\mu = \cos\theta_\mathrm{W} W_\mu^3 - \sin\theta_\mathrm{W} B_\mu \tag{3.20}$$

This leads to a mass for the Z-boson of $m_Z = \frac{gv}{2\cos\theta_\mathrm{W}} = \frac{m_W}{\cos\theta_\mathrm{W}}$ and a vanishing mass for the photon.

Using the definitions in Equation (3.20) for the neutral part of the covariant derivative

$$D_\mu = \partial_\mu - \mathrm{i}eA_\mu \left(T^3 + Y\mathbb{1}\right) - \mathrm{i}eZ_\mu \left(\cot\theta_\mathrm{W} T^3 - \tan\theta_\mathrm{W} Y\mathbb{1}\right), \tag{3.21}$$

with $e = g\sin\theta_\mathrm{W}$, reveals the definition of the electric charge $Q = T^3 + Y$.

The mass of fermionic fields is generated by the gauge invariant Yukawa term

$$\mathcal{L}_\mathrm{Yukawa} = -Y_{ij}^d \bar{Q}^i H d_\mathrm{R}^j - Y_{ij}^u \bar{Q}^i \tilde{H} u_\mathrm{R}^j - Y_{ij}^\ell \bar{L}^i \tilde{H} \ell_\mathrm{R}^j + h.c. \tag{3.22}$$

with $\tilde{H} = \mathrm{i}\sigma_2 H^*$ and the dimensionless 3×3 Yukawa matrices $Y^{d/u/\ell}$.

This thesis deals mostly with leptons, nevertheless at first we demonstrate the mass generation in the quark sector and show afterwards the differences and challenges in the lepton sector. After symmetry breaking the quark mass terms of $\mathcal{L}_\mathrm{Yukawa}$ become

$$\mathcal{L}_\mathrm{mass}^Q = -\frac{v}{\sqrt{2}} \left[\bar{d}_\mathrm{L} Y_d d_\mathrm{R} + \bar{u}_\mathrm{L} Y_u u_\mathrm{R}\right] + h.c.. \tag{3.23}$$

The Yukawa matrices can be diagonalized via

$$Y_d = U_d M_d K_d^\dagger, \qquad Y_u = U_u M_u K_u^\dagger, \tag{3.24}$$

with the diagonal matrices $M_{d/u}$ and the unitary matrices $U_{d/u}$ and $K_{d/u}$. Using this diagonalization and redefining the fields via $d'_\mathrm{R} = K_d d_\mathrm{R}$, $u'_\mathrm{R} = K_u u_\mathrm{R}$, $d'_\mathrm{L} = U_d d_\mathrm{L}$ and $u'_\mathrm{L} = U_u u_\mathrm{L}$ yields the Lagrangian in the mass basis

$$\mathcal{L}_\mathrm{mass}^Q = -m_j^d \bar{d}_\mathrm{L}^{\prime j} d_\mathrm{R}^{\prime j} - m_j^u \bar{u}_\mathrm{L}^{\prime j} u_\mathrm{R}^{\prime j} + h.c., \tag{3.25}$$

with the diagonal entries $m_j^{d/u} = \frac{v}{\sqrt{2}} M_{d/u}^{jj}$. In this basis the kinetic terms and the interaction terms with the gauge bosons read

$$\begin{aligned}\mathcal{L}_{\text{kin}}^{Q} =& \frac{e}{\sin\theta_W} Z_\mu J_\mu^Z + eA_\mu J^{\mu,\text{EM}} - m_j^d \left(\bar{d}_{\text{L}}^{\prime j} d_{\text{R}}^{\prime j} + \bar{d}_{\text{R}}^{\prime j} d_{\text{L}}^{\prime j}\right) - m_j^u \left(\bar{u}_{\text{L}}^{\prime j} u_{\text{R}}^{\prime j} + \bar{u}_{\text{R}}^{\prime j} u_{\text{L}}^{\prime j}\right) \\ &+ \frac{e}{\sqrt{2}\sin\theta_W} \left[W_\mu^+ \bar{u}_{\text{L}}^{\prime i} \gamma^\mu \left(V_{\text{CKM}}\right)^{ij} d_{\text{L}}^{\prime j} + W_\mu^- \bar{d}_{\text{L}}^{\prime i} \gamma^\mu \left(V_{\text{CKM}}^\dagger\right)^{ij} u_{\text{L}}^{\prime j} \right],\end{aligned} \tag{3.26}$$

with the neutral currents $J_\mu^{\text{EM}} = \sum_i Q_i \left(\bar{\psi}_{\text{L}}^i \gamma^\mu \psi_{\text{L}}^i + \bar{\psi}_{\text{R}}^i \gamma^\mu \psi_{\text{R}}^i\right)$, $J_\mu^3 = \sum_i \bar{\psi}_{\text{L}}^i \gamma^\mu T^3 \psi_{\text{L}}^i$ and $J_\mu^Z = \frac{1}{\cos\theta_W}\left(J_\mu^3 - \sin^2\theta_W J_\mu^{\text{EM}}\right)$. The neutral currents are not affected by the basis transformation performed, unlike the charged currents. Here, the unitary matrix mixing matrix

$$V_{\text{CKM}} = U_u^\dagger U_d \tag{3.27}$$

arises. In general V_{CKM} is not restricted besides being unitary. This means that the mixing matrix does not need to be diagonal and therefore can potentially lead to flavor changing charged currents. If V_{CKM} was the identity matrix, the so called flavor basis and the mass basis would be the same and all families would be completely separated.

In general a unitary 3×3 matrix has 9 independent real parameters, three angles and six phases. The number of phases can be reduced to one, since each quark field can be redefined by an arbitrary $\text{U}(1)$ symmetry transformation.

The procedure followed in the quark sector can also be performed in the lepton sector with one important difference. Since there is no right handed neutrino ν_{R} in the SM, we only have *one* Yukawa matrix Y_ℓ to be diagonalized:

$$\mathcal{L}_{\text{mass}}^{lep} = -\frac{v}{\sqrt{2}} \bar{\ell}_{\text{L}} Y_\ell \ell_{\text{R}}, \tag{3.28}$$

$$Y_\ell = U_\ell M_\ell K_\ell^\dagger. \tag{3.29}$$

Using a redefinition analogously to the quark sector, $\ell_{\text{L}}^\prime = U_\ell \ell_{\text{L}}$ and $\ell_{\text{R}}^\prime = K_\ell \ell_{\text{R}}$, and writing the resulting kinetic leptonic Lagrangian in the mass basis leads to a diagonal structure in the neutral currents as well. Furthermore, due to the lack of neutrino mass terms, the left handed neutrino field can be redefined freely with an arbitrary transformation $\nu_{\text{L}}^\prime = U_\nu \nu_{\text{L}}$. Setting $U_\nu = U_\ell$, all flavor changing charged currents are removed in the lepton sector, since the resulting mixing matrix satisfies $V_{\text{lepton}} = U_\nu^\dagger U_\ell = \mathbb{1}$.

The essential result of this is that without a mass term in the neutrino sector, there are no flavor changing charged currents in tree level processes in the lepton sector. In other words, if there are no neutrino masses, the mass basis in the neutrino sector is not well defined and can always be matched to the charged lepton mass basis.

In the next chapter we discuss the experimental evidence of neutrino oscillations and its interpretation as a necessity of neutrino masses. The theoretical description of neutrino mass generation is discussed in the succeeding chapter

3.2. The Experimental Evidence of Neutrino Oscillations and its Conclusions

The experimental discovery and direct detection of the neutrino was performed via inverse β decay. The different flavors of the neutrinos were determined by the produced charged lepton, which in turn could be distinguished via the different masses.

Neutrino oscillations were discovered by the SNO [11] and Super-Kamiokande [12]. Figure 3.1 shows the Feynman diagram for a neutrino flavor conversion. While the produced neutrino flavor is determined by the charged lepton at the source, the charged lepton at the target determines the neutrino flavor after a travelling distance or baselength L. The deficit of the initial neutrino flavor at the target (disappearance) or an excess of one of the other flavors at the target (appearance) indicate a flavor conversion. This flavor conversion can only be explained by

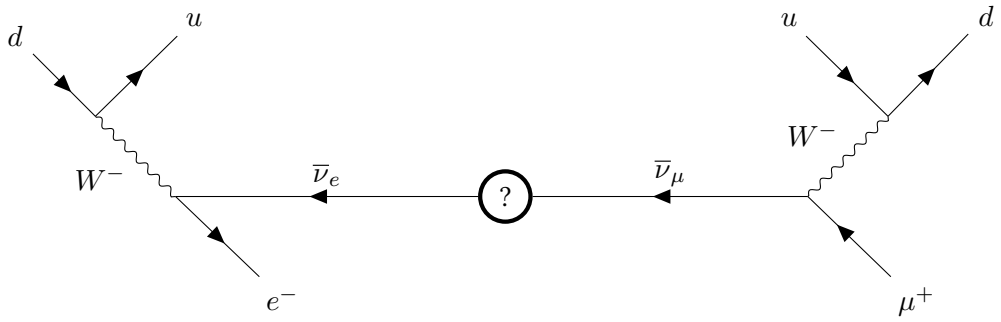

Figure 3.1.: Feynman diagram for antineutrino flavor conversion as measured e.g. in reactor neutrino experiments (this and all following Feynman diagrams are generated with TikZ-Feynman [13]).

introducing neutrino masses. If the neutrino mass basis and the charged lepton mass basis is not the same, flavor changing charged currents naturally arise analogously to the quark sector.

For simplicity we introduce a right handed neutrino ν_{R}, which is a singlet under the SM and therefore impossible to detect directly. With this ν_{R}, a mass term can be introduced like

$$\mathcal{L}^{\nu}_{\mathrm{mass}} = -\frac{v}{\sqrt{2}} \left[\bar{\ell}_{\mathrm{L}} Y_\ell \ell_{\mathrm{R}} + \bar{\nu}_{\mathrm{L}} Y_\nu \nu_{\mathrm{R}} \right]. \tag{3.30}$$

The generation of such neutrino mass terms will be handled with more detail in Section 3.3. Analogously to the quark sector, we transform the Yukawa matrices via a bi-unitary diagonalization

$$Y_\ell = U_\ell M_\ell K_\ell^\dagger, \qquad Y_\nu = U_\nu M_\nu K_\nu^\dagger, \tag{3.31}$$

with the diagonal matrices $M_{\ell/\nu}$ and the unitary matrices $U_{\ell/\nu}$ and $K_{\ell/\nu}$. Redefining the fields via $\ell'_{\mathrm{R}} = K_d \ell_{\mathrm{R}}$, $\nu'_{\mathrm{R}} = K_\nu \nu_{\mathrm{R}}$, $\ell'_{\mathrm{L}} = U_\ell \ell_{\mathrm{L}}$ and $\nu'_L = U_\nu \nu_L$ yields the Lagrangian in the mass basis

$$\mathcal{L}^{\nu}_{\mathrm{mass}} = -m^{\ell}_j \bar{\ell}'^j_L \ell'^j_R - m^{\nu}_j \bar{\nu}'^j_L \nu'^j_R + h.c.. \tag{3.32}$$

with the diagonal entries $m^{\ell/\nu}_j = \frac{v}{\sqrt{2}} M^{jj}_{\ell/\nu}$. Similar to the quark sector we can reformulate the kinetic terms of the Lagrangian in the mass basis yielding

$$\begin{aligned}\mathcal{L}^{\mathrm{mass}}_{\mathrm{kin}} =& \frac{e}{\sin\theta_{\mathrm{W}}} Z_\mu J^Z_\mu + e A_\mu J^\mu_{\mathrm{EM}} - m^{\ell}_j \left(\bar{\ell}'^j_{\mathrm{L}} \ell'^j_{\mathrm{R}} + \bar{\ell}'^j_{\mathrm{R}} \ell'^j_{\mathrm{L}}\right) - m^{\nu}_j \left(\bar{\nu}'^j_{\mathrm{L}} \nu'^j_{\mathrm{R}} + \bar{\nu}'^j_{\mathrm{R}} \nu'^j_{\mathrm{L}}\right) \\ &+ \frac{e}{\sqrt{2}\sin\theta_{\mathrm{W}}} \left[W^+_\mu \bar{\nu}'^i_{\mathrm{L}} \gamma^\mu \left(\mathbf{U}\right)_{ij} \ell'^j_{\mathrm{L}} + W^-_\mu \bar{\ell}'^i_{\mathrm{L}} \gamma^\mu \left(\mathbf{U}^\dagger\right)_{ij} \nu'^j_{\mathrm{L}}\right],\end{aligned} \tag{3.33}$$

Again, flavor changing charged currents are generated via the unitary mixing matrix

$$\mathbf{U} = U^\dagger_\nu U_\ell, \tag{3.34}$$

also known as the Pontecorvo-Maki-Nakagawa-Sakata (PMNS) named after Pontecorvo who predicted neutrino oscillations [14] and Maki, Nakagawa, and Sakata, who introduced this matrix [15].

As we can see in (3.33), the neutral currents are independent of any choice of basis for the leptons. The charged currents, on the other hand, depend on the choice of basis but only in the combination of both transformations, U_ℓ and U_ν (see Equation (3.34)). Therefore, we can set without loss of generality $U_\ell = \mathbb{1}$, so that $U_\nu = \mathbf{U}^\dagger$. With this definition two distinct bases for the neutrinos arise. The mass basis, in which the mass term for the neutrinos is diagonal $\nu_i = \delta_{ij} \nu'^j$ and the flavor basis, where $\mathbf{U}$ is absorbed so that the charged current becomes diagonal, $\nu_\alpha = \mathbf{U}_{\alpha j} \nu'^j_{\mathrm{L}}$.

From here on, every time we use the Dirac notation for the neutrino states, Latin indices indicate the mass basis, and Greek indices indicate the flavor basis. The transformation from one basis to the other is performed with $\mathbf{U}$.

$$|\nu_\alpha\rangle = \left(\mathbf{U}\right)_{\alpha i} |\nu_i\rangle\,, \qquad |\nu_i\rangle = \left(\mathbf{U}^\dagger\right)_{\alpha i} |\nu_\alpha\rangle\,. \tag{3.35}$$

Figure 3.2 shows the Feynman diagram for neutrino oscillations in the above introduced definition. In contrast to Figure 3.1 here we focus on neutrino oscillations instead of antineutrino oscillations. In the limit of small neutrino masses compared to the momentum, and the long distance interaction, the propagator $S^c_i(p, L)$ of a neutrino ν_i can be written as [16]

$$S^c_i(p, L) = \mathrm{i} \frac{\not{p}}{2p^0} \mathrm{e}^{-\mathrm{i}\frac{m^2_i - p^2}{2|\vec{p}|} L}. \tag{3.36}$$

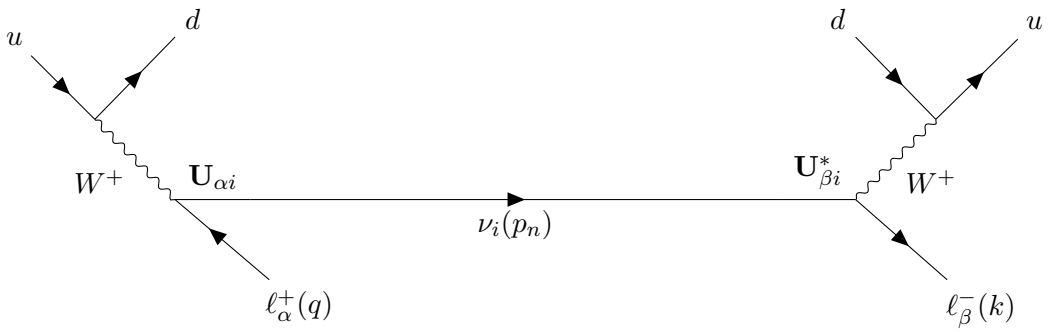

Figure 3.2.: Feynman diagram for general neutrino oscillations $\nu_\alpha \to \nu_\beta$.

With the help of the propagator it is straightforward to write out the amplitude of the process, when the heavy gauge boson is integrated out, and summed over all three neutrino mass eigenstates.

$$\mathcal{M} = -\mathrm{i}\frac{G_F^2}{4p^0}\sum_{i=0}^{3}\left[\mathbf{U}_{\alpha i}\mathbf{U}^*_{\beta i}\mathrm{e}^{-\mathrm{i}\frac{m_i^2-p^2}{2p^0}L} j_\rho^{(2)}\bar{u}(k)\gamma^\rho\left(1-\gamma^5\right)\not{p}\gamma^\mu\left(1-\gamma^5\right)v(q)j_\mu^{(1)}\right], \quad (3.37)$$

where q and k are the momenta of the charged lepton at the source and at the target, respectively, and $j_\mu^{(1)}$ and $j_\rho^{(2)}$ correspond to the matrix elements of the charged weak hadronic currents.

The resulting squared amplitude averaged over the polarizations of the incoming and summed over the polarisations of the outgoing hadronic parts reads

$$\left\langle|\mathcal{M}|^2\right\rangle = \frac{4G_F^4}{\left(p^0\right)^2}W^{(1)}_{\mu\nu}A^{\mu\nu\rho\sigma}W^{(2)}_{\rho\sigma}\cdot P_{\nu_\alpha\to\nu_\beta}, \quad (3.38)$$

with

$$\begin{aligned}A^{\mu\nu\rho\sigma} = \frac{1}{64}\,\mathrm{tr}\,\big[&\not{p}\gamma^\mu\left(1-\gamma^5\right)\left(\not{q}-m_\alpha\right)\gamma^\nu\left(1-\gamma^5\right)\not{p}\gamma^\sigma\left(1-\gamma^5\right)\\ &\left(\not{k}+m_\beta\right)\gamma^\rho\left(1-\gamma^5\right)\big],\end{aligned} \quad (3.39)$$

and

$$W^{(1)}_{\mu\nu} = \left\langle j_\mu^{(1)}\left(j_\nu^{(1)}\right)^\dagger\right\rangle, \qquad W^{(2)}_{\rho\sigma} = \left\langle j_\rho^{(2)}\left(j_\sigma^{(2)}\right)^\dagger\right\rangle. \quad (3.40)$$

The angle brackets denote the averaging and summation of incoming and outgoing particle polarisations. The first part in (3.38) can also be factorized. For more details see [16].

In the following focus on the last part $P_{\nu_\alpha \to \nu_\beta} = P_{\alpha\beta}$ which we will call the neutrino oscillation probability. This part is only dependent on the neutrino properties like mass and energy, the leptonic mixing matrix $\mathbf{U}$ and the baselength L. Using the above definition leads to

$$P_{\nu_\alpha \to \nu_\beta} = \sum_{k,j=1}^{3} \left(\mathbf{U}^*_{\alpha k} \mathbf{U}_{\beta k} \mathbf{U}_{\alpha j} \mathbf{U}^*_{\beta j} \cdot \mathrm{e}^{-\mathrm{i} \frac{m_k^2 - m_j^2}{2E} L} \right). \tag{3.41}$$

This oscillation probability is the starting point of all further calculations in this thesis.

It is also possible to calculate the above oscillation probability with basic quantum mechanics. The oscillation probability is then calculated via

$$P_{\nu_\alpha \to \nu_\beta} = |\langle \nu_\beta | \nu_\alpha(L) \rangle|^2 \tag{3.42}$$

as the probability of a neutrino starting with the flavor α and travelling the distance L ending up with the flavor β. The state $|\nu_\alpha(L)\rangle$ is a linear superposition of the mass eigenstates $|\nu_i\rangle$

$$|\nu_\alpha\rangle = (\mathbf{U})_{\alpha i} |\nu_i\rangle \tag{3.43}$$

which are also the propagation eigenstates. The propagation of the mass eigenstates are determined by the plane wave solution

$$\begin{aligned} |\nu_i(t)\rangle &= \mathrm{e}^{-E_i t - \vec{p}_i \vec{x}} |\nu_i(0)\rangle \\ &\approx \mathrm{e}^{-\mathrm{i} \frac{m_i^2}{2E} L} |\nu_i(0)\rangle . \end{aligned} \tag{3.44}$$

where we used the ultrarelativistic limit of $p_i \gg m_i$ and neglect common phases which do not contribute to the oscillation probability. Note that here we use the oscillation distance L and the travelling time t interchangeably due to a travelling speed close to light speed and the use of natural units.

The oscillation probability now reads

$$\begin{aligned} P_{\alpha\beta} = P_{\nu_\alpha \to \nu_\beta} &= |\langle \nu_\beta | \nu_\alpha(L) \rangle|^2 = \left| \sum_{j=1}^{3} \mathbf{U}^*_{\beta j} \mathbf{U}_{\alpha j} \mathrm{e}^{-\mathrm{i} \frac{m_j^2}{2E} L} \right|^2 \\ &= \sum_{k,j=1}^{3} \left(\mathbf{U}^*_{\alpha k} \mathbf{U}_{\beta k} \mathbf{U}_{\alpha j} \mathbf{U}^*_{\beta j} \cdot \mathrm{e}^{-\mathrm{i} \frac{m_k^2 - m_j^2}{2E} L} \right) \\ &= \delta_{\alpha\beta} - 4 \sum_{k>j}^{3} \mathrm{Re} \left(\mathbf{U}^*_{\alpha k} \mathbf{U}_{\beta k} \mathbf{U}_{\alpha j} \mathbf{U}^*_{\beta j} \right) \sin^2 \left(\frac{m_k^2 - m_j^2}{4E} L \right) \\ &\quad + 2 \sum_{k>j}^{3} \mathrm{Im} \left(\mathbf{U}^*_{\alpha k} \mathbf{U}_{\beta k} \mathbf{U}_{\alpha j} \mathbf{U}^*_{\beta j} \right) \sin \left(\frac{m_k^2 - m_j^2}{4E} L \right). \end{aligned} \tag{3.45}$$

This basic neutrino oscillation probability shows some significant features we want to highlight:

- The oscillation probability is solely dependent on the mass squared differences $\Delta m^2_{kj} \equiv m^2_k - m^2_j$ and independent of the absolute mass scale as long as the kinematic approximations are valid.

- The dependence on $\frac{L}{E}$ is tested by various experiments with either variable baselength, variable energy or both and among different experiments. The oscillatory behaviour with the different frequencies Δm^2_{kj} gives rise to the name neutrino oscillations.

- The energy and baselength scale for experiments to detect neutrino oscillations is determined by the mass squared differences: If $\frac{E}{L} \ll \Delta m^2_{kj}$, the argument of $\sin$ becomes small compared to 1 and therefore the oscillatory feature will vanish. If $\frac{E}{L} \gg \Delta m^2_{kj}$, the argument becomes large compared to 1 and the oscillations will become too fast to be resolved experimentally and the oscillation will be "averaged out" due to the limited resolution of detectors in either E or L or both. Integrating over the bin width or spatial expansion of the detector makes it is possible to approximate $\sin \Delta m^2_{kj} \frac{L}{4E} \sim 0$ and $\sin^2 \Delta m^2_{kj} \frac{L}{4E} \sim \frac{1}{2}$.

The leptonic mixing matrix $\mathbf{U}$ can be parametrized in numerous ways. The standard parametrization reads

$$\begin{aligned}
\mathbf{U} &= U_{12}U_{13}U_{23} \\
&= \begin{pmatrix} 1 & 0 & 0 \\ 0 & c_{23} & s_{23} \\ 0 & -s_{23} & c_{23} \end{pmatrix} \begin{pmatrix} c_{13} & 0 & s_{13}\mathrm{e}^{-\mathrm{i}\delta_{CP}} \\ 0 & 1 & 0 \\ -s_{13}\mathrm{e}^{+\mathrm{i}\delta_{CP}} & 0 & c_{13} \end{pmatrix} \begin{pmatrix} c_{12} & s_{12} & 0 \\ -s_{12} & c_{12} & 0 \\ 0 & 0 & 1 \end{pmatrix} \\
&= \begin{pmatrix} c_{12}c_{13} & s_{12}c_{13} & s_{13}\mathrm{e}^{-\mathrm{i}\delta_{CP}} \\ -s_{12}c_{23} - c_{12}s_{23}s_{13}\mathrm{e}^{\mathrm{i}\delta_{CP}} & c_{12}c_{23} - s_{12}s_{23}s_{13}\mathrm{e}^{\mathrm{i}\delta_{CP}} & s_{23}c_{13} \\ s_{12}s_{23} - c_{12}c_{23}s_{13}\mathrm{e}^{\mathrm{i}\delta_{CP}} & -c_{12}s_{23} - s_{12}c_{23}s_{13}\mathrm{e}^{\mathrm{i}\delta_{CP}} & c_{23}c_{13} \end{pmatrix},
\end{aligned} \tag{3.46}$$

with $s_{ij} \equiv \sin\theta_{ij}$ and $c_{ij} \equiv \cos\theta_{ij}$. The current global best fit values are shown in Table 3.2. Note that we do not use historically introduced parameters like θ_{atm}, θ_{sol}, $\theta_{\mathrm{reactor}}$, $\Delta m^2_{\mathrm{atm}}$ or $\Delta m^2_{\mathrm{atm}}$. The actual definition of these parameters are changing throughout the literature and the above parametrization is more intuitive and clearer.

As mentioned before, the neutrino oscillation probability is only sensitive to mass squared differences Δm^2_{kj} and not to the absolute mass values. In the standard three neutrino approach, there are only three independent masses, and therefore only two independent mass squared differences. As we will see later in III, the neutrino oscillation probability is only at higher orders sensitive to the ordering of the neutrino masses. Without information about the relative sign of Δm^2_{31} or Δm^2_{32} it is impossible to deduce whether $m^2_1 < m^2_2 < m^2_3$, called normal ordering (NO) or $m^2_3 < m^2_1 < m^2_2$, called inverted ordering (IO). Current global fits report a preference for normal ordering at a significance of more than $3\,\sigma$ [17–19]. The different possibilities of orderings also provide different values for the parameters in the global fits,

which is also indicated in Table 3.2. We did not include a value for the Dirac phase δ_{CP}, since there are only first indications for $\delta_{\mathrm{CP}} \neq 0$ at the $2\,\sigma$ level [82].

Parameter	value
$\sin^2\theta_{12}$	0.297
$\sin^2\theta_{23}$ (NO)	0.437
$\sin^2\theta_{23}$ (IO)	0.569
$\sin^2\theta_{13}$ (NO)	0.0214
$\sin^2\theta_{13}$ (IO)	0.0218
$\Delta_{21}[10^{-5}\ \mathrm{eV}^2]$	7.37
$\Delta_{31}[10^{-3}\ \mathrm{eV}^2]$ (NO)	2.50
$\Delta_{32}[10^{-3}\ \mathrm{eV}^2]$ (IO)	-2.46

Table 3.2.: Standard parameters used in throughout this thesis, with different values for normal (NO) and inverted ordering (IO). Values taken from [20].

Figure 3.3 shows all different probabilities $P_{\alpha\beta}$ in dependence of $\frac{L}{E}$. Due to the large difference between the two mass squared differences Δm^2_{21} and Δm^2_{31} one can clearly see the different regimes of the oscillation modes. For small values of $\frac{L}{E}$, only the oscillation triggered by Δm^2_{31} is relevant and the oscillation frequency Δm^2_{21} can be neglected, while for larger values of $\frac{L}{E}$, the oscillation is driven by Δm^2_{21} and the fast oscillation over Δm^2_{31} averages out.

3.3. Neutrino Mass Generation in the Standard Model and Beyond

This section is based on the review articles [21] and [22]. Since neutrinos are the only electrically neutral fermions in the SM, additionally to the common Dirac-mass term, a Majorana term is also possible. The most general mass Lagrangian then reads

$$\mathcal{L}^{\nu}_{\mathrm{mass}} = \underbrace{-m_D \overline{\nu_{\mathrm{L}}}\nu_{\mathrm{R}}}_{\text{Dirac Mass Term}} \underbrace{-M^{\mathrm{R}}_{\mathrm{maj}} \overline{\nu_{\mathrm{R}}}\,(\nu_{\mathrm{R}})^C}_{\text{Majorana Mass Term}} + h.c. \tag{3.47}$$

where the superscript C indicates the charge conjugation of the Dirac spinor defined as

$$\psi^C \equiv \mathcal{C}\psi \equiv -\mathrm{i}\gamma^2\psi^*. \tag{3.48}$$

To conserve electric charge, the Majorana mass term is only allowed if the Majorana condition

$$\psi^C = \psi \tag{3.49}$$

is satisfied. The Majorana condition is also often referred to as the particle being its own antiparticle.

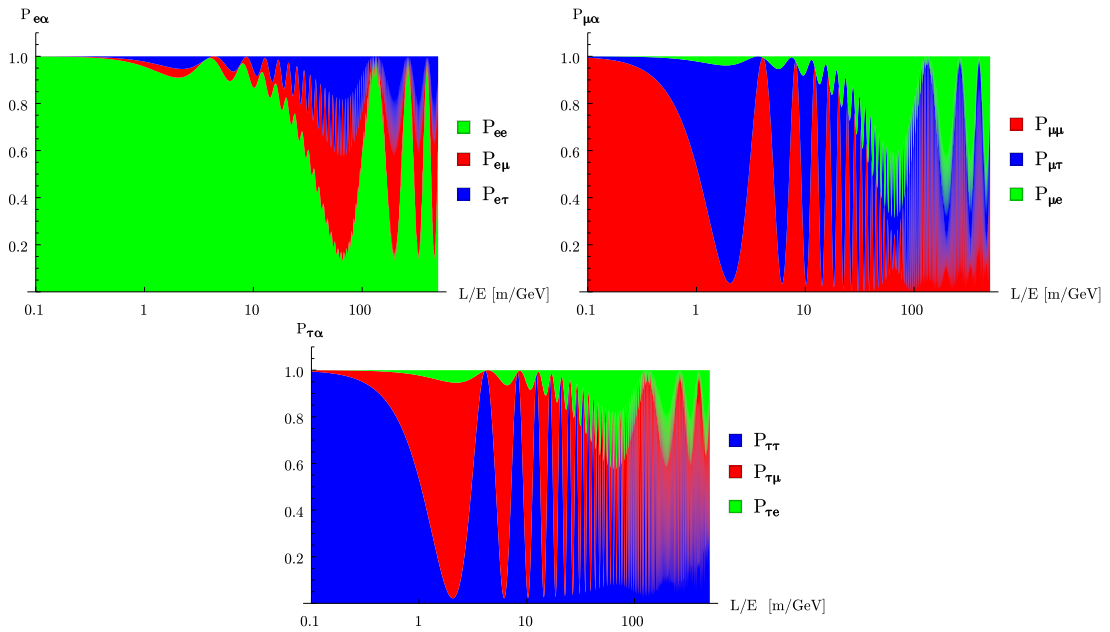

Figure 3.3.: Neutrino oscillation probabilities for normal ordering and parameter values taken from Table 3.2.

A possible Majorana term for the left handed neutrino $M^{\mathrm{L}}_{\mathrm{maj}}\overline{\nu_{\mathrm{L}}}\,(\nu_{\mathrm{L}})^{C}$ is not allowed in the SM due to conservation of hypercharge.

Equation (3.47) also indicates that the mass eigenstates are linear combinations of the right handed and left handed neutrinos. The mass eigenstates can be found by diagonalizing the total mass matrix

$$M = \begin{pmatrix} 0 & m_D \\ m_D & M^{\mathrm{R}}_{\mathrm{maj}} \end{pmatrix}. \tag{3.50}$$

This also shows that the often used terms “heavy right handed neutrinos” or “light left handed neutrinos” are not exact. Those terms are used in the case that $m_D \ll M^{\mathrm{R}}_{\mathrm{maj}}$ so that the heavy mass eigenstates are “mostly” right handed and the light eigenstates are “mostly” left-handed. This will be handled in more detail in Section 3.3.2 about the Seesaw mechanism.

Due to the Majorana condition (3.49) a general neutrino Majorana term violates Lepton number. Lepton number is only an accidental symmetry in the SM and therefore in general not guaranteed. Several Experiments are looking for signals of lepton number violation, for example in the search for neutrinoless double beta decay.

Another approach to generate a neutrino mass without specifying new particles in the UV-completion is the introduction of an effective dimension 5 operator

$$\mathcal{L}_{\text{Weinberg}} = -M_{ij}\left(\bar{L}^i\tilde{H}\right)\left(\tilde{H}\bar{L}^i\right)^\dagger, \tag{3.51}$$

the so called Weinberg-Operator. This effective operator is generated for example by integrating out the right handed neutrino in Equation (3.47).

3.3.1. Implications of Majorana Mass

As already mentioned, a Majorana mass term breaks the accidental symmetry of lepton number by two units. A process generated by this Majorana mass term is the neutrinoless double beta decay, shown in Figure 3.4. Two electrons and no neutrinos are produced and therefore the lepton number is not conserved. A detailed review about neutrinoless double beta decay can be found in [23, 24]. In [25] and later in [26, 27] it is shown that a black box argument can be made regarding this process: If one detects neutrinoless double beta decay, there is a nonzero contribution to a Majorana mass term for neutrinos. This argument also holds "the other way": If a Majorana mass term for neutrinos exists, a neutrinoless double beta decay is, possible unless specific parameter combinations are realized. The essential parameter involved in neutrinoless

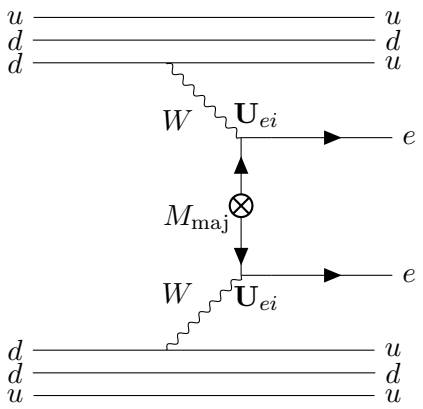

Figure 3.4.: Feynman diagram for $0\nu\beta\beta$-decay

double beta decay is the effective mass

$$m_{\beta\beta} = \left|\sum_{i=1}^{3} \mathrm{e}^{\mathrm{i}\xi_i}\left|\mathbf{U}_{ei}^2\right| m_i\right|, \tag{3.52}$$

where ξ_i are the so called Majorana phases. These phases arise, since the Majorana condition (3.49) fixes the neutrino fields, and a redefinition by a $\mathrm{U}(1)$ symmetry transformation is not

possible. Therefore, only three phases of the lepton mixing matrix can be absorbed in the charged lepton fields, and three phases are left, instead of only one in case of Dirac neutrinos. The two additional phases are the Majorana phases, which affect neutrinoless double beta decay but have no impact on neutrino oscillation processes.

As can be seen in Equation (3.52), due to the Majorana phases, it is possible, that parts of the sum cancel, which is also shown in Figure 3.5. We use the current best fit values from Table 3.2 and calculate the largest and smallest possible mass $m_{\beta\beta}$ dependent on the lightest neutrino mass m_{lightest}. There is a significant difference between the possible orderings, due to the different admixtures of ν_e in the different mass eigenstates. For large m_{lightest}, there is as expected, no difference between the mass orderings. In the normal ordering a vanishing $m_{\beta\beta}$ is possible for $2 \cdot 10^{-3}\,\text{eV} \lesssim m_{\text{lightest}} \lesssim 6 \cdot 10^{-3}\,\text{eV}$, since for these masses, it is possible with significant fine tuning that the sum in (3.52) cancels out exactly. If this is the case, no neutrinoless double beta decay will be measurable although there is a Majorana mass term. Measuring the neutrinoless double beta decay and determining $m_{\beta\beta}$ can also be used to determine the mass ordering.

Currently several experiments are searching for neutrinoless double beta decay, like COBRA [28], CUORE [29], EXO-200 [30], GERDA [31], and KamLAND-Zen [32]. The process is yet unobserved, but all experiments set lower bounds on the lifetime of the process. Theoretical calculations of the matrix elements depend on non trivial nuclear physics and different methods come to different results. Therefore, the upper bounds for $m_{\beta\beta}$ are often presented as an interval depending on the calculation method of the matrix elements. The strongest bound is currently set by KamLAND-Zen with the isotope ^{136}XE to a 90% C.L. upper limit of $m_{\beta\beta} < (61 - 165)$ meV [33]. This upper limit is not far away from the interesting parameter space, where normal and inverted ordering are distinguishable. The lightest neutrino mass m_{lightest} can be restricted by cosmological experiments, where an upper bound on the sum of all neutrino masses $m_\Sigma = m_1 + m_2 + m_3$ can be extracted from the cosmic microwave background. The Planck collaboration released the most current upper bounds in [34]. Since the upper bound is highly dependent on the cosmological model and the actual analysis, we only use the most conservative bound of $m_\Sigma < 0.54$ eV at 95% C.L. This bound, converted to a bound on m_{lightest}, depends on the ordering, but the difference at current significance is negligible. Both bounds are shown in Figure 3.5.

One of the most appealing arguments for looking for neutrinoless double beta decay, and therefore for a Majorana mass term, is the possibility of solving the longstanding cosmological question of the origin of the baryon asymmetry of the universe, which cannot be explained in the SM. A Majorana mass could fulfill one of the Sakharov conditions [35] since a lepton number violating process could induce a lepton asymmetry which can be transferred to a baryon asymmetry via SM sphaleron processes.

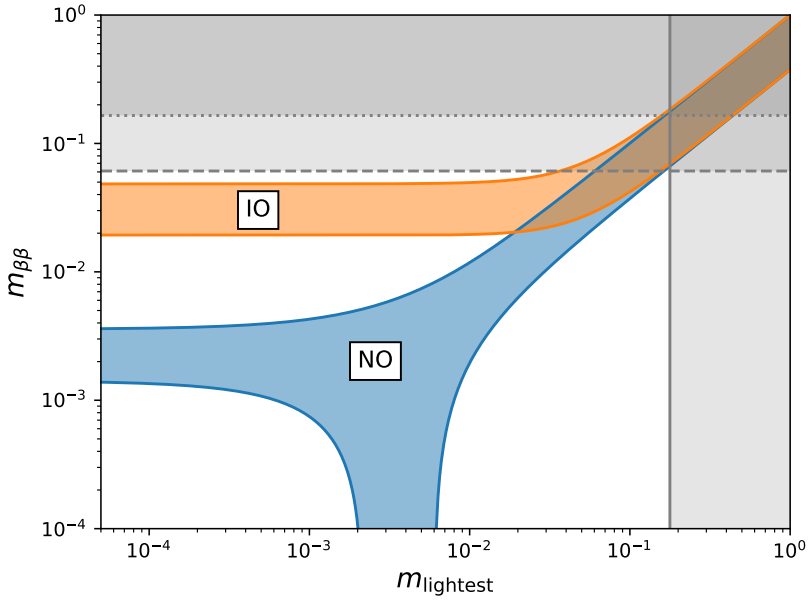

Figure 3.5.: Possible values for $m_{\beta\beta}$ depending on the lightest neutrino mass m_{lightest} for normal ordering (NO) in blue and inverted ordering (IO) in orange. The horizontal grey lines correspond to the bounds from KamLAND-Zen [33], while the dotted and dashed lines correspond to different theoretical calculations of the nuclear matrix elements. The vertical solid line correspond to the most conservative cosmological bound on m_Σ from the Planck collaboration [34].

3.3.2. Beyond Standard Model Realization of Neutrino Masses

The already mentioned absence of neutrino masses in the SM is a theoretical issue which needs explanation. Additionally the experimental values for the neutrino masses turn out to be orders of magnitude smaller than all other fermionic particles. If the neutrino masses are also generated via the Higgs mechanism as a Dirac mass by introducing the undetectable right handed field ν_{R}, this would yield a Yukawa coupling for the neutrinos of $y_\nu \sim 10^{-13}$ compared to the Yukawa coupling of the top quark of $y_t \sim 1$. Although possible, such a small coupling seems unappealing. Therefore, lots of beyond standard model (BSM) approaches of neutrino mass generation also try to explain the smallness of neutrino masses by the mass mechanism itself.

The most popular neutrino mass mechanisms are the so called Seesaw mechanisms [36–40]. They provide a renormalizable tree-level realization of the non-renormalizable Weinberg operator (3.51) by introducing new heavy particles. The three different types, shown in Figure 3.6, differ in the newly introduced particle. Type I introduces a right handed neutrino ν_{R} with

a large Majorana mass, Type II and III each use a heavy $SU(2)_L$ triplet, the bosonic Δ^0 for type II and the fermionic Σ for type III.

For each type of Seesaw mechanism, the light neutrino masses can be determined by integrating out the heavy particle and diagonalizing the resulting mass matrix. For Type I Seesaw the mass matrix is given by Equation (3.50) and diagonalization leads to light neutrino masses of $m_\nu \sim -m_D \left(M^{\mathrm{R}}_{\mathrm{Maj}}\right)^{-1} m_D^T$. The Type II and III masses read $m_\nu \sim \lambda_\Delta Y_\Delta \frac{v_u^2}{M_\Delta}$ and $m_\nu \sim -m_D M_\rho^{-1} m_D^T$, respectively.

It can be seen that for all Seesaw mechanisms the light neutrino masses are suppressed by the heavy masses of the newly introduced particles. Generating a neutrino mass in the eV-range and using natural couplings and Dirac-masses at the EW-scale automatically leads to masses of the heavy particles around the GUT-scale, which are undetectable by the Large Hadron Collider (LHC). A rough estimate from basic principles in [41] gives an upper bound for the scale of $m_{\mathrm{Maj}} < \mathcal{O}(10^{16})$ GeV. In contrast to the Seesaw-mechanisms, renormalizable realizations of

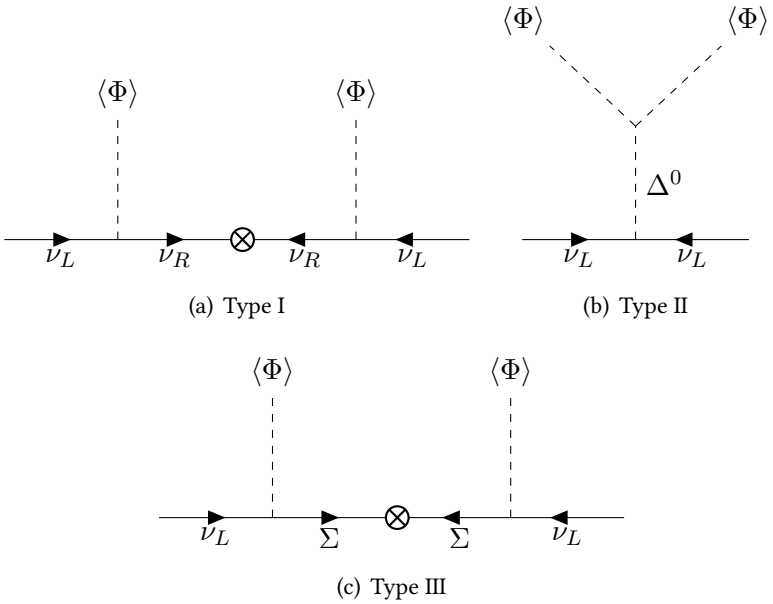

Figure 3.6.: Feynman diagrams for Seesaw Mechanism Type I, II and III.

(3.51) at loop-level generate the small neutrino masses via loop suppressions. The most famous models are the Zee- [42, 43], the Zee-Babu- [44, 45] and the scotogenic [46] model. The Zee- and Zee-Babu-model do not propose right handed neutrinos, but extend the scalar sector by either an additional doublet Φ_2 and a singly charged singlet h^+ (Zee model) or two additional singlets h^+ and k^{++} (Zee-Babu model). The generation of the neutrino masses occur at one- and two-loop level, respectively. The scotogenic model in contrast introduces right handed

neutrinos with a large Majorana mass and an additional scalar doublet. The neutrino mass is generated at one loop level and the new neutral scalar serves as a potential dark matter candidate. The corresponding Feynman diagrams generating the neutrino masses are shown in Figure 3.7. In general, the above mentioned neutrino mass models can explain the smallness of the neutrino masses, but lack additional testable predictions. The newly introduced particles are either too heavy or too weakly coupled to be tested at a current collider like the LHC. Most mass generation mechanisms also predict a Majorana mass, but as shown in Section 3.3.1 a null result for neutrinoless double beta decay does not rule out these models due to possible cancellations of the Majorana phases.

Predictions for values or patterns in the leptonic mass or mixing matrix can only be made by imposing additional constraints like flavor symmetries, which are covered in the next section.

3.3.3. Predictions for Leptonic Mixing via Discrete Symmetries and Texture Zeros

In every mechanism generating fermionic masses, the specific entries in the mass matrices are in general determined by free coupling parameters, e.g. the Yukawa couplings y_Ψ. Without imposing restrictions on the specific coupling parameters the mass matrices are expected to lack any structure. Looking at the experimentally determined values of the masses and mixing matrices in the quark and lepton sector the naive expectations are not met [20]. While the quark mixing matrix is almost diagonal and can be written in the Wolfenstein parametrization with the Wolfenstein parameter $\lambda_\mathrm{W} \sim 0.22$ as

$$|V_\mathrm{CKM}| = \begin{pmatrix} 1-\frac{\lambda_\mathrm{W}^2}{2} & \lambda_\mathrm{W} & \lambda_\mathrm{W}^3 \\ \lambda_\mathrm{W} & 1-\frac{\lambda_\mathrm{W}^2}{} & \lambda_\mathrm{W}^2 \\ \lambda_\mathrm{W}^3 & \lambda_\mathrm{W}^2 & 1 \end{pmatrix} + \mathcal{O}(\lambda_\mathrm{W}^4) \approx \begin{pmatrix} 0.974 & 0.225 & 0.004 \\ 0.225 & 0.974 & 0.041 \\ 0.009 & 0.040 & 0.999 \end{pmatrix}, \tag{3.53}$$

the leptonic mixing matrix does not show structure at the first glance

$$|V_\mathrm{PMNS}| \approx \begin{pmatrix} 0.829 & 0.539 & 0.146 \\ 0.490 & 0.576 & 0.654 \\ 0.268 & 0.614 & 0.742 \end{pmatrix}. \tag{3.54}$$

A possible explanation for a structure among the different generations arises from imposing a horizontal flavor symmetry on the corresponding fields. Starting with a flavor symmetry, most generally an $SU(3)$, all fields are assigned to multiplet representations of this symmetry. Typically the structure is imposed by charging the different generations differently. Additionally so called flavon fields are introduced, which are typically singlets under the SM-gauge group but charged under the flavor symmetry.

Except for the Yukawa terms, all terms in the Lagrangian are automatically invariant under the new flavor symmetry. To make Yukawa terms invariant under the flavor symmetry, different powers of the flavon fields are needed. If the flavon field acquires a VEV, the flavor

symmetry is broken, and the Yukawa terms for different fields are suppressed by different powers of the VEV of the flavon according to their charges. A hierarchical structure in the Yukawa matrix can therefore be imposed.

The more democratic structure in the leptonic sector cannot be explained by such an abelian group. Before the measurement of θ_{13} a common approximation of the PMNS matrix was the so called tri-bi-maximal mixing

$$V^{\mathrm{TBM}} = \begin{pmatrix} \sqrt{\frac{2}{3}} & \frac{1}{\sqrt{3}} & 0 \\ -\frac{1}{\sqrt{6}} & \frac{1}{\sqrt{3}} & \frac{1}{\sqrt{2}} \\ \frac{1}{\sqrt{6}} & -\frac{1}{\sqrt{3}} & \frac{1}{\sqrt{2}} \end{pmatrix} \tag{3.55}$$

first proposed in [47] corresponding to $\sin\theta_{12}^{\mathrm{TBM}} = \frac{1}{\sqrt{3}}$, $\theta_{23}^{\mathrm{TBM}} = \frac{\pi}{4}$ and $\theta_{13}^{\mathrm{TBM}} = 0$. This mixing matrix is automatically generated if the neutrino mass matrix in flavor basis takes the form

$$M_\nu = \begin{pmatrix} x & y & y \\ y & x+v & y-v \\ y & y-v & x+v \end{pmatrix} \tag{3.56}$$

Such a structure of the neutrino mass matrix can be generated e.g. by charging the neutrinos under the discrete symmetry group A_4, a subgroup of $\mathrm{SU}(3)$ [48]. Several other approaches were proposed to generate this kind of structure, e.g. structure zeros, but all models had to be extended due to the measurement of nonzero θ_{13}.

In general flavor models predicting the structure of the mixing or mass matrix make precise predictions that can be tested in experiments but all simple models fail to explain current data and more general extensions usually lack predictability.

3.4. Experimental Hints for Neutrino-Physics Beyond Standard Model

Apart from theoretically motivated models to explain either the neutrino mass generation itself or the values of the masses and mixing parameters, there are currently several experimental anomalies that cannot be explained by solely three massive neutrinos.

The LSND experiment was an accelerator based experiment and searched for $\bar{\nu}_\mu \to \bar{\nu}_e$ oscillations, with a baselength of ~ 30 m and neutrino energies between 20 and 60 MeV. Due to the setup of the experiment it was sensitive to mass squared differences of $\Delta m_{\mathrm{SB}} \sim 1\mathrm{eV}^2$. In 2001 the collaboration reported a significant excess of electron events in the detector [49] and interpreted this as an oscillation from muon antineutrinos into electron antineutrinos. Since at this setup, oscillations with Δm_{21}^2 or Δm_{31}^2 are negligible, it can be interpreted as a third mass squared difference, and therefore a hint for a fourth neutrino species. To further investigate

this so called short baseline oscillation the experiments MiniBooNE and MicroBooNE has been developed, which are also accelerator-based and sensitive to such mass squared differences. Recent results by MiniBooNE also show a significant excess which can be interpreted as such oscillations [50]. We will focus on this result in Part IV.

In addition to the LSND experiment, the Gallium-anomaly also provide hints for a mass squared difference of $\Delta m_{SB} \sim 1\mathrm{eV}^2$ at around 2.7σ [51]. To test the solar neutrino experiments GALLEX [52–54] and SAGE [55–58] artificial radioactive sources made of $^{51}\mathrm{Cr}$ and $^{37}\mathrm{Ar}$ have been placed into the detectors. The measured number of events turned out to be significantly lower than predicted. One possible explanation is that the electron antineutrinos, produced in the radioactive decay of the sources, oscillated into another flavor.

A third hint for short baseline oscillation is the reactor anomaly [59], where the flux of electron antineutrino from fission reactors show a deficit of $\sim 5\%$ compared to the predictions. The Daya Bay collaboration claims to find a correlation between the different fuel components in the reactor and the flux deficit and suggests that the anomaly may be explained by an incorrect calculation of the spectrum of ^{235}U [60]. Nevertheless, this interpretation has been contradicted by the global analysis in [61].

All anomalies combined seem to hint in the same direction of a fourth neutrino state. On the other hand this simplest explanation is inconsistent with several other neutrino experiments like atmospheric or accelerator based experiments. This issue is handled in more detail in Part IV.

Additionally a fourth neutrino state is highly unmotivated from a theoretical point of view. There is no evidence of a fourth charged lepton and therefore the fourth neutrino would not fit in the doublet structure of the SM. Additionally, the precision measurement of the decay width of the Z-boson [62] determines the number of neutrinos coupling to the Z to three and excludes a light neutrino participating in the weak interaction. Therefore this additional fourth neutrino has to be sterile.

Summarizing, theoretical and experimental approaches in neutrino physics currently provide lots of open questions for further research: On the one hand there is no experimental evidence for theoretically well motivated mechanisms that could explain the origin of neutrino masses, on the other hand there is no theoretical approach to explain all current neutrino data and anomalies.

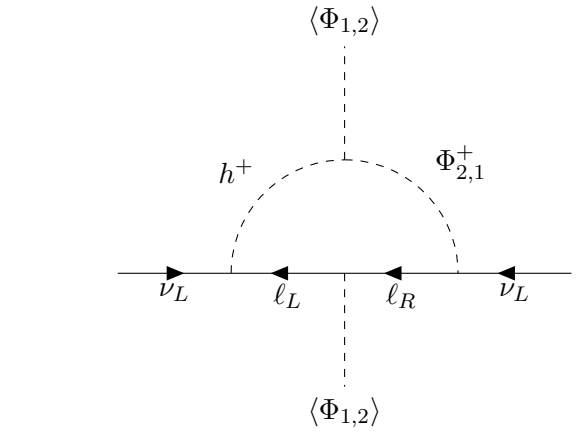

(a) Zee model

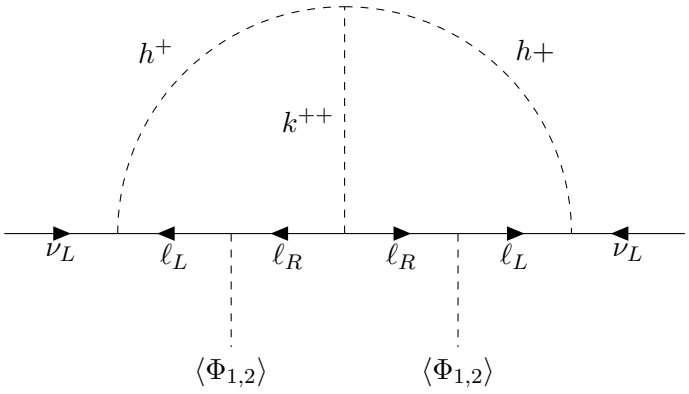

(b) Zee-Babu model

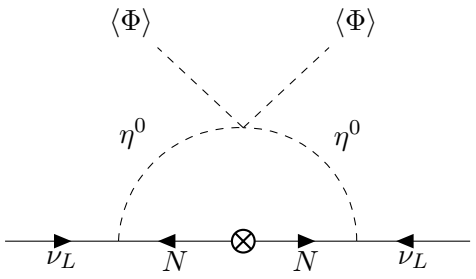

(c) Scotogenic model

Figure 3.7.: Feynman diagrams for different models generating neutrino masses by loop effects [13].

Part II.

A Novel Approach to Analyze Neutrino Oscillations in the Light of New Physics

4. Model Independent Description of Neutrino Oscillations

In the beginning of neutrino oscillation physics approximations , e.g. a two neutrino scheme, were used to simplify the analyses. Due to increasing number of neutrino experiments and their increasing sensitivity, neutrino oscillation physics in recent years approaches the era of high precision physics. Becoming more and more precise, more exact analytical formulations for the oscillation probability are needed. For example the analysis in [63] from the T2K collaboration uses the following probability for the neutrino and antineutrino channel

$$P(\overset{(-)}{\nu}_\mu \to \overset{(-)}{\nu}_e) \simeq \sin^2\theta_{23}\sin^2 2\theta_{13}\sin^2\frac{\Delta m^2_{31}L}{4E} \\ \overset{(+)}{-}\frac{\sin 2\theta_{12}\sin 2\theta_{23}}{2\sin\theta_{13}}\sin\frac{\Delta m^2_{21}L}{4E}\sin^2 2\theta_{13}\sin^2\frac{\Delta m^2_{31}L}{4E}\sin\delta_{\mathrm{CP}} + \dots . \tag{4.1}$$

Note the second term, which provides non-leading contribution to the oscillation probability, but is sensitive to the CP phase δ_{CP}, whose measurement is one of the main goals of T2K. This analysis adopts the three neutrino paradigm without any potential sources of new physics beyond the SM. Since there is no stringent evidence for BSM physics, the approach is of course justified and the first step to discover CP violation in neutrino oscillations. Nevertheless, several authors already claimed that new physics models can introduce "fake" CP violation spoiling an analysis based on the three neutrinos paradigm [64–68]. Such analyses are therefore highly dependent on the specific underlying model.

Moreover, experiments like T2K or NOvA rely on parameter inputs from different experiments like reactor or atmospheric neutrino experiments. This ansatz can be made if no new physics is involved, but it is not clear whether the measured parameters at different experiments coincide with each other when new physics is applied.

Taking above mentioned discussion into account, in this part of the thesis we introduce a novel approach to analyze neutrino oscillations, which is independent of a specific model of new physics and also independent of other experimental results. Due to the smaller number of parameters we focus on CP violation in neutrino oscillations but the approach can in principle also be extended to other neutrino experiments.

New physics can impact predictions of the SM in various ways. Here we focus solely on implications, which manifest themselves in deviation from expectations in neutrino oscilla-

tions. Therefore we start at the underlying Lagrangian responsible for neutrino oscillations, the charged current interaction:

$$\mathcal{L}_{CC} \propto \sum_{\alpha\in\{e,\mu,\tau\}} \sum_{k=1} \overline{\ell_\alpha}\gamma^\mu(1-\gamma^5)U_{\alpha k}\nu_k W_\mu^- \quad + \quad \overline{\nu_k}\gamma^\mu(1-\gamma^5)U_{\alpha k}^*\ell_\alpha W_\mu^+ \tag{4.2}$$

The coupling of the charged leptons with the physical neutrino mass eigenstates is described by the mixing matrix U and plays a significant role in this part.

While the mixing matrix U in the SM is a 3×3 unitary mixing matrix, this assumption does not hold for all BSM models. The unitarity of the mixing matrix can be violated in two different ways:

- direct unitarity violation is generated by introducing additional light sterile neutrinos. The kinematically accessible neutrino mass eigenstates are more than three and the neutrinos can actually oscillate into these states. As a result, the enlarged mixing $N_{\text{light}} \times N_{\text{light}}$ is still unitary, but not the reduced 3×3 mixing matrix.

- indirect unitarity violation is generated by additional heavy right handed neutrinos e.g. in a Seesaw mechanism which are kinematically forbidden in typical energy ranges for neutrino oscillations. Therefore the 3×3 mixing matrix is also not unitary, but additional constraints are not obvious.

We assume in any case, that the complete high energy theory fulfills basic quantum mechanical principles. The low energy effective theory in contrast, might violate quantum mechanical principles like a non-unitary mixing matrix, a non hermitian effective Hamiltonian or a flavor basis, which is ill defined. Our approach is based on the search for these violations. The neutrino mass eigenstates are still physically well defined and so

$$\langle\nu_i|\nu_j\rangle = \delta_{ij} \tag{4.3}$$

holds, while the same is not true for the "flavor states" described by the interaction with the charged leptons. The flavor states do not built up a complete eigenbasis. A transition from the mass eigenbasis to the "flavor space" is generated by the (in general) non-unitary mixing matrix U:

$$|\nu_\alpha\rangle = U_{\alpha i}\,|\nu_i\rangle \qquad \langle\nu_\alpha| = \langle\nu_i|\,U_{\alpha i}^\dagger \tag{4.4}$$

$$\Rightarrow \langle\nu_\beta|\nu_\alpha\rangle = \left(U^\dagger U\right)_{\beta\alpha} \neq \delta_{\alpha\beta} \tag{4.5}$$

With this relation it is straightforward to deduce the neutrino oscillation probability analogously to Section 3.2, but with the emphasis of not using unitarity implicitly.

$$P_{\nu_\alpha \to \nu_\beta} = \underbrace{\sum_{k,j}^{N_{\text{light}}} (U^*_{\alpha k} U_{\beta k} U_{\alpha j} U^*_{\beta j})}_{\text{zero distance effect}} - 4 \sum_{k>j}^{N_{\text{light}}} \underbrace{\text{Re}(U^*_{\alpha k} U_{\beta k} U_{\alpha j} U^*_{\beta j})}_{\mathcal{R}^{kj}_{\alpha\beta}} \sin^2\left(\frac{\Delta m^2_{kj} L}{4E}\right) \tag{4.6}$$

$$+ 2 \sum_{k>j}^{N_{\text{light}}} \underbrace{\text{Im}(U^*_{\alpha k} U_{\beta k} U_{\alpha j} U^*_{\beta j})}_{\mathcal{A}^{kj}_{\alpha\beta}} \sin\left(\frac{\Delta m^2_{kj} L}{2E}\right) \tag{4.7}$$

The first term reduces to $\delta_{\alpha\beta}$ in case of unitarity or direct unitarity violation due to basic unitarity conditions. Since it is independent of baselength, it is often referred to as a zero distance effect. We do not focus any further on this specific effect, since most experiments are not sensitive to this, but it has to be taken into account as a flux normalization effect independent of the energy.

Most approaches for SM or BSM physics currently use specific parametrizations of the mixing matrix U or use approximations suitable for specific experiments. We will be more general and focus on the newly introduced parameters $\mathcal{A}^{kj}_{\alpha\beta}$ and $\mathcal{R}^{kj}_{\alpha\beta}$, describing CP conserving and CP violating processes. These parameters are in fact observables and hence independent of any parametrization, as already pointed out in [69, 70]. Nevertheless, there are strict and specific predictions for these parameters in case of the SM or direct unitarity violation. Analytic predictions will be covered in the following section.

5. Analytic Predictions for CP violating Amplitudes

In Chapter 4 we introduced the CP conserving and the CP violating amplitudes

$$\mathcal{R}^{kj}_{\alpha\beta} = \mathrm{Re}\left(U^*_{\alpha k} U_{\beta k} U_{\alpha j} U^*_{\beta j}\right) , \tag{5.1}$$

$$\mathcal{A}^{kj}_{\alpha\beta} = \mathrm{Im}\left(U^*_{\alpha k} U_{\beta k} U_{\alpha j} U^*_{\beta j}\right) . \tag{5.2}$$

From the definition it is easy to deduce some general relations among the amplitudes.

The CP conserving amplitudes are symmetric under interchange of indices

$$\mathcal{R}^{kj}_{\alpha\beta} = \mathcal{R}^{kj}_{\beta\alpha} , \tag{5.3}$$

$$\mathcal{R}^{kj}_{\alpha\beta} = \mathcal{R}^{jk}_{\alpha\beta} , \tag{5.4}$$

while the CP violating amplitudes are anti-symmetric under interchange of indices

$$\mathcal{A}^{kj}_{\alpha\beta} = -\mathcal{A}^{kj}_{\beta\alpha} , \tag{5.5}$$

$$\mathcal{A}^{kj}_{\alpha\beta} = -\mathcal{A}^{jk}_{\alpha\beta} . \tag{5.6}$$

Consequently, the CP violating amplitudes vanish for two identical indices,

$$\mathcal{A}^{kj}_{\alpha\alpha} = 0 , \tag{5.7}$$

$$\mathcal{A}^{kk}_{\alpha\beta} = 0 . \tag{5.8}$$

These relations reduce the total number of possible amplitudes of an $N \times N$ mixing matrix from N^4 of CP violating and N^4 of CP conserving amplitudes to only $\left(\frac{N(N+1)}{2}\right)^2$ CP conserving plus $\left(\frac{(N-1)N}{2}\right)^2$ CP violating amplitudes. Note, that these relations are independent of whether the mixing matrix U is unitary or not. They are simply deduced from the basic definition of the amplitudes.

To determine further analytic relations among the amplitudes it is necessary to be more model dependent. The most obvious approach is to assume a unitary mixing matrix, which will be done in the following section.

5.1. General Constraints due to Unitarity

If one considers the free low energy Hamiltonian to be hermitian, it is possible to diagonalize it with a unitary matrix U. The unitary matrix U is considered to be an $N \times N$ matrix, without specifying N directly in this step. Usually N corresponds also to the number of light neutrinos in this context. The basic condition for unitarity $U^{-1} = U^\dagger$ can be rewritten as

$$\begin{aligned} UU^\dagger &= 1\,, \\ \Rightarrow \sum_k U_{\alpha k} \left(U^\dagger\right)_{k\beta} &= \sum_k U_{\alpha k} U^*_{\beta k} = \delta_{\alpha\beta}\,. \end{aligned} \tag{5.9}$$

as well as

$$\begin{aligned} U^\dagger U &= 1\,, \\ \Rightarrow \sum_\alpha \left(U^\dagger\right)_{k\alpha} U_{\alpha j} &= \sum_\alpha U^*_{\alpha k} U_{\alpha j} = \delta_{kj}\,. \end{aligned} \tag{5.10}$$

From these relations it is easy to see that the relation

$$\begin{aligned} \sum_\alpha^N \mathcal{A}^{kj}_{\alpha\beta} &= \sum_\alpha^N \mathrm{Im}\left(U^*_{\alpha k} U_{\beta k} U_{\alpha j} U^*_{\beta j}\right) \\ &= \mathrm{Im}\left(\sum_\alpha^N \left(U^*_{\alpha k} U_{\alpha j}\right) U_{\beta k} U^*_{\beta j}\right) \\ &= \mathrm{Im}\left(\delta_{kj} U_{\beta k} U^*_{\beta j}\right) \\ &= 0\,, \end{aligned} \tag{5.11}$$

holds. Generalizing these constraints for each index and also to the CP conserving amplitudes we end up with following relations:

$$\sum_\alpha^N \mathcal{A}^{kj}_{\alpha\beta} = 0\,, \qquad \sum_\beta^N \mathcal{A}^{kj}_{\alpha\beta} = 0\,, \tag{5.12}$$

$$\sum_k^N \mathcal{A}^{kj}_{\alpha\beta} = 0\,, \qquad \sum_j^N \mathcal{A}^{kj}_{\alpha\beta} = 0\,, \tag{5.13}$$

$$\sum_\alpha^N \mathcal{R}^{kj}_{\alpha\beta} = \delta_{jk} \left|U_{\beta k}\right|^2\,, \qquad \sum_\beta^N \mathcal{R}^{kj}_{\alpha\beta} = \delta_{jk} \left|U_{\alpha k}\right|^2\,, \tag{5.14}$$

$$\sum_k^N \mathcal{R}^{kj}_{\alpha\beta} = \delta_{\alpha\beta} \left|U_{\alpha j}\right|^2\,, \qquad \sum_j^N \mathcal{R}^{kj}_{\alpha\beta} = \delta_{\alpha\beta} \left|U_{\alpha k}\right|^2\,. \tag{5.15}$$

From these unitarity relations for amplitudes it is straightforward to calculate the specific relations for a specific number of N. Keep in mind, that the relations are directly deduced from unitarity of the mixing matrix and that they are exact.

5.2. Two Neutrinos

Since there is already evidence for three neutrinos, the two neutrino case is not realistic. Nevertheless it is instructive to stress some details.

From Equations (5.12) and (5.13) it is easy to see that all $\mathcal{A}^{kj}_{\alpha\beta}$ vanish. Therefore no CP violation can be measured in case of only two neutrinos and unitary mixing. This behavior is well known and also corresponds to the missing CP phase in the typical parametrization. Additionally, from Equations (5.14) and (5.15) all CP conserving amplitudes are determined by only one free parameter corresponding to the single mixing angle in a two neutrino scheme.

5.3. Three Neutrinos

The first proof of only one independent CP violating amplitude in the case of three generations has been presented in [71] by Jarlskog via the commutator of mass matrices in the quark sector. We will come back to this method in Section 7.3. The method of invariant amplitudes also provides a simple proof of a single uniform CP violating amplitude. Using Equations (5.12) and (5.13) and implying the basic relations from Equations (5.5) and (5.6) directly leads to

$$\mathcal{A}^{21}_{e\mu} = \mathcal{A}^{32}_{e\mu} = -\mathcal{A}^{31}_{e\mu} = -\mathcal{A}^{21}_{e\tau} = -\mathcal{A}^{32}_{e\tau} = \mathcal{A}^{31}_{e\tau} = \mathcal{A}^{21}_{\mu\tau} = \mathcal{A}^{32}_{\mu\tau} = -\mathcal{A}^{31}_{\mu\tau}. \tag{5.16}$$

Apart from the sign, all amplitudes are the same.

This uniform CP violating amplitude corresponds to only one CP phase in a 3×3 unitary matrix. A direct consequence from this is that the magnitude of CP violation is the same for all neutrino oscillation channels and modes. A direct comparison between different experiments is therefore a stringent test of the three neutrino hypothesis. This relation is independent of parametrization or actual mixing angles and has to be satisfied regardless of specific values. One test for this uniform CP violating amplitude is the famous CKM unitarity triangle in the quark sector. Similar analyses have also been worked out in the lepton sector [72–77]. While this provides a precise test for the unitarity of the 3×3 mixing matrix, the insights of unitarity triangles are limited in cases where the triangle does not close. The source of unitarity violation cannot be determined.

With this analysis we focus at sums and ratios of the CP amplitudes itself and show that the emerging correlations depend on the specific BSM model and therefore provide a useful test for new physics.

5.4. Analytic Treatment of 3+1 ν

As mentioned before in Section 3.4 the introduction of a light sterile neutrino is motivated by several experimental hints and currently under investigation. Albeit a light sterile neutrino lacks theoretical motivation the tensions among different experiments have to be taken seriously. Therefore in this section we focus on adding exactly one light sterile neutrino to the standard model content.

Considering an additional light sterile neutrino, the assumption of hermiticity of the free Hamiltonian, results in unitarity of the 4×4 mixing matrix. Note especially that now the 3×3 mixing matrix is *not* unitary anymore. The conclusions we draw in the previous section do not hold anymore, so in general we have more CP violating amplitudes than just a single one. By exploiting these relations in the context of the quark sector it has been shown for four flavors that all amplitudes can be reduced to only three independent CP violating and six CP conserving amplitudes [78]. In the following, we follow these arguments translated to the notation commonly used in neutrino physics. All relations rely on [78] where these relations have been proven for general unitary 4×4 matrices.
In total there exist $4 \times 4 \times 4 \times 4 = 256$ ($\alpha, \beta \in \{e, \mu, \tau, s\}$ and $k, j \in \{1, 2, 3, 4\}$) different CP violating amplitudes $\mathcal{A}^{kj}_{\alpha\beta} = \mathrm{Im}(U^*_{\alpha k} U_{\beta k} U_{\alpha j} U^*_{\beta j})$. Due to the general relations (5.5) - (5.8) it is sufficient to only consider $\mathcal{A}^{kj}_{\alpha\beta}$ where $\alpha < \beta$ and $k > j$, which reduces the number of CP violating amplitudes to 36. These 36 amplitudes are not independent due to the unitarity relations (5.12) and (5.13) and can be expressed via only nine amplitudes (see Appendix A). Again, these nine amplitudes can be expressed by three remaining amplitudes via the following expression

$$\begin{pmatrix} \mathcal{A}^{32}_{e\mu} \\ \mathcal{A}^{43}_{e\mu} \\ \mathcal{A}^{21}_{\mu\tau} \\ \mathcal{A}^{43}_{\mu\tau} \\ \mathcal{A}^{21}_{\tau s} \\ \mathcal{A}^{32}_{\tau s} \end{pmatrix} = \mathbf{M}^{-1} \begin{pmatrix} \mathcal{R}^{32}_{e\mu} \mathcal{A}^{21}_{e\mu} \\ \mathcal{R}^{43}_{\mu\tau} \mathcal{A}^{43}_{\tau s} \\ \mathcal{R}^{21}_{\mu\tau} \mathcal{A}^{21}_{e\mu} \\ \mathcal{R}^{32}_{\tau s} \mathcal{A}^{43}_{\tau s} \\ (\mathcal{R}^{32}_{\tau\tau} + \mathcal{R}^{32}_{e\mu}) \mathcal{A}^{32}_{\mu\tau} \\ (\mathcal{R}^{33}_{\mu\tau} + \mathcal{R}^{32}_{e\mu}) \mathcal{A}^{32}_{\mu\tau} \end{pmatrix}, \tag{5.17}$$

with $\mathbf{M}^{-1}$ defined by the inverse of

$$\mathbf{M} = \begin{pmatrix} -(\mathcal{R}^{22}_{e\mu} + \mathcal{R}^{21}_{e\mu}) & \mathcal{R}^{22}_{e\mu} & 0 & 0 & 0 & 0 \\ 0 & \mathcal{R}^{43}_{\tau\tau} & 0 & -(\mathcal{R}^{43}_{\tau\tau} + \mathcal{R}^{43}_{\tau s}) & 0 & 0 \\ 0 & 0 & -(\mathcal{R}^{21}_{\mu\mu} + \mathcal{R}^{21}_{e\mu}) & 0 & \mathcal{R}^{21}_{\mu\mu} & 0 \\ 0 & 0 & 0 & 0 & \mathcal{R}^{33}_{\tau s} & -(\mathcal{R}^{33}_{\tau s} + \mathcal{R}^{43}_{\tau s}) \\ \mathcal{R}^{32}_{\tau\tau} & 0 & 0 & 0 & 0 & -\mathcal{R}^{32}_{\mu\tau} \\ 0 & 0 & -\mathcal{R}^{33}_{\mu\tau} & -\mathcal{R}^{32}_{\mu\tau} & 0 & 0 \end{pmatrix}. \tag{5.18}$$

The amplitudes $\mathcal{R}^{kj}_{\alpha\beta} = \mathrm{Re}(U^*_{\alpha k} U_{\beta k} U_{\alpha j} U^*_{\beta j})$ correspond to the CP conserving amplitudes in neutrino oscillations. These relations therefore provide a connection between the CP violating

and the CP conserving processes.
To emphasize the differences between 3ν and $3+1\nu$ we want to highlight the following relations:

$$\mathcal{A}^{31}_{e\mu} = -\mathcal{A}^{32}_{e\mu} + \mathcal{A}^{43}_{e\mu} \tag{5.19}$$
$$\mathcal{A}^{21}_{e\tau} = -\mathcal{A}^{32}_{\mu\tau} + \mathcal{A}^{43}_{\tau s} \tag{5.20}$$
$$\mathcal{A}^{31}_{e\tau} = -\mathcal{A}^{32}_{e\tau} - \mathcal{A}^{32}_{\tau s} + \mathcal{A}^{43}_{\tau s} \tag{5.21}$$

The relations reduce to the 3ν case, if no mixing with the sterile neutrino takes place, corresponding to vanishing non diagonal elements in the fourth line and column of U. Consequently, all amplitudes vanish if $\alpha \vee \beta = s$ or $k \vee j = 4$. Due to the expected smallness of mixing with sterile states, the deviations from uniform amplitudes in the 3×3 sector could be treated in a perturbative approach.

5.5. Two Sterile Neutrinos

In general this method can be extended for an arbitrary amount of additional light sterile neutrinos. Before starting rather annoying calculations one has to consider whether comparable relations might be interesting at all.

The weak Eigenbasis is determined via the weak interaction with the charged leptons. Since there are no additional generations of charged leptons, it is impossible to define a weak Eigenbasis in the sterile sector. The transformation from mass to weak Eigenbasis is determined via the mixing matrix U

$$|\nu_\alpha\rangle = U_{\alpha i} \, |\nu_i\rangle \, . \tag{5.22}$$

Due to the arbitrariness in the sterile sector, one can always rotate the mixing matrix U in the 4-5 plane by an arbitrary angle θ_{45} without changing the physics. The unitarity conditions for U then read for example

$$\mathcal{A}^{21}_{e\mu} + \mathcal{A}^{31}_{e\mu} + \mathcal{A}^{41}_{e\mu} + \mathcal{A}^{51}_{e\mu} = 0 \tag{5.23}$$

Since all $\mathcal{A}^{kj}_{\alpha\beta}$ with $\alpha, \beta \in \{e, \mu, \tau\}$ and $k, j \in \{1, 2, 3\}$ are invariant under a rotation in the 4-5 plane, we can deduce

$$\mathcal{A}^{41}_{e\mu}(\theta_{45}) + \mathcal{A}^{51}_{e\mu}(\theta_{45}) = \mathcal{A}^{41}_{e\mu}(\theta^*_{45}) + \mathcal{A}^{51}_{e\mu}(\theta^*_{45}) \tag{5.24}$$

This sum of the additional amplitudes can be renamed so that the original unitarity relations from the $3+1\nu$ model emerge. This argument can be made for all other unitarity relations, and by renaming the involved sums we end up at exactly the same relations as in the chapter before.

There are a few annotations to the above made argument. First of all, unless additional interactions of the sterile neutrinos are found, it is impossible to differentiate between the two different sterile neutrino states. Therefore it is experimentally impossible to distinguish $P(\nu_e \to \nu_{s_1})$ from $P(\nu_e \to \nu_{s_2})$ and therefore to distinguish e.g. the amplitudes $\mathcal{A}^{21}_{es_1}$ and $\mathcal{A}^{21}_{es_2}$ where ν_{s_1} and ν_{s_2} indicate the two sterile states (not to confuse with the additional mass eigenstates ν_4 and ν_5 which are actually well defined).

In contrast, it is generally possible to measure the difference between e.g. $\mathcal{A}^{41}_{e\mu}$ and $\mathcal{A}^{51}_{e\mu}$ if the additional frequencies in the $\frac{L}{E}$ spectrum induced by the additional independent mass squared differences Δm^2_{41} and Δm^2_{51} are determined. Currently some short baseline experiments are taking data looking for such a direct proof of more than three light neutrino generations. In this thesis we want to focus on the case where these additional frequencies do not show up in the experiments. Most of the current experiments are not sensitive to additional frequencies in the range of $\Delta m^2 \gtrsim 0.1\ \mathrm{eV}^2$, due to the long distance between source and detector. In such experiments the additional frequencies would be averaged out and the only measurable amplitudes would be $\mathcal{A}^{kj}_{\alpha\beta}$ with $\alpha, \beta \in \{e, \mu, \tau\}$ and $k, j \in \{1, 2, 3\}$. In this case the amplitudes $\mathcal{A}^{41}_{\alpha\beta}$ and $\mathcal{A}^{51}_{\alpha\beta}$ are only measurable in combination.

Focussing on only the amplitudes with $\alpha, \beta \in \{e, \mu, \tau\}$ and $k, j \in \{1, 2, 3\}$, there is no difference between models with one additional light neutrino or more additional light neutrinos. The naively expected larger freedom for the amplitudes due to the higher number of free parameters in the larger mixing matrix, is hidden in the sterile sector.

5.6. General Non-Unitarity-Approach

In general a non-unitary 3×3 matrix U_{NU} can be described by a matrix product of a unitary matrix $\mathbf{U}_{\mathrm{unitary}}$ and a triangular matrix $(\mathbb{1} - \alpha)$ (see for instance [79–81])

$$U_{\mathrm{NU}} = (\mathbb{1} - \alpha)\, \mathbf{U}_{\mathrm{unitary}} = \begin{pmatrix} 1 - \alpha_{ee} & 0 & 0 \\ \alpha_{e\mu} & 1 - \alpha_{\mu\mu} & 0 \\ \alpha_{\tau e} & \alpha_{\mu\tau} & 1 - \alpha_{\tau\tau} \end{pmatrix} \mathbf{U}_{\mathrm{unitary}}, \tag{5.25}$$

where α_{ee}, $\alpha_{\mu\mu}$ and $\alpha_{\tau\tau}$ are real and $\alpha_{e\mu}$, $\alpha_{\tau e}$ and $\alpha_{\mu\tau}$ are complex parameters. If all α vanish, the resulting matrix is unitary. By varying the parameters α, it is possible to generate a general non-unitary quadratic matrix. For suitable parameter combinations it is also possible with this approach to mimic a mixing matrix from a 3+1 ν model, where also the above analytic relations follow. We want to be most general and do not apply any restrictions on the parameters α and therefore no general analytic predictions for the amplitudes can be made.

By applying total freedom on all parameters α it is possible to violate probability conservation. In the case of direct unitarity violation mentioned above it was only possible that probability seems to vanish in the 3×3 region since the sterile state is not measurable. Similar effects can also happen in the general non-unitarity approach, where new effects like new heavy neutrino states or non standard interactions at production or detection can be the cause

of loss of probability. For suitable combinations of α it is also possible to seemingly generate probability, if the inequality $\sum_{\alpha\in\{e,\mu,\tau\}} \left|(U_{NU})_{\alpha j}\right|^2 > 1$ holds. While by violating basic quantum mechanical rules on this level, it might be possible to effectively generate such an effect by rather speculative models like neutrino decay. Therefore, we distinguish between the two different cases of general non-unitarity, with and without possibility to effectively generate probability.

Since general analytic relations are not deducible the following chapter follows a numerical approach.

6. Numerical Analysis

As pointed out in the previous chapter it is not possible to find analytic constraints for the framework of general non-unitary mixing matrices. Therefore we focus in this chapter on a numerical approach.

6.1. A Numerical Method to Predict Amplitudes

One of the basic goals for this new method to analyze neutrino oscillations is to achieve the highest independence possible . Especially we want to establish a method to analyze experimental data without using external data from different experiments. For instance, the significance of the determination of the CP phase δ_{CP} at T2K increases substantially by including the measurements of the mixing angle θ_{13} from reactor experiments [82]. This method works fine, if both analyses use the same underlying model. But if T2K wants to look for the CP phases in a $3+1$ model, the results from reactor experiments have to be used with a lot of care.

For a model independent analysis it is also necessary to be as independent as possible from assumptions made in previous analyses. If these analyses made intrinsic unknown assumptions the new analysis can be corrupted and lead to incorrect results.

Without imposing any constraints on the elements of the mixing matrix we can achieve a maximum of independence. Depending on the model, the absolute values of the linear independent amplitudes $\mathcal{A}^{kj}_{\alpha\beta}$ are not bound and not correlated at all. Therefore it is impossible to find constraints apart from the analytic constraints in case of direct unitarity violation presented in the previous chapter.

Following this approach on the other hand, would totally ignore all previously made experimental discoveries in the neutrino sector. Fortunately in [83] a global analysis for the elements of the mixing matrix is performed without implying unitarity or a specific new physics model. These bounds on elements of the mixing matrix play a central role in the numerical analysis.

$$|U|^{3\times 3}_{3\sigma} = \begin{pmatrix} 0.76 \to 0.85 & 0.50 \to 0.60 & 0.13 \to 0.16 \\ 0.21 \to 0.54 & 0.42 \to 0.70 & 0.61 \to 0.79 \\ 0.18 \to 0.58 & 0.38 \to 0.72 & 0.40 \to 0.78 \end{pmatrix} \tag{6.1}$$

To find numerical relations among the in general independent amplitudes we perform the analysis based on the different models. For each model we pick random numbers for all involved parameters in the specific model, the SM parameters $\sin^2\theta_{12}$, $\sin^2\theta_{13}$, $\sin^2\theta_{23}$, and δ_{31} are drawn from a flat distribution in the range $[0,1]$ and $[0,2\pi]$, respectively.

If the resulting mixing matrix U satisfy the bounds in Equation (6.1), the parameter combination is considered viable and for each viable parameter combination all accessible amplitudes $\mathcal{A}^{kj}_{\alpha\beta}$ are calculated and extracted. For each model we extract $100,000$ viable combinations.

We compare six different approaches of neutrino physics beyond the three neutrino paradigm:

(i) a $3+1\nu$ model with a light sterile neutrino participating in the neutrino oscillations. The additional angles $\sin^2\theta_{41}$, $\sin^2\theta_{42}$ and $\sin^2\theta_{43}$, as well as the CP phases δ_{41} and δ_{43} are sampled from a flat distribution in the range $[0,1]$ and $[0,2\pi]$, respectively.

(ii) a $3+2\nu$ model with two additional light sterile neutrinos similar to the case (i). The additional angles and phases are drawn accordingly. The main reason is to check whether the analytic prediction made in Section 5.5 that a $3+n\nu$ model behaves like a $3+1\nu$ model holds in the numeric analysis.

(iii) a $3+1\nu$ model with the best fit constraint from the recent analysis in [84] respecting recent results from NEOS and DANSS collaborations. The extracted constraint on an additional element of the mixing matrix reads

$$|U_{e4}| = 0.012 \pm 0.003. \tag{6.2}$$

(iv) the general non-unitarity approach introduced in Section 5.6 without any additional bounds. The parameters are drawn from flat distribution in the range $[0,1]$ for the absolute values and $[0,2\pi]$ for the phases of the off-diagonal elements.

(v) the general non-unitarity approach introduced in Section 5.6 with the additional bound of $\sum_{\alpha\in\{e,\mu,\tau\}}|U_{\alpha j}|^2 \leq 1$ corresponding to no emergence of probability.

(vi) a non-unitarity approach according to (iv) and (v) but with additional constraints determined from rare decays and EW precision observables presented in [85], called minimal unitarity violation (MUV),

$$\begin{aligned} \alpha_{ee} &< 1.3\cdot 10^{-3}, & |\alpha_{\mu e}| &< 6.8\cdot 10^{-4}, \\ \alpha_{\mu\mu} &< 2.0\cdot 10^{-4}, & |\alpha_{\tau e}| &< 2.7\cdot 10^{-3}, \\ \alpha_{\tau\tau} &< 2.8\cdot 10^{-3}, & |\alpha_{\tau\mu}| &< 1.2\cdot 10^{-3}. \end{aligned} \tag{6.3}$$

The absolute values of the parameters are drawn from a flat distribution in the range corresponding to the above constraints. The phases of the off-diagonal elements are drawn analogously to (iv).

For all of the above models, we create a scatter plot of all viable combinations of the corresponding amplitudes. As an example, Figures 6.1 - 6.6 show the resulting scatter plots in the $\left(\mathcal{A}^{21}_{e\mu}-\mathcal{A}^{32}_{e\mu}\right)$- $\left(\mathcal{A}^{31}_{e\mu}+\mathcal{A}^{32}_{e\mu}\right)$ plane, as well as in the $\left(\mathcal{A}^{21}_{\mu\tau}/\mathcal{A}^{32}_{\mu\tau}\right)$- $\left(\mathcal{A}^{31}_{\mu\tau}/\mathcal{A}^{32}_{\mu\tau}\right)$ plane. The exact SM predictions are single points $(0,0)$ and $(1,-1)$ in these plots, due to unitarity.

As can clearly be seen there is a significant difference among some of the scenarios. In particular the analytic result from Section 5.5 can be confirmed, since no difference between the $3+1\nu$ and the $3+2\nu$ model can be observed. Therefore from here on, we neglect the special case of the $3+2\nu$ model. As expected the region of viable amplitudes for the NEOS/DANSS case is smaller compared to the free $3+1\nu$ model, due to the constraint on $|U_{e4}|$.

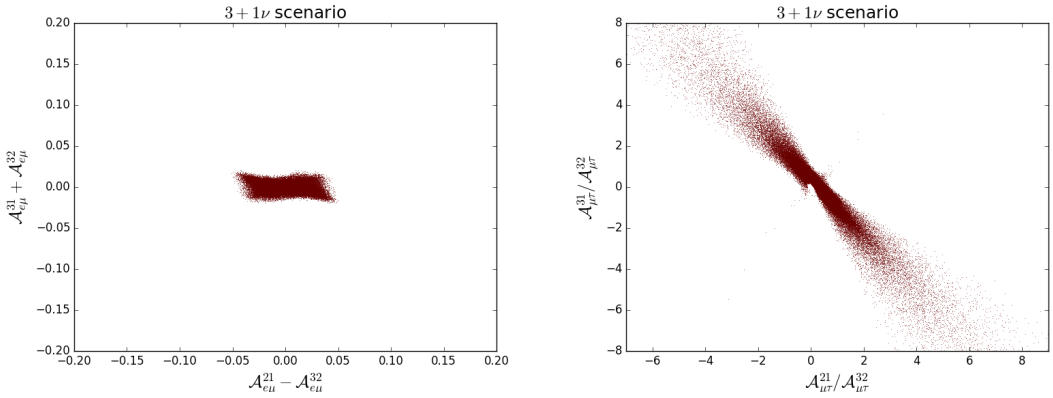

Figure 6.1.: Scatter plots of viable parameter combinations for the $3+1\nu$ model. On the left (right) the differences (ratios) of the three different CP violating amplitudes in the $\nu_e \to \nu_\mu$-channel ($\nu_\mu \to \nu_\tau$- channel) are shown. The SM exact prediction is the single point $(0,0)$ (left) and $(1,-1)$ (right).

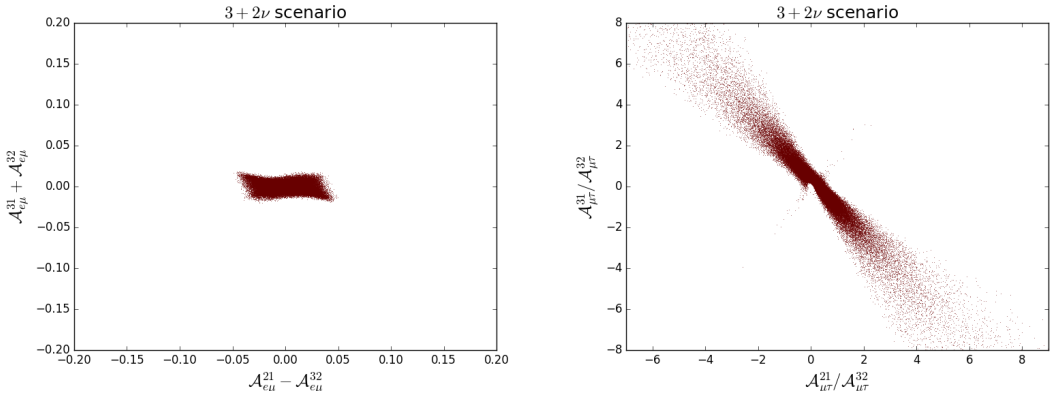

Figure 6.2.: Scatter plots of viable parameter combinations for the $3+2\nu$ model. On the left (right) the differences (ratios) of the three different CP violating amplitudes in the $\nu_e \to \nu_\mu$-channel ($\nu_\mu \to \nu_\tau$- channel) are shown. The SM exact prediction is the single point $(0,0)$ (left) and $(1,-1)$ (right).

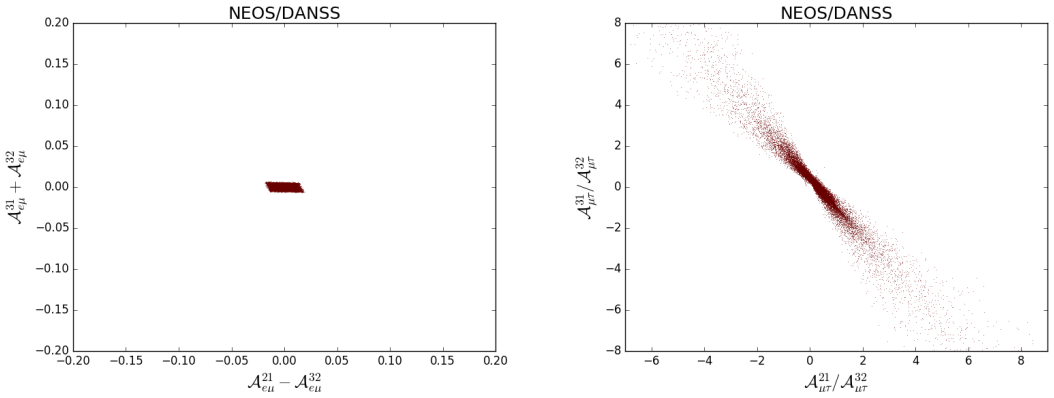

Figure 6.3.: Scatter plots of viable parameter combinations for the NEOS/DANSS scenario. On the left (right) the differences (ratios) of the three different CP violating amplitudes in the $\nu_e \to \nu_\mu$-channel ($\nu_\mu \to \nu_\tau$- channel) are shown. The SM exact prediction is the single point $(0, 0)$ (left) and $(1, -1)$ (right).

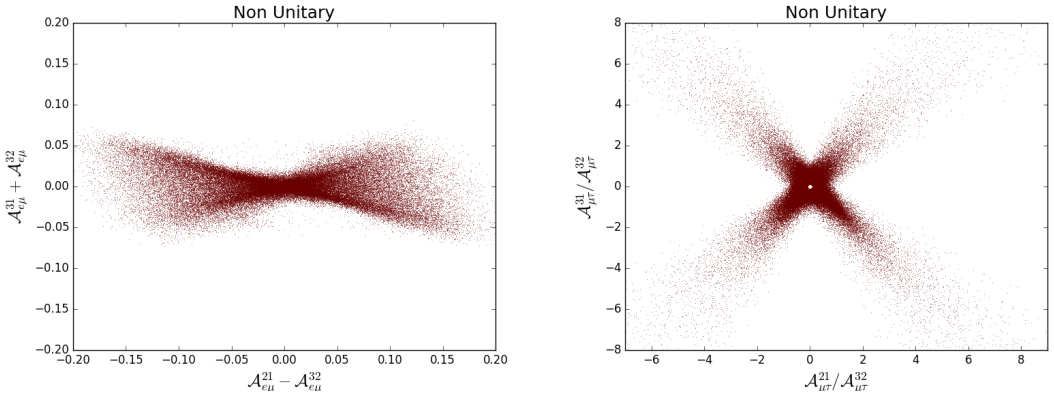

Figure 6.4.: Scatter plots of viable parameter combinations for the general non-unitary approach. On the left (right) the differences (ratios) of the three different CP violating amplitudes in the $\nu_e \to \nu_\mu$-channel ($\nu_\mu \to \nu_\tau$- channel) are shown. The SM exact prediction is the single point $(0, 0)$ (left) and $(1, -1)$ (right).

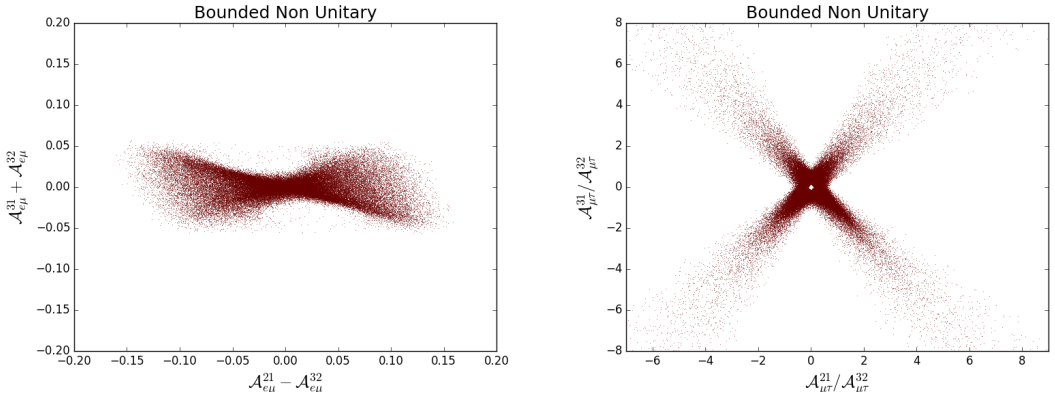

Figure 6.5.: Scatter plots of viable parameter combinations for the bounded non-unitarity approach with $\sum_i |U_{ij}|^2 \leq 1$. On the left (right) the differences (ratios) of the three different CP violating amplitudes in the $\nu_e \to \nu_\mu$-channel ($\nu_\mu \to \nu_\tau$- channel) are shown. The SM exact prediction is the single point $(0, 0)$ in this plane.

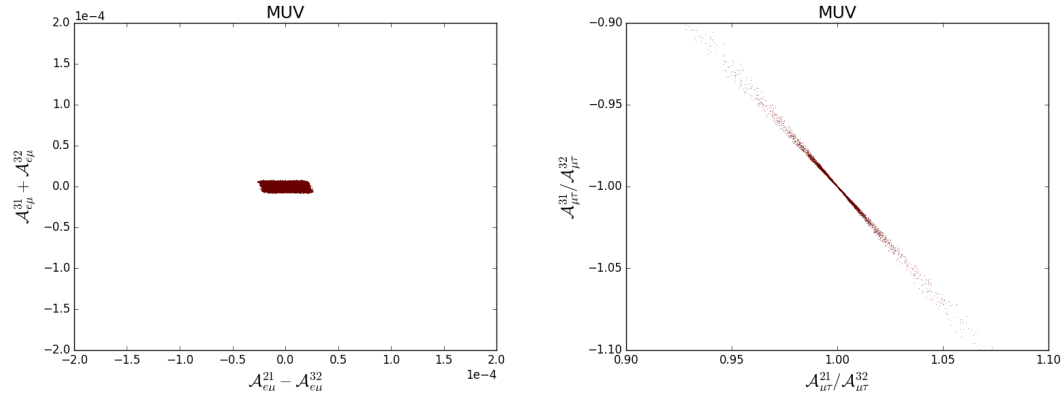

Figure 6.6.: Scatter plots of viable parameter combinations for the MUV approach with bounds from EW precision measurements. Note that the scale is adjusted compared to the other plots in 6.1 to 6.5 due to the strict constraints on the parameters. On the left (right) the differences (ratios) of the three different CP violating amplitudes in the $\nu_e \to \nu_\mu$-channel ($\nu_\mu \to \nu_\tau$- channel) are shown. The SM exact prediction is the single point $(0, 0)$ in this plane.

For a better comparison we calculate the kernel density estimations (KDE) from the above scatter plots and show the 95% CL regions in Figures 6.7 and 6.8. As can be seen clearly for the scenarios with additional light neutrinos and non-unitarity without constraints from EW precision measurements, the corresponding parameter spaces allow for significant deviation

from the SM prediction of uniform CP violation. The MUV scenario albeit provides only small allowed regions due to the strict constraints on the parameters.

The difference between the general non-unitary approach and the approach with bounded matrix elements via $\sum_i |U_{ij}|^2 \leq 1$ is not extreme. Due to the constraints in Equation (6.1), there are not many viable parameter combinations, where the condition $\sum_i |U_{ij}|^2 \leq 1$ is not fulfilled. Nevertheless, current uncorrelated bounds on the matrix elements still do not rule out emergence of probability yet.

The main result from the numerical analysis is the huge differences of the viable parameter spaces for the general non-unitary approach and the scenario of additional light sterile neutrinos. Since the direct unitarity violation due to light sterile neutrinos still imply unitarity of the $(3 + N_{\text{light}}) \times (3 + N_{\text{light}})$ mixing matrix, the viable parameter space is significantly smaller compared to the general non-unitary or indirect unitarity violation approach, where these restrictions are not present. Also there are large areas in the general non-unitary approach, which do not align with the additional light neutrino scenario.

In conclusion, it becomes obvious that there is plenty of room for new physics models, not only to rule out the SM prediction of uniform CP violation, but also to differentiate among direct and indirect unitarity violation for suitable parameter combinations. On the other hand a determination of a unique CP violating amplitude would be in agreement with both, the three neutrino model but also with specific parameter combinations of the new physics models and none of these models could be rejected completely.

In the next section we show, that current experiments are sensitive enough to actually discriminate between different models with this novel approach.

6.2. Analysis with GLoBES

To demonstrate the potential of this newly introduced approach, we perform a pseudo data analysis with the General Long Baseline Experiment Simulator (GLoBES) [86–88]. The Simulation calculates the cross sections based on [89, 90] and we use the pre-built experimental setups for T2K, based on [91, 92] and NOvA, based on [93, 94]. With the GLoBES package we are able to simulate data at T2K or NOvA with the previously introduced approach. We assume rather extreme values as "true" input parameters in the general non-unitary approach as presented in Table 6.1. The resulting mixing matrix reads

$$U_{3\times3}^{\text{true}} = \begin{pmatrix} 0.85 & 0.56 & 0.07 + 0.11\text{i} \\ -0.14 + 0.35\text{i} & 0.63 + 0.23\text{i} & 0.69 + 0.06\text{i} \\ -0.14 - 0.19\text{i} & -0.29 - 0.35\text{i} & 0.41 - 0.28\text{i} \end{pmatrix}, \tag{6.4}$$

fulfilling the bounds set by Equation (6.1).

The probability engine in the GLoBES program is modified to suit the proposed approach at this stage, for example the matter effect is turned off by hand. With these inputs we generate

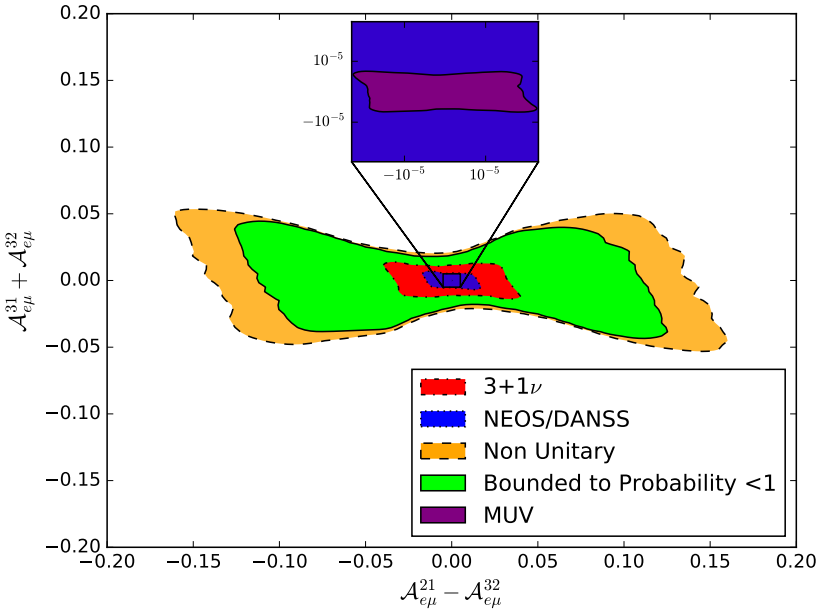

Figure 6.7.: Kernel density estimates for the different scenarios: $3{+}1\nu$ in red, $3{+}1\nu$ with bounds from NEOS/DANSS in blue, general non-unitarity in orange, non-unitarity with the bound $\sum_i |U_{ij}|^2 \leq 1$ in green and minimal unitarity violation in purple. The colored areas correspond to the 95% CL of the KDE. The SM prediction corresponds to the point at $(0, 0)$. Due to the strong constraints for MUV, the viable region is extremely small and deviations from the three neutrino predictions will be hard to measure. Shown are the differences of the three different CP violating amplitudes in the $\nu_e \to \nu_\mu$-channel.

pseudo data, that would resemble the data measured by T2K or NOvA, if the parameters in nature actually have the above shown values.

In the following analyses all neutrino masses are fixed to the current best fit values from Table 3.2 and are not marginalized. Additionally, we restrict ourselves to normal ordering.

This generated pseudo data is then analyzed by the inbuilt SM fit and by a fit to the parameters in the novel model independent approach. The SM fit leads to an extremely large value for the χ^2 at the best fit point of $\chi^2_{\text{best fit}}/\text{dof} = 367$, which would automatically lead to the conclusion that the three neutrino SM model cannot be used to explain the generated pseudo data. This result is expected, since the mixing matrix we used is highly non-unitary.

The analysis, in case of the general approach, is performed by scanning over all values of $\mathcal{A}^{21}_{e\mu}$, $\mathcal{A}^{31}_{e\mu}$ and $\mathcal{A}^{32}_{e\mu}$ in the region $[-1; 1]$. We marginalize all other CP violating and CP conserving amplitudes, that are contributing to the oscillation probabilities of the considered experiments.

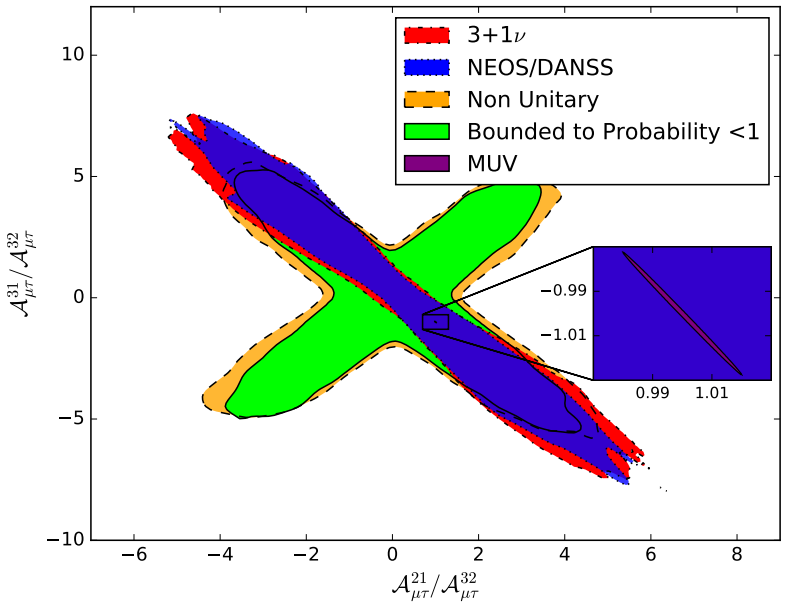

Figure 6.8.: Kernel density estimates for the different scenarios: $3{+}1\nu$ in red, $3{+}1\nu$ with bounds from NEOS/DANSS in blue, general non-unitarity in orange, non-unitarity with the bound $\sum_i |U_{ij}|^2 \leq 1$ in green and minimal unitarity violation in purple. The colored areas correspond to the 95% CL of the KDE. The SM prediction corresponds to the point at $(0, 0)$. Due to the strong constraints for MUV, the viable region is extremely small and deviations from the three neutrino predictions will be hard to measure. Shown are the ratios of the three different CP violating amplitudes in the $\nu_\mu \to \nu_\tau$-channel.

Figures 6.9 and 6.10 show the χ^2 regions corresponding to 68%, 95% and 99% confidence level intervals in the corresponding plane with the KDE plots from the previous chapter in the background.

The analyses of both experiments show the significant feature of a band, restricting the sum $\mathcal{A}^{31}_{e\mu} + \mathcal{A}^{32}_{e\mu}$ but not restricting $\mathcal{A}^{21}_{e\mu} - \mathcal{A}^{32}_{e\mu}$ at all. This effect can be explained by the setup of the experiments. Both, T2K and NOvA aim to measure CP violation in the SM case and therefore have a baselength and energy combination suitable for measuring the oscillation driven by the large mass squared differences Δm^2_{32} and Δm^2_{31}. Therefore it is possible to determine the corresponding amplitudes. The term in the oscillation probability driven by the smaller mass squared difference Δm^2_{21} can be approximated to zero for these setups, and therefore the amplitude $\mathcal{A}^{21}_{e\mu}$ cannot be restricted much by T2K and NOvA.

Parameter	value	Parameter	value
$\sin^2\theta_{12}^{\text{true}}$	0.3054	$\text{abs}(\alpha_{e\mu}^{\text{true}})$	-0.4481
$\sin^2\theta_{23}^{\text{true}}$	0.5876	$\text{abs}(\alpha_{e\tau}^{\text{true}})$	-0.5017
$\sin^2\theta_{13}^{\text{true}}$	0.0166	$\text{abs}(\alpha_{\mu\tau}^{\text{true}})$	-0.3435
$\delta_{13}^{\text{true}}$	5.2809	$\arg(\alpha_{e\mu}^{\text{true}})$	4.0291
$\alpha_{ee}^{\text{true}}$	-0.0238	$\arg(\alpha_{e\tau}^{\text{true}})$	0.9736
$\alpha_{\mu\mu}^{\text{true}}$	0.0644	$\arg(\alpha_{\mu\tau}^{\text{true}})$	2.1732
$\alpha_{\tau\tau}^{\text{true}}$	0.6215		

Table 6.1.: Input parameters for the GLoBES analysis in the general non-unitary approach.

While both analyses share similar features, there is a huge difference between the T2K and NOvA analysis. While T2K does not restrict the viable parameter space, since they all lie in the 68% confidence level region (see Figure 6.9, NOvA is able not only to exclude the SM but also to distinguish between direct and indirect unitarity violation. At the best fit point, the analyses leads to $\chi^2_{\text{BF}} = 0.105$ which indicates overfitting due to the large amount of free parameters in the proposed approach. For the actual true input values used to generate the data, the difference to χ^2_{BF} is determined to $\Delta\chi^2_{\text{true}} = 1.5$. The SM can be excluded due to the large value of $\Delta\chi^2_{\text{SM}} = 31.5$. The significantly better sensitivity of NOvA compared to T2K can be explained by the general setups of these experiments. Both experiments are off-Axis accelerator experiments, which results in a narrow energy spectrum for both experiments. While both experiments are designed to measure the oscillation driven by Δm^2_{31}, the location of the peak energy differs. At T2K, the peak energy is designed to be near the first oscillation maximum [95], where

$$\frac{\Delta m^2_{31} L^{\text{T2K}}}{4E^{\text{T2K}}_{\text{peak}}} \approx \frac{\pi}{2}. \tag{6.5}$$

Comparing this to Equation (4.7), leads to small value for $\sin\left(\frac{\Delta m^2_{31} L^{\text{T2K}}}{2E^{\text{T2K}}_{\text{peak}}}\right) \approx \sin(\pi) = 0$ governing the impact of the CP violating amplitudes. On the other hand, the peak energy and baselength at NOvA is designed as [96]

$$\frac{\Delta m^2_{31} L^{\text{NOvA}}}{4E^{\text{NOvA}}_{\text{peak}}} \approx 1.1, \tag{6.6}$$

leading to a large value of $\sin\left(\frac{\Delta m^2_{31} L^{\text{NOvA}}}{2E^{\text{NOvA}}_{\text{peak}}}\right) \approx \sin(2.2) = 0.8$. Therefore the contribution of the CP violating amplitudes to the probability is significantly higher at NOvA, resulting in a higher sensitivity to $\mathcal{A}^{31}_{e\mu} + \mathcal{A}^{32}_{e\mu}$ for NOvA compared to T2K.

For a further restrictions of these amplitudes, other experiments are necessary. We concentrate on accelerator experiments, since they are the only experiments providing both neutrino

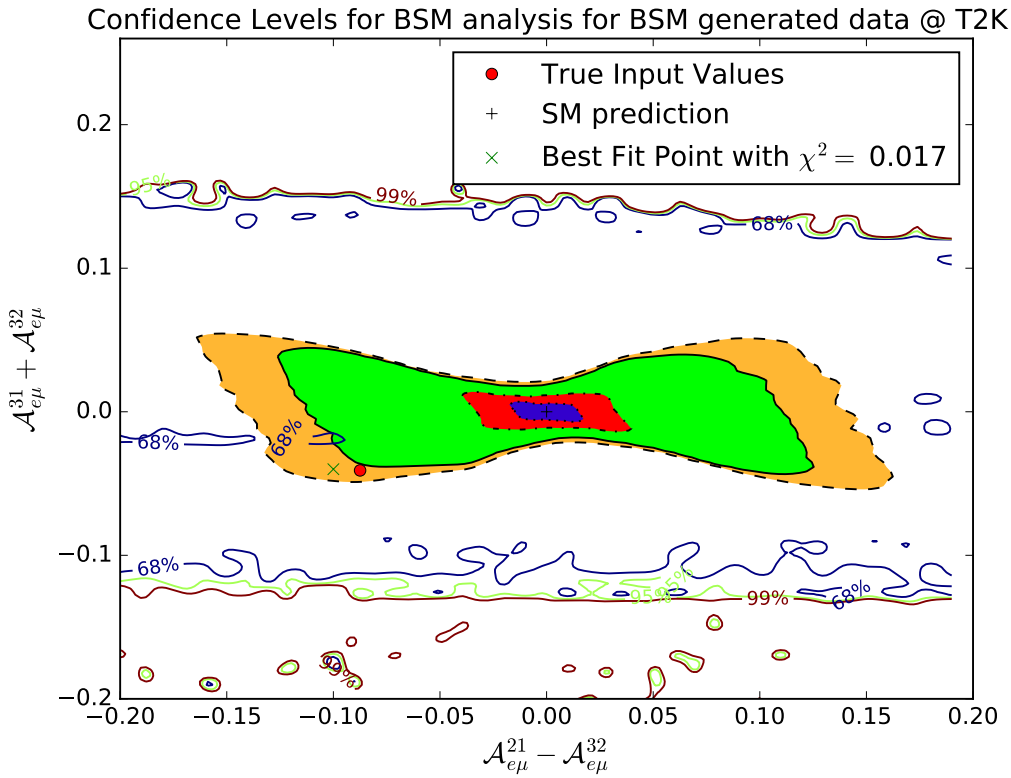

Figure 6.9.: Confidence level intervals for the new proposed method to analyze T2K data generated with the input values indicated by the red dot. The GLoBES-package is used to generate the pseudo data and calculate the χ^2-values.

and antineutrinos with the source under human control. To be sensitive to $\mathcal{A}^{21}_{e\mu}$, the oscillation driven by Δm^2_{21} has to contribute significantly to the oscillation probability. Therefore, either the energy or the baseline has to be adjusted. The energy is difficult to adjust, due to the production process from Pion decays. Therefore we artificially create an experiment in the GLoBES framework with the same specifics as T2K but enlarged baseline by the factor of 17, corresponding to a maximization of the oscillation driven by Δm^2_{21}. The running time is also adjusted accordingly by a factor of 17^2, which is of course unrealistic, but necessary to get the desired number of events in the detector, since the flux in the detector scales with $\frac{1}{L^2}$. We are aware of the problems due to running time and logistics of this setup, but want to emphasize this as a proof of concept. The resulting confidence levels for the analysis can be seen in Figure 6.11. The SM prediction can be excluded, and, comparable to the NOvA analysis, also a large part of the viable parameter space for direct unitarity violation. Combining both anal-

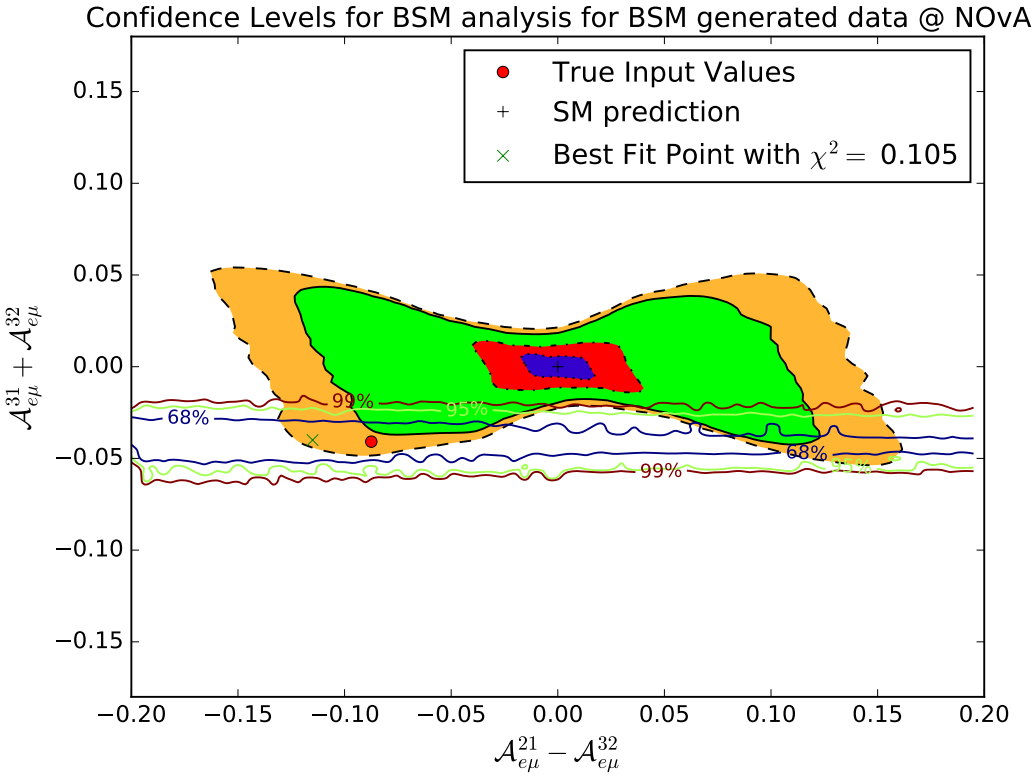

Figure 6.10.: Confidence level intervals for the new proposed method to analyze NOvA data generated with the input values indicated by the red dot. The GLoBES-package is used to generate the pseudo data and calculate the χ^2-values.

ysis, NOvA and T2K with longer baseline, can therefore restrict the CP violating amplitudes consequently.

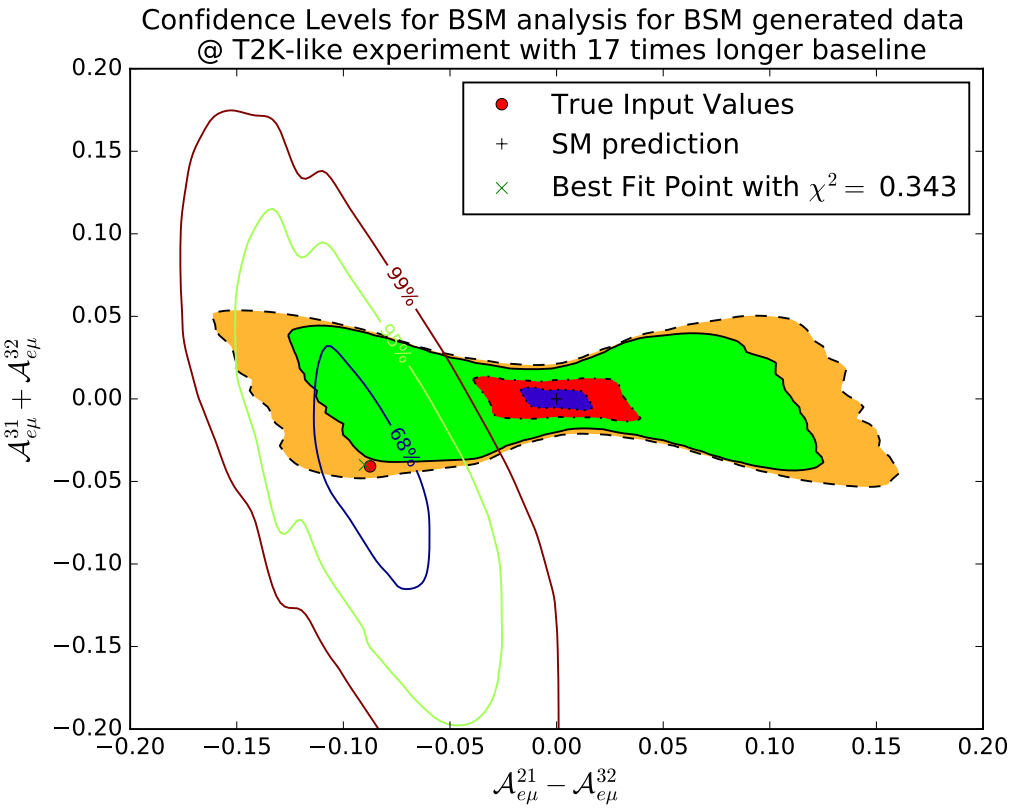

Figure 6.11.: Confidence level intervals for the new proposed method to analyze T2K-like data generated with the input values indicated by the red dot. In contrast to Figure 6.9, the baseline is expanded by a factor of 17 and the running time by a factor of 17^2 to be sensitive to $A^{21}_{e\mu}$. For details see the text. The GLoBES-package is used to generate the pseudo data and calculate the χ^2-values.

7. Matter Effects

7.1. Introduction

The method introduced in the previous chapter investigates CP violation of neutrino oscillations in vacuum. Current oscillation experiments, which are sensitive enough to measure a (possible) CP violation usually use long baselines. Therefore the neutrinos travel through Earth's matter and interact weakly with the constituents, also affecting the effective mixing matrix and therefore the CP violating amplitudes. The analytic relations presented in Section 5 still hold for a specific experiment and energy. The constraints presented in Section 6 on the other hand are based on vacuum values for all mixing parameters and therefore these constraints do not apply anymore, once matter effects are taken into account.

In this Section we examine how matter effects impact the previously introduced novel method.

7.2. Oscilllation Probabilities in Matter or Other Additional Potentials

The effect of matter on neutrino oscillations with unitarity violation has been studied previously in [97]. We follow the general approach and apply the formulation to our method.

In any model of BSM physics, only light neutrinos, active and sterile, participate in the actual oscillation. Therefore the resulting Hamiltonian in flavor space reads

$$H_{Flav}^{n\times n} = \frac{1}{2E} U_{n\times n} M_{n\times n} U_{n\times n}^{\dagger} + \left(U_{n\times n} U_{n\times n}^{\dagger}\right) V \left(U_{n\times n} U_{n\times n}^{\dagger}\right), \tag{7.1}$$

where n is the number of light neutrinos. Again, the impact of, for example, heavy neutrino states is indirectly taken care of in the non-unitarity of the $n \times n$ mixing matrices.

In case of only direct unitarity violation the mixing matrix $U_{n\times n}$ is unitary and $U_{n\times n} U_{n\times n}^{\dagger} = \mathbb{1}_{n\times n}$ holds.

The Potential V for matter effects, e.g. in the earths mantle, can be described as

$$V = \begin{pmatrix} V_{CC} + V_{NC} & 0 & 0 & \cdots \\ 0 & V_{NC} & 0 & \cdots \\ 0 & 0 & V_{NC} & \cdots \\ \vdots & \vdots & \vdots & 0 \end{pmatrix} \tag{7.2}$$

$$V_{CC} = \sqrt{2} G_F N_e, \qquad V_{NC} = -\frac{\sqrt{2}}{2} G_F N_n \tag{7.3}$$

with the Fermi constant G_F and the electron- (neutron-) density $N_{e(n)}$. The charged current interaction with the electron is described by V_{CC}, while the neutral current interaction with protons neutrons and electrons is described by V_{NC}. In SM approaches with three light active neutrinos the neutral current potential is often neglected because it is proportional to the unit matrix and is therefore not measurable. By introducing direct or indirect unitarity violation the neutral current cannot be neglected anymore and has to be taken into account

For antineutrinos the effective potential flips its sign, resulting in an intrinsic CP violation due to the matter effect. The potential V can also be generalized for BSM effects like non standard interactions (NSI) during propagation (see [98] for a review). Nevertheless we suppose the potential is given in flavor space.

Following the standard approach with the Hamiltonian in the flavor eigenbasis leads to

$$\begin{aligned} \mathrm{i}\frac{\mathrm{d}}{\mathrm{d}t} |\nu_\alpha\rangle &= \frac{1}{2E} (U_{n\times n} M_{n\times n} U_{n\times n}^\dagger) |\nu_\alpha\rangle + \left(U_{n\times n} U_{n\times n}^\dagger\right) V \left(U_{n\times n} U_{n\times n}^\dagger\right) |\nu_\alpha\rangle \\ &= \frac{1}{2E} \sum_{i,j,\beta}^{n} (U_n)_{\alpha i} (M_n)_{ij} (U_n^\dagger)_{j\beta} |\nu_\beta\rangle + \sum_{\beta\rho\sigma} (U_n U_n^\dagger)_{\alpha\rho} (V)_{\rho\sigma} (U_n U_n^\dagger)_{\sigma\beta} |\nu_\beta\rangle \\ &= \frac{1}{2E} \sum_{\beta} (K_n)_{\alpha\beta} |\nu_\beta\rangle . \end{aligned} \tag{7.4}$$

To calculate the transition probability it is necessary to diagonalize the non-diagonal $n \times n$ matrix K_n. If at least one heavy neutrino is involved, K_n is not even hermitian . Especially, the transformation to the vacuum mass eigenbasis does not diagonalize this Hamiltonian anymore, and therefore the propagation eigenstates do not match the vacuum mass eigenstates.

To find the eigenspace in matter we, have to diagonalize the matrix K. We use an invertible matrix S, which rotates K into the new propagation eigenspace. These propagation eigenstates are denoted by a capital Latin letter as $|\nu_J\rangle$. The new effective masses are given as the eigenvalues of K, or the diagonal entries D_J of $D = S^{-1} K S$, which leads to the Schrödinger equation in propagation eigenspace

$$\mathrm{i}\frac{d}{dt} |\nu_J\rangle = \frac{1}{2E} D_J |\nu_J\rangle \tag{7.5}$$

So far neither U nor S are assumed to be unitary. If U is unitary and the effective potential is hermitian, the new mixing matrix S will be unitary as well. Since we found an eigenspace of the Hamiltonian, we can follow the usual way to calculate the oscillation probability:

$$\begin{aligned} P_{\nu_\alpha \to \nu_\beta} = |\langle \nu_\beta | \nu_\alpha(L) \rangle|^2 &= \left| \sum_{I,J} \langle \nu_J | \, S^*_{\beta J} S_{\alpha I} \, | \nu_I(t) \rangle \right|^2 \\ &= \sum_{J,K} S^*_{\beta J} S_{\alpha J} S_{\beta K} S^*_{\alpha K} \cdot \mathrm{e}^{\left(+\mathrm{i}\frac{\Delta D_{KJ}}{2E} L\right)}, \end{aligned} \tag{7.6}$$

with $\Delta D_{KJ} = D_K - D_J$. This probability can be rewritten to a more common form for neutrino oscillations

$$P_{\nu_\alpha \to \nu_\beta} = P_0 - 4 \sum_{K>J} \mathcal{R}^{KJ}_{\alpha\beta} \sin^2\left(\frac{\Delta D_{KJ}}{4E} L\right) + 2 \sum_{K>J} \mathcal{A}^{KJ}_{\alpha\beta} \sin\left(\frac{\Delta D_{KJ}}{2E} L\right) \tag{7.7}$$

$$P_0 = \sum_{K,J} \left(S^*_{\alpha K} S_{\beta K} S_{\alpha J} S^*_{\beta J} \right) \tag{7.8}$$

$$\mathcal{R}^{KJ}_{\alpha\beta} = \mathrm{Re}\left[S^*_{\alpha K} S_{\beta K} S_{\alpha J} S^*_{\beta J} \right] \tag{7.9}$$

$$\mathcal{A}^{KJ}_{\alpha\beta} = \mathrm{Im}\left[S^*_{\alpha K} S_{\beta K} S_{\alpha J} S^*_{\beta J} \right], \tag{7.10}$$

where P_0 denotes the zero-distance effect which only arises in case of indirect non-unitarity. The limit of vanishing effective potential can be obtained by setting the matrix V to zero. In that case the mass basis corresponds to the propagation basis and the transformation matrix S is equal to the vacuum mixing matrix U. Having that in mind, the corresponding amplitudes $\mathcal{R}$ and $\mathcal{A}$ can be reduced to the vacuum case and the oscillation probability reduces to the well known vacuum case, as expected.

For large potentials, i.e. high densities or high energies in matter, the first term in Equation (7.1) is negligible and the transformation matrix S reads

$$S_{\text{High Energy}} = \left(U U^\dagger \right). \tag{7.11}$$

In case of only direct unitarity violation S becomes the unit matrix and the electron neutrino is completely decoupled.

The derivations above hold for neutrinos and antineutrinos separately. Nevertheless, due to the possibility of non-unitarity of U, the diagonalization performed in Equation (7.5) for neutrinos does not match the diagonalization for antineutrinos.

$$H_{\text{Mass}} \neq \overline{H}_{\text{Mass}} \tag{7.12}$$

$$H_{\text{Mass}} = \frac{1}{2E}\left[M + (U)^{-1} V \left(U^{\dagger}\right)^{-1}\right] \tag{7.13}$$

$$\begin{aligned}\overline{H}_{\text{Mass}} &= \frac{1}{2E}\left[M + (U^*)^{-1} \overline{V} \left((U^*)^{\dagger}\right)^{-1}\right] \\ &= \frac{1}{2E}\underbrace{\left[M + (U^*)^{-1} \overline{V} \left(U^{T}\right)^{-1}\right]}_{\overline{K}}\end{aligned} \tag{7.14}$$

Only if $V = \overline{V}$ and U is real, both Hamiltonians match and the same diagonalization S can be used for neutrino and antineutrino and the same eigenvalues D arise. In this case, it follows that neutrino and antineutrino behave exactly the same and no CP violation is observable.

For complex values in U, neither S nor D match for the neutrino and antineutrino cases. Moreover, the potential V does not have to be the same for neutrino and antineutrino, for example in the case of matter effects in earth or sun. The diagonalization of $\overline{H}_{\text{Mass}}$ is performed analogously to the neutrino case with the invertible matrix $\overline{S}$ and the diagonal matrix $\overline{D}$ satisfying $\overline{D} = \overline{S}^{-1}\overline{K}\overline{S}$. Therefore, the rather simple calculation for CP violating amplitudes in vacuum becomes significantly more complex:

$$\begin{aligned}P_{\nu_\alpha\to\nu_\beta} - P_{\overline{\nu}_\alpha\to\overline{\nu}_\beta} =& P_0 - \overline{P_0} \\ &- 4\sum_{K>J}\left(\mathcal{R}^{KJ}_{\alpha\beta}\sin^2\left(\frac{\delta D_{KJ}}{4E}L\right) - \overline{\mathcal{R}^{KJ}_{\alpha\beta}}\sin^2\left(\overline{\frac{\delta D_{KJ}}{4E}}L\right)\right) \\ &+ 2\sum_{K>J}\left(\mathcal{A}^{KJ}_{\alpha\beta}\sin\left(\frac{\delta D_{KJ}}{2E}L\right) - \overline{\mathcal{A}^{KJ}_{\alpha\beta}}\sin\left(\overline{\frac{\delta D_{KJ}}{2E}}L\right)\right),\end{aligned} \tag{7.15}$$

with the definition for the antineutrino parts as

$$\overline{P_0} = \sum_{K,J}\left(\overline{S}^*_{\alpha K}\overline{S}_{\beta K}\overline{S}_{\alpha J}\overline{S}^*_{\beta J}\right) \tag{7.16}$$

$$\overline{\mathcal{R}^{KJ}_{\alpha\beta}} = \text{Re}\left[\overline{S}^*_{\alpha K}\overline{S}_{\beta K}\overline{S}_{\alpha J}\overline{S}^*_{\beta J}\right] \tag{7.17}$$

$$\overline{\mathcal{A}^{KJ}_{\alpha\beta}} = \text{Im}\left[\overline{S}^*_{\alpha K}\overline{S}_{\beta K}\overline{S}_{\alpha J}\overline{S}^*_{\beta J}\right] \tag{7.18}$$

$$\overline{\delta D_{KJ}} = \overline{D}_{KK} - \overline{D}_{JJ}\,, \tag{7.19}$$

similar to the neutrino case. The energy spectrum of the CP violation $P_{\nu_\alpha\to\nu_\beta} - P_{\overline{\nu}_\alpha\to\overline{\nu}_\beta}$ differs significantly from the vacuum case. For non-unitary U, we expect six (instead of three) terms proportional to $\sin\left(\frac{\delta D_{KJ}}{2E}L\right)$ and six (instead of zero) terms proportional to $\sin^2\left(\frac{\delta D_{KJ}}{4E}L\right)$.

Investigating the differences of probabilities from neutrino and antineutrino in vacuum had the advantage of cancelling real parts of U and the $\sin^2$ terms. Since these terms do not cancel anymore due to different D and different $\mathcal{R}$, an exclusive focus at CP violating amplitudes is not adequate.

To conclude we want to highlight three main differences between vacuum oscillations and oscillations with an effective potential induced e.g. by matter effects.

- the amplitudes and mass squared differences are in general energy dependent. Due to the different energy dependence of the mass term and the potential in the Hamiltonian, the diagonalization differs for different energies. Therefore there are no uniform amplitudes and mass squared differences for the whole energy spectrum of an experiment.
- the diagonalization for the neutrino and antineutrino Hamiltonian is different and therefore an intrinsic CP violation. A measured difference in the probabilities of neutrinos and antineutrinos is not necessarily a proof of CP violation on the fundamental level.
- the amplitudes are not independent of the vacuum values of the mass squared differences or the mass ordering anymore.

7.3. Commutator of Mass Matrices Applied to Non-Unitarity

The aforementioned energy dependence of the amplitudes and the effective mass squared differences in case of matter effects has already been studied analytically in [71, 99–102]. In contrast to this work those analyses focus on the three neutrino case and unitary mixing. A relation between the amplitudes, effective mass squared differences depending on the energy and effective potential has been found. This kind of relation would make it possible to use the above introduced general approach also in the context of matter effects to deduce the vacuum values for the amplitudes and mass squared differences from the measured ones and compare them among different experiments. We follow the approach in the above publications without assuming unitarity of the 3×3 mixing matrix $U_{3\times3}$.

The already introduced Jarlskog invariant J was originally determined in the quark sector by the commutator of the up type and the down type mass matrices since the commutator quantifies the alignment of both bases. Transferred to the lepton sector, we define the Jarlskog invariant with the charged lepton mass matrix M_ℓ with eigenvalues $\{m_e, m_\mu, m_\tau\}$ and the neutrino mass matrix M_ν with eigenvalues $\{m_1, m_2, m_3\}$ via the determinant of the commutator

$$\det\left[M_\ell M_\ell^\dagger, M_\nu M_\nu^\dagger\right] = 2\mathrm{i}Jv_{M_\ell}v_{M_\nu}, \tag{7.20}$$

with $v_{M_\ell} = \left(m_e^2 - m_\mu^2\right)\left(m_\mu^2 - m_\tau^2\right)\left(m_\tau^2 - m_e^2\right)$ and $v_{M_\nu} = \left(m_1^2 - m_2^2\right)\left(m_2^2 - m_3^2\right)\left(m_3^2 - m_1^2\right)$ and the Jarlskog invariant

$$J = \mathrm{Im}\left(\mathbf{U}_{\alpha k}^* \mathbf{U}_{\beta k} \mathbf{U}_{\alpha j} \mathbf{U}_{\beta j}^*\right). \tag{7.21}$$

This definition holds as long as unitarity of the 3×3 mixing matrix is imposed. On the one hand, the commutator is not defined, if we want to add an additional light neutrino due to the different dimensions of the mass matrices. On the other hand, by using a generalized non-unitary 3×3 leptonic mixing matrix, the determinant does not factorize anymore

$$\begin{aligned}\det\left[M_\ell M_\ell^\dagger, M_\nu M_\nu^\dagger\right] =& v_{M_l} \cdot \left[\sum_{i,j,k} m_i^2 m_j^2 m_k^2 \cdot \left(U_{ei}U_{\mu i}^* U_{\mu j} U_{\tau j}^* U_{\tau k} U_{ek}^* - U_{ei} U_{\tau i}^* U_{\mu j} U_{ej}^* U_{\tau k} U_{\mu k}^*\right)\right] \\ =& v_{M_l} \cdot \left[\sum_{i\neq j} 2\mathrm{i} \cdot m_i^4 m_j^2 \left(|U_{\mu i}|^2 \mathcal{A}_{e\tau}^{ij} - |U_{ei}|^2 \mathcal{A}_{\mu\tau}^{ij} - |U_{\tau i}|^2 \mathcal{A}_{e\mu}^{ij}\right)\right. \\ & \left. + m_1^2 m_2^2 m_3^2 \sum_{i\neq j\neq k\neq i} \left(U_{ei}U_{\mu i}^* U_{\mu j} U_{\tau j}^* U_{\tau k} U_{ek}^* - U_{ei} U_{\tau i}^* U_{\mu j} U_{ej}^* U_{\tau k} U_{\mu k}^*\right)\right].\end{aligned} \tag{7.22}$$

As expected, the commutator becomes much more complicated, due to non-unitarity, but nevertheless we follow the arguments to find out whether relations between the vacuum and matter can be deduced.

Without loss of generality we start in the flavor basis, which means we set the mass matrix of the charged leptons to be diagonal i.e. $M_\ell = \mathrm{diag}\{m_e, m_\mu, m_\tau\}$. In this basis, the mass matrix for the neutrinos can be deduced from the free Hamiltonian

$$H_{\mathrm{vac}}^{3\times 3} = \frac{1}{2E} U\, \mathrm{diag}\{m_1^2, m_2^2, m_3^2\} U^\dagger, \tag{7.23}$$

while the effective Hamiltonian in matter reads

$$\begin{aligned} H_{\mathrm{eff}}^{3\times 3} &= \frac{1}{2E} U\, \mathrm{diag}\{m_1^2, m_2^2, m_3^2\} U^\dagger + \left(UU^\dagger\right) V \left(UU^\dagger\right) \\ &= \frac{1}{2E} M_\nu^{\mathrm{eff}} \left(M_\nu^{\mathrm{eff}}\right)^\dagger. \end{aligned} \tag{7.24}$$

with the potential V and the mixing matrix U being the generally non-unitary 3×3 mixing matrix parametrized by

$$U = \underbrace{(\mathbb{1} - \alpha)}_{A} \mathbf{U}_{\mathrm{unitary}} = \begin{pmatrix} 1-\alpha_{11} & 0 & 0 \\ \alpha_{21} & 1-\alpha_{22} & 0 \\ \alpha_{31} & \alpha_{32} & 1-\alpha_{33} \end{pmatrix} \mathbf{U}_{\mathrm{unitary}}. \tag{7.25}$$

With this parametrization of U it is possible to generate any 3×3 matrix by a unitary matrix $\mathbf{U}$ and the non-unitary term $A = (\mathbb{1} - \alpha)$, similar to the approach of general unitarity violation in Section 6.

The effective potential V itself is, in case of matter effects, diagonal in flavor space:

$$V = \begin{pmatrix} V_{cc} + V_{nc} & 0 & 0 \\ 0 & V_{nc} & 0 \\ 0 & 0 & V_{nc} \end{pmatrix} \tag{7.26}$$

$$V_{cc} = \sqrt{2} G_F N_e, \qquad V_{nc} = -\frac{\sqrt{2}}{2} G_F N_n \tag{7.27}$$

This leads to a general diagonal term in the effective Hamiltonian in case U is unitary, and a non-diagonal term in case U is not.

The commutator now reads

$$\begin{aligned} \left[M_\ell M_\ell^\dagger, M_\nu^{\text{eff}} \left(M_\nu^{\text{eff}} \right)^\dagger \right] &= \left[M_\ell M_\ell^\dagger, U \,\text{diag}\{m_1^2, m_2^2, m_3^2\} U^\dagger + 2E \cdot \left(U U^\dagger \right) V \left(U U^\dagger \right) \right] \\ &= \left[M_\ell M_\ell^\dagger, M_\nu^{\text{vac}} \left(M_\nu^{\text{vac}} \right)^\dagger \right] + 2E \cdot \left[M_\ell M_\ell^\dagger, \left(A A^\dagger \right) V \left(A A^\dagger \right) \right] \end{aligned} \tag{7.28}$$

For $A A^\dagger = 1$ and a diagonal potential V, one can relate the effective masses and mixing parameters to the vacuum ones via Equation (7.20), reproducing the Naumov relation [103]

$$J \delta m_{21}^2 \delta m_{31}^2 \delta m_{32}^2 = \tilde{J} \delta \tilde{m}_{21}^2 \delta \tilde{m}_{31}^2 \delta \tilde{m}_{32}^2, \tag{7.29}$$

which is the basic result of the above mentioned papers.

For general non-unitarity the term $\left(A A^\dagger \right) V \left(A A^\dagger \right)$ is not diagonal in flavor space and generates additional terms in the relation. The resulting system of nonlinear equation is not solvable in all generality. A further analytical study of the parameters in matter has not been performed, although for specific parameter setups it might be possible to calculate the dependencies of the masses and mixing parameters.

7.4. Numerical Analysis of T-Violation in the presence of Matter Effects

One of the main features of the new approach to analyze CP violation in vacuum neutrino oscillation introduced in Section 4 was that all CP conserving amplitudes cancel. This cancellation reduces the number of free parameters significantly and clear predictions can be made. As

shown in the previous section, this is not possible anymore, once matter effects are involved. A possible way out is focussing on T violating instead of CP violating processes, which read

$$\begin{aligned} P_{\nu_\alpha\to\nu_\beta} - P_{\nu_\beta\to\nu_\alpha} =& P^0_{\alpha\beta} - P^0_{\beta\alpha} \\ &- 4\sum_{K>J}^{3}\left(\mathcal{R}^{KJ}_{\alpha\beta}\sin^2\left(\frac{\delta D_{KJ}}{4E}L\right) - \mathcal{R}^{KJ}_{\beta\alpha}\sin^2\left(\frac{\delta D_{KJ}}{4E}L\right)\right) \\ &+ 2\sum_{K>J}^{3}\left(\mathcal{A}^{KJ}_{\alpha\beta}\sin\left(\frac{\delta D_{KJ}}{2E}L\right) - \mathcal{A}^{KJ}_{\beta\alpha}\sin\left(\frac{\delta D_{KJ}}{2E}L\right)\right) \\ =& +4\sum_{K>J}^{3}\left(\mathcal{A}^{KJ}_{\alpha\beta}\sin\left(\frac{\delta D_{KJ}}{2E}L\right)\right) \end{aligned} \tag{7.30}$$

Note that the difference between T violation and CP violation in the presence of matter effects is not a violation of the CPT theorem. Since the considered matter in earth or sun is made almost purely out of matter and not antimatter, the background itself already violates CP and this extrinsic CP violation generates the difference between CP and T violation. The CPT conservation becomes obvious comparing the probabilities $P_{\nu_\alpha\to\nu_\beta}$ in matter and $P_{\overline{\nu}_\beta\to\overline{\nu}_\alpha}$ in antimatter, which is experimentally impossible. In the vacuum case, CPT is conserved and therefore the T violation and the CP violation is equal, which can also be seen in Equation (7.30). While the CP violating oscillations become significantly more complex if matter effects are taken into account (see Equation (7.15)), the T violating processes preserve the cancellation of the real amplitudes. Therefore a focus on the amplitudes $\mathcal{A}^{KJ}_{\alpha\beta}$ is possible, but due to the energy dependence of $\mathcal{A}^{KJ}_{\alpha\beta}$ and δD_{KJ}, a more careful analysis is needed.

While being theoretically simpler, the T violation (7.30) is experimentally challenging. An analysis would require sources, that produce neutrinos with different flavors with comparable energies at sufficient rates which is hard to realize due to the huge differences in the masses of the charged leptons. Additionally, a complete model independent analysis requires a fit of the amplitudes for each energy bin separately. This fit is only possible if the probabilities are measured at sufficiently many different base lengths, corresponding to multiple detectors with a high spatial resolution at different distances from the source.

To analyze the imaginary amplitudes $\mathcal{A}^{kj}_{\alpha\beta}$ in greater detail, one has to examine the effect of the matter potential further. Due to the different potentials for ν_e and $\nu_{\mu/\tau}$, the possibility of resonant mixing arises. For neutrinos, the electron neutrino becomes effectively heavier for larger energies, while the muon and tau neutrino become lighter, due to the different prefactor in the potential. With this behaviour also the mixing with the mass eigenstates changes. For large energies, the electron neutrino decouples completely from the other two and the heaviest propagation eigenstates corresponds to the electron neutrino. Depending on the mass ordering this results in different possibilities of resonant mixing. At the resonance, the mixing is maximal, i.e. the off-diagonal elements of the mixing matrix become large, which causes large values for the amplitude $\mathcal{A}^{kj}_{\alpha\beta}$ with ν_k and ν_j as the corresponding resonant propagation

eigenstates. Figures 7.1 and 7.2 show the energy dependence of the mass eigenvalues and the corresponding amplitudes $\mathcal{A}^{kj}_{e\mu}$ between 10 MeV and 100 GeV, for normal and inverted ordering and for neutrinos and antineutrinos. To demonstrate the effect, we used vacuum mixing values with large unitarity violation, but still satisfying the bounds in Equations (6.1). The electron density is set to the value of the earth mantle $N_e^{\text{mantle}} \sim 2.2\text{cm}^{-3} N_A$ with N_A the Avorgadro number. In all cases the lightest neutrino mass is set to zero, and the dashed lines in the plots correspond to negative values for the effective masses m_j^2. For different setups, different possibilities of resonant mixing occur, which also results in different behavior of the amplitudes.

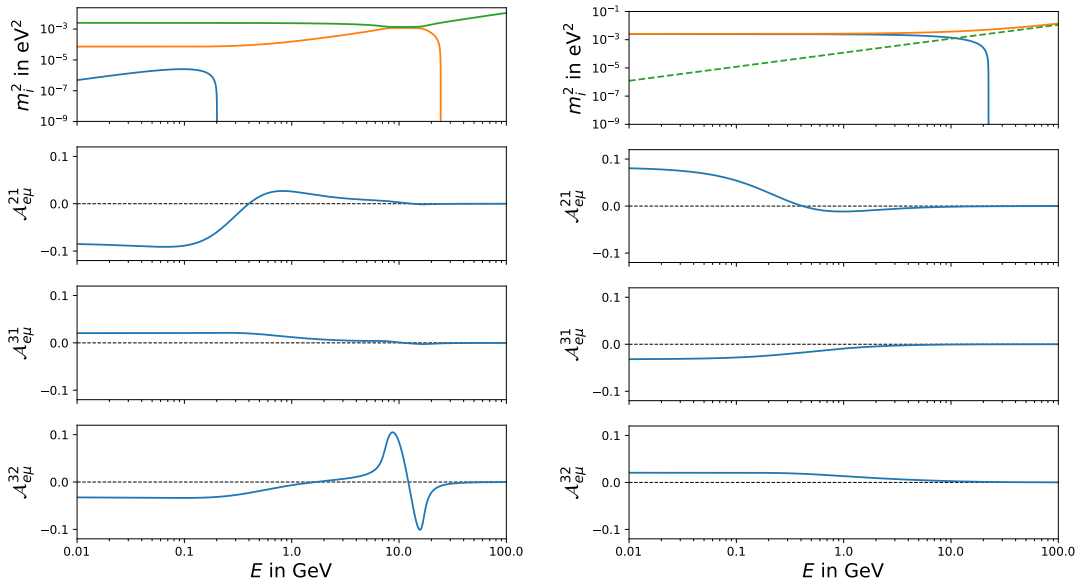

Figure 7.1.: Energy dependence of imaginary amplitudes of one specific setting for neutrinos with normal (left) and inverted ordering (right). The squared masses are shown as m_1^2 in blue, m_2^2 in orange and m_3^2 in green. The dashed line for m_3^2 for inverted ordering corresponds to negative values of the squared effective mass.

Figures 7.3 and 7.4 show the dependence of energy of the amplitudes over an energy range from 10 MeV to 100 GeV for different vacuum parameter combinations in the $\left(\mathcal{A}^{21}_{e\mu} - \mathcal{A}^{32}_{e\mu}\right)$–$\left(\mathcal{A}^{31}_{e\mu} + \mathcal{A}^{32}_{e\mu}\right)$ plane. Again, the vacuum values satisfy the constraints given in Equation (6.1). For large energies all parameter combinations show the same behaviour. As expected for large energies, no oscillation will be measurable since the flavor states correspond to the propagation eigenstates. This translates to all amplitudes approaching zero and the point $(0, 0)$ in the considered plane.

The different possibilities of resonant mixing result in different general features. If there is no resonant behavior (neutrinos with inverted ordering, and antineutrinos with normal or-

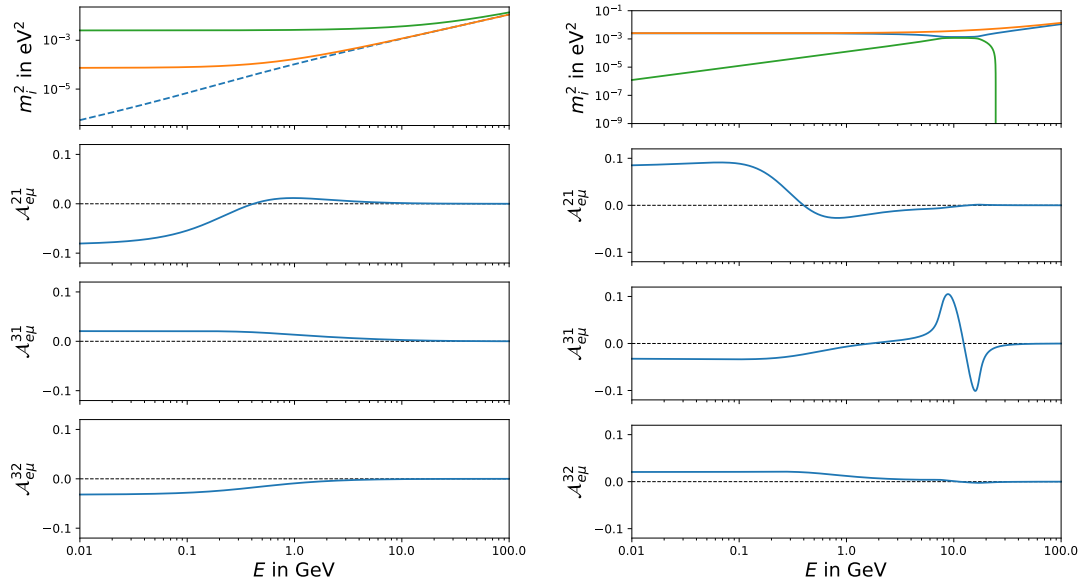

Figure 7.2.: Energy dependence of imaginary amplitudes of one specific setting for antineutrinos with normal (left) and inverted ordering (right). The squared masses are shown as m_1^2 in blue, m_2^2 in orange and m_3^2 in green. The dashed line for m_1^2 for normal ordering corresponds to negative values of the squared effective mass.

dering), all amplitudes slowly converge to zero for large energies. With resonant mixing the corresponding amplitude ($\mathcal{A}_{e\mu}^{32}$ for neutrinos with normal ordering, and $\mathcal{A}_{e\mu}^{31}$ for antineutrinos with inverted ordering) approach large absolute values before reaching zero eventually. While this resonant enhancement for neutrinos with normal ordering or antineutrinos with inverted ordering depends on the specific parameter combinations, the possibility of enlarged unitarity violation due to the matter effect is an important feature.

In general, the experimental determination of the energy dependent amplitudes $\mathcal{A}_{\alpha\beta}^{kj}$ with included matter effect is not trivial and out of reach of current experimental setups as described above. Nevertheless, due to the possibility of resonant enhancement at specific energies, it may be possible to detect unitarity violation more easily than in the vacuum case.

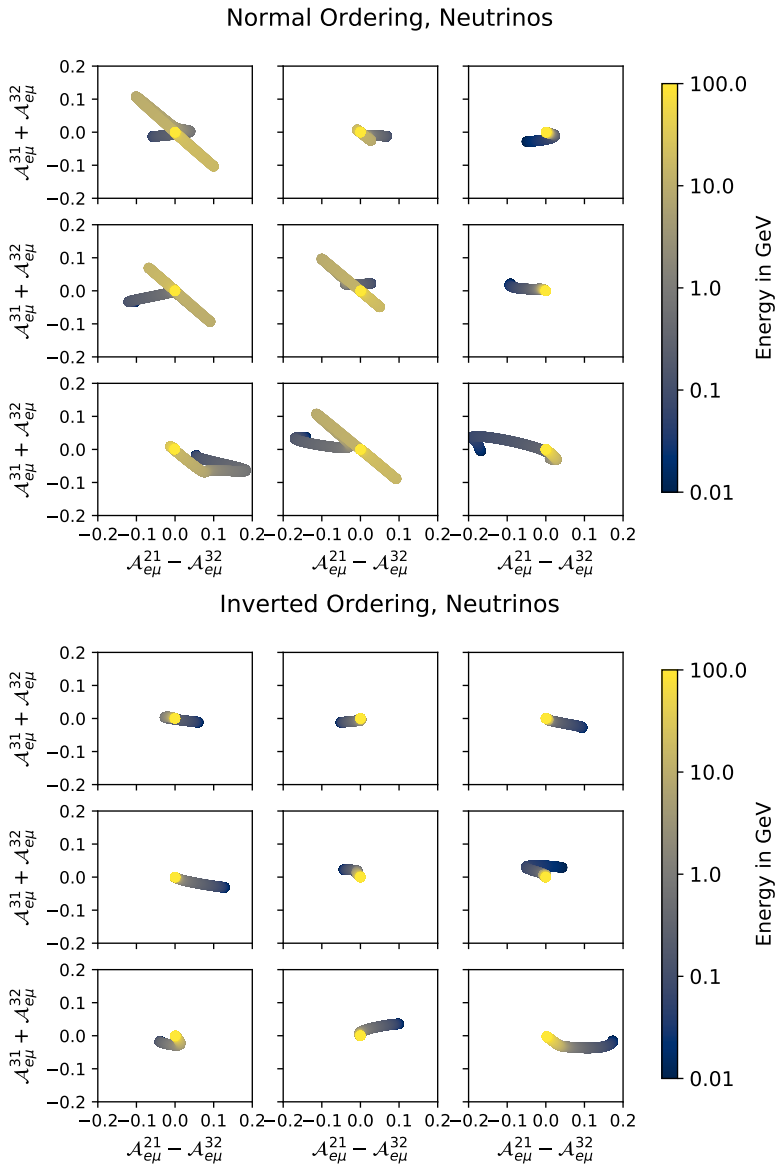

Figure 7.3.: Energy dependence of nine different parameter settings in the $\left(\mathcal{A}_{e\mu}^{21} - \mathcal{A}_{e\mu}^{32}\right)$– $\left(\mathcal{A}_{e\mu}^{31} + \mathcal{A}_{e\mu}^{32}\right)$ plane for neutrinos with normal (top) and inverted ordering (bottom).

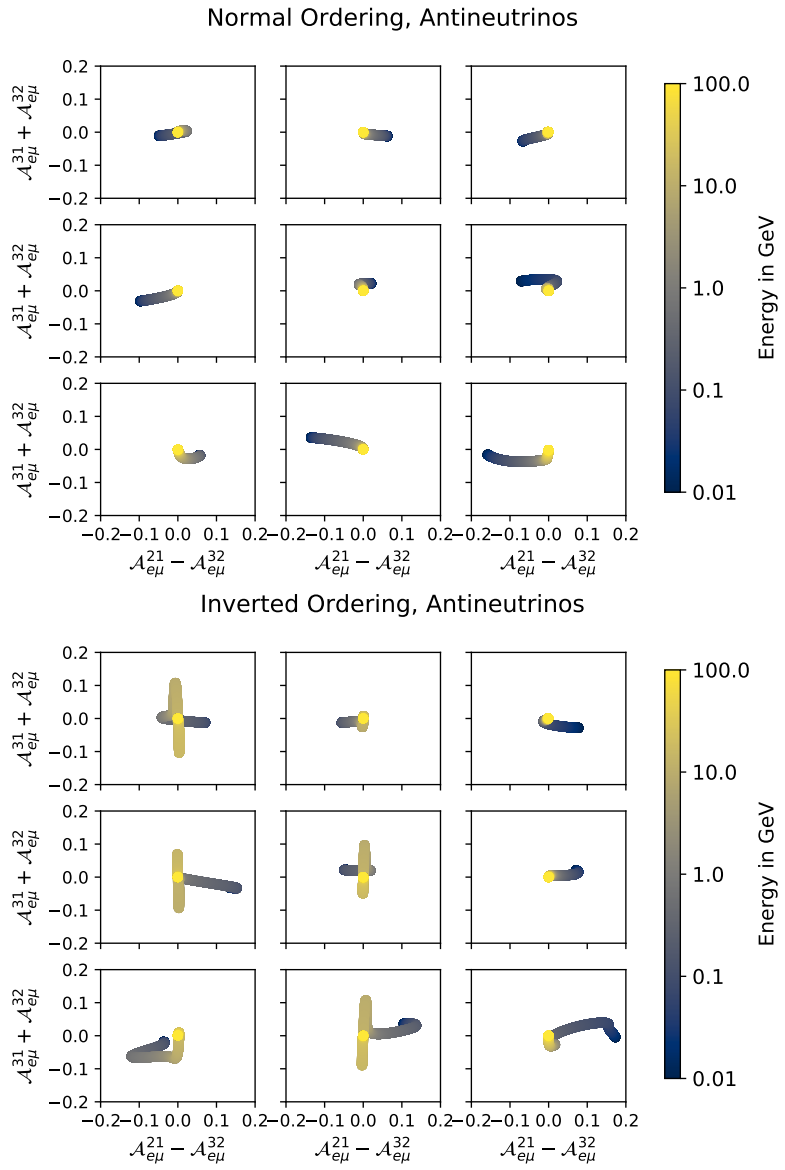

Figure 7.4.: Energy dependence of nine different parameter settings in the $\left(\mathcal{A}^{21}_{e\mu} - \mathcal{A}^{32}_{e\mu}\right)$– $\left(\mathcal{A}^{31}_{e\mu} + \mathcal{A}^{32}_{e\mu}\right)$ plane for antineutrinos with normal (top) and inverted ordering (bottom).

8. Summary

In this part we have introduced a new model independent method to investigate CP violation in neutrino oscillations. Due to the high sensitivity of current neutrino oscillation experiments it is possible to compare these experiments in an independent way without implying a specific model or parameters determined by other experiments. Our method relies on the observable CP violating amplitudes $\mathcal{A}^{kj}_{\alpha\beta}$ instead of specific parametrizations.

We have shown that there is a generic difference between the minimal model of three light active neutrinos and extensions like additional light sterile neutrinos or non-unitarity mixing due to heavy neutrinos or non standard interactions. Specifically the strong prediction of a uniform value for all amplitudes (the Jarlskog invariant) in the minimal three neutrino case, does not hold for any extension of a unitary 3×3 mixing matrix.

For direct unitarity violation we have deduced analytic relations among the amplitudes for the $3 + 1\nu$ case and have also shown, that the addition of even more light sterile states can always be reduced to the special $3 + 1\nu$ case.

To compare direct and indirect unitarity violation, we have performed an extensive numerical analysis, where possible combinations of different amplitudes has been calculated based on bounds for the elements of the mixing matrix without implying unitarity. We have shown that the viable combinations of amplitudes differ significantly for different sources of unitarity violation.

With the help of the GLoBES package we have simulated the current experiments T2K and NOvA looking for CP violation in neutrino oscillations. The simulated pseudo data has been generated by the assumption of extreme but still allowed unitarity violation. Analyzing this generated pseudo data by the newly introduced method has led to the possibility of not only excluding the minimal three neutrino case but also direct unitarity violation as the source. With this proof of concept we are confident that this newly introduced method is a powerful tool to investigate CP violation in neutrino oscillations.

To also include matter effects we have shown the difficulties arising due to the different effect on neutrinos and antineutrinos. Due to the energy dependent effective potential, also the CP violating amplitudes become dependent on the mass squared differences and the energy. Without implying any model dependent relations, this leads to a huge number of free parameters. We have investigated the approach of commutators of the mass matrices with the aim to find a generalized version of the Naumov relation, which has failed in all generality. An extensive reduction of free parameters can be made by focusing on T violation instead of CP violation. Albeit being experimentally more challenging, theoretical predictions can be

made, and we have shown the energy dependence of the CP violating amplitudes for different parameter combinations.

To summarize, the newly introduced method provides a powerful model independent tool to analyze neutrino oscillations already with current experiments. With the presented approach it is not only possible to reject the standard three neutrino hypothesis but also to determine the source of the new effects for specific parameter combinations. The inclusion of matter effects leads to challenges for the method and opens a path for further investigation.

Part III.

Impact of Light Sterile Neutrinos on Determination of the Mass Ordering at Juno

9. Determination of the Mass Ordering at JUNO in the 3ν Case

As pointed out in Section 3.2 one of the yet undetermined properties in the neutrino sector is the mass ordering of the three mass eigenstates m_1^2, m_2^2 and m_3^2. While each mixing angle and mass squared difference can be in the leading term of oscillation probabilities at suitable baselength and energy, the ordering has always only a sub-leading contribution. Oscillation experiments therefore need a high sensitivity to determine the mass ordering. The JUNO experiment is a reactor based experiment designed especially for this determination. Sensitivity studies have shown that JUNO can achieve a median sensitivity of $\sim 3\sigma$ after six years of running time. [128]

In this part we will shortly review the significant features of JUNO and its searches and show afterwards whether a light sterile neutrino can impact the search so that a simple three neutrino analysis leads to a wrong determination of the mass ordering. The JUNO experiment is measuring the survival probability of electron antineutrinos ($\overline{\nu_e}$):

$$P_{(\overline{\nu_e}\to\overline{\nu_e})} = 1 - 4\sum_{i<j}^{N} |\mathbf{U}_{ei}|^2 |\mathbf{U}_{ej}|^2 \sin^2 F_{ij}, \text{ with } \begin{cases} F_{ij} \equiv \frac{\Delta_m^2 ijL}{4E}, \\ \Delta_m^2 ij \equiv m_j^2 - m_i^2, \end{cases} \tag{9.1}$$

with N being the total number of light neutrinos (active or sterile) involved in the neutrino oscillation processes and the mixing matrix $\mathbf{U}$ is a $N \times N$ unitary matrix.

The analysis in [128] relies on the standard case with $N = 3$. The mass ordering is only a sub-leading effect in the probability and cannot be seen directly in the above form. The following parametrizations and redefinitions are used to highlight the impact of the mass ordering: We use the standard parametrization from Equation (3.46) so that

$$\mathbf{U}_{e1} = c_{12}c_{13}, \qquad \mathbf{U}_{e2} = s_{12}c_{13}, \qquad \mathbf{U}_{e3} = \hat{s}_{13}^*, \tag{9.2}$$

where $\hat{s}_{ij} \equiv s_{ij}e^{i\delta_{ij}}$ and $s_{ij} \equiv \sin\theta_{ij}$, $c_{ij} \equiv \cos\theta_{ij}$ with the mixing angles θ_{ij} and the CP-phases δ_{ij}.

We also define $F_* \equiv \frac{\Delta m^2_* L}{4E}$ with $\Delta m^2_* \equiv \Delta m^2_{31} + \Delta m^2_{32}$. The survival probability follows as

$$\begin{aligned} P^{3\nu}_{(\overline{\nu_e}\to\overline{\nu_e})} =& 1 - 4|\mathbf{U}_{e1}|^2|\mathbf{U}_{e2}|^2 \sin^2 F_{21} - 4|\mathbf{U}_{e1}|^2|\mathbf{U}_{e3}|^2 \sin^2 F_{31} \\ & - 4|\mathbf{U}_{e2}|^2|\mathbf{U}_{e3}|^2 \sin^2 F_{32} \\ =& 1 - c^4_{13} \sin^2 2\theta_{12} \sin^2 F_{21} - \sin^2 2\theta_{13} \left(c^2_{12} \sin^2 F_{31} + s^2_{12} \sin^2 F_{32}\right) \\ =& 1 - c^4_{13} \sin^2 2\theta_{12} - \sin^2 2\theta_{13} + \sin^2 2\theta_{13} \cos F_* \cos F_{21} \\ & + \sin^2 2\theta_{13} \sin F_* \cos 2\theta_{12} \sin F_{21}. \end{aligned} \tag{9.3}$$

The impact of the mass ordering becomes visible in Equation (9.3): Normal ordering (NO) (i.e. $m_3 > m_2 > m_1$) results in $\Delta_* > 0$, while inverse ordering (IO) (i.e. $m_2 > m_1 > m_3$) results in $\Delta^2_m * < 0$. Therefore, all terms in (9.3) which are proportional to $\cos F_*$ are not sensitive to the mass ordering, but the terms proportional to $\sin F_*$ are. So only the last term is responsible for JUNO being sensitive to the mass ordering. Note, that this effect is a non-leading effect and a high energy resolutions and high statistics is necessary to determine the mass ordering.

The difference between the two mass orderings can be seen in Figure 9.1 where we used the values for the mixing parameters from Table 3.2 and a CP phase of $\delta_{\mathrm{CP}} = 0$. As can be clearly seen, the different mass orderings result in a shift of the fast oscillating mode. Due to a high energy resolution and a peak in the energy spectrum at $3 - 5$ MeV, JUNO is able to measure this shift and therefore determine the mass hierarchy.

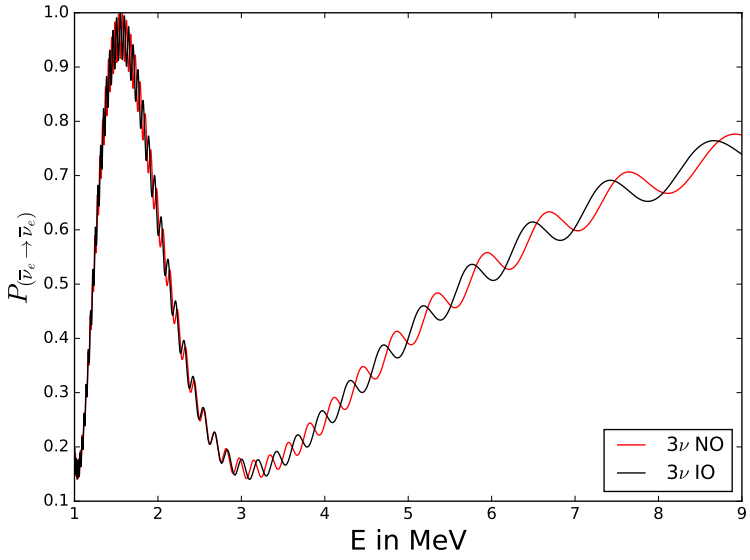

Figure 9.1.: Electron antineutrino survival probability at relevant energies for JUNO for normal ordering (red) and inverted ordering (black).

10. Addition of one Light Sterile Neutrino

The $3+1\nu$ case can now be examined by a analogue treatment. With the corresponding elements of the mixing angles and a redefinition of the new mass square differences $\Delta m'^2_* \equiv \Delta m^2_{41} + \Delta m^2_{42}$ and accordingly $F'_* = \frac{\Delta m'^2_* L}{4E}$ the survival probability can be written as

$$\begin{aligned} P^{4\nu}_{(\overline{\nu_e}\to\overline{\nu_e})} =& \underbrace{1 - 4|V_{e1}|^2|V_{e2}|^2 \sin^2 F_{21} - 4|V_{e1}|^2|V_{e3}|^2 \sin^2 F_{31} - 4|V_{e2}|^2|V_{e3}|^2 \sin^2 F_{32}}_{\text{standard terms}} \\ & \underbrace{-4|V_{e1}|^2|V_{e4}|^2 \sin^2 F_{41} - 4|V_{e2}|^2|V_{e4}|^2 \sin^2 F_{42} - 4|V_{e3}|^2|V_{e4}|^2 \sin^2 F_{43}}_{\text{light sterile terms}} \\ =& 1 - c^4_{13}c^4_{14} \sin^2 2\theta_{12} - c^4_{14} \sin^2 2\theta_{13} - c^2_{13} \sin^2 2\theta_{14} - s^2_{13} \sin^2 2\theta_{14}. \\ & + c^4_{14} \sin^2 2\theta_{13} \cos F_* \cos F_{21} + c^2_{13} \sin^2 2\theta_{14} \cos F'_* \cos F_{21} \\ & + s^2_{13} \sin^2 2\theta_{14} \cos F'_* \cos F_* \\ & - \left(c^4_{14} \sin^2 2\theta_{13} \sin F_* + c^2_{13} \sin^2 2\theta_{14} \sin F'_*\right) \cos 2\theta_{12} \sin F_{21} \\ & + s^2_{13} \sin^2 2\theta_{14} \sin F'_* \sin F_*. \end{aligned} \tag{10.1}$$

Again, the term $\sin F_*$ is sensitive to the mass hierarchy. In contrast to the simple 3ν case, in the $3+1\nu$ case, there arises an additional term proportional to $\sin F'_*$ which can in principle cancel out the standard term.

For a suitable parameter combination, it is possible that the additional term not only cancels out the standard term but generates a term that can spoil the mass hierarchy. This is the case if

$$2 \cdot c^4_{14} \sin^2 2\theta_{13} \sin F_* = -c^2_{13} \sin^2 2\theta_{14} \sin F'_*. \tag{10.2}$$

Note that this relation can in principle be fulfilled with numerous parameter combinations and depends on the energy due F_* and F'_*. Nevertheless, JUNO does not measure this term separately but can only deduce the complete survival probability (10.1), which we focus on in the following.

To show the actual impact of such a light sterile neutrino, we show in Figure 10.1 the survival probability (10.1) in the energy region JUNO is sensitive to. We used different values for the mixing parameters of the fourth neutrino. For the standard mixing parameters, we used the best fit values shown in Table 3.2. It can be easily seen, that the actual impact of the light sterile neutrino is highly dependent on the mixing angle and the mass squared difference.

To investigate whether a misinterpretation of the mass ordering is possible in case of one additional light sterile neutrino, we define the quantity

$$Q(E) = \left| \frac{P_{4\nu}^{\mathrm{NO/IO}}(E) - P_{3\nu}^{\mathrm{IO/NO}}(E)}{P_{4\nu}^{\mathrm{NO/IO}}(E)} \right| \tag{10.3}$$

to measure the deviation of the survival probability with one additional sterile neutrino ($P_{4\nu}$) from the survival probability without any additional light sterile neutrino ($P_{3\nu}$) calculated by Equation (10.1) for opposite orderings of the three neutrinos ν_1, ν_2 and ν_3. This quantity obviously depends on Δm^2_{41}, θ_{14} and the energy. Figures 10.2 and 10.3 show Q as scans over the mixing parameters for different combination of the orderings. For specific energies, it is possible to find specific combinations of θ_{14} and Δm^2_{41} so that the relative deviation Q becomes small ($\lesssim 5\%$). A naive guess could be, that if θ_{14} becomes closer to 0, also Q becomes negligible due to decoupling of the sterile state. However this effect can be observed, even for $\sin^2(2\theta_{14} = 10^{-3}$, the deviation due to the additional sterile state is significant and expected to be measurable by JUNO. The minima in parameter space are indicated by the dark blue region and have a not trivial shape depending on the energy. In general these region also do not align for different energies, as expected due to Equation (10.2).

Due to the broad energy spectrum at JUNO, it is possible to test the hypothesis of a specific mass ordering at different energies at the same time. A weighted analysis with the actual spectrum at JUNO is not done here due to lack of insight into the specifics of the experiment. Therefore we simply calculate the averaged value of $Q(E)$ for $N_{\mathrm{bins}} = 200$ equal sized bins in the energy region from 1.8 MeV to 8.0 MeV, matching the analysis in [128] as

$$\overline{Q} = \frac{1}{N_{\mathrm{bins}}} \sum_{i}^{N_{\mathrm{bins}}} Q(E_i), \tag{10.4}$$

with the energy E_i of the i-th bin.

Since the specifics of the used reactors and detectors are not publicly available, it is not possible to deduce whether JUNO can resolve the difference between 3ν and $3+1\nu$ for parameter combinations where $\overline{Q}$ is large. Nevertheless, if there are parameter combinations of θ_{14} and Δm^2_{41} where $\overline{Q}$ s negligible, JUNO is not able to measure any deviation to a supposed 3ν analysis, and therefore might claim a wrong mass hierarchy without being able to notice.

Figures 10.5 and 10.4 show the two different possibilities of combination of the mass orderings for $\overline{Q}$. The averaged deviation is for all parameter combinations at least 3% and for a huge parameter space even significantly bigger. We therefore suspect that JUNO is able to detect these deviations.

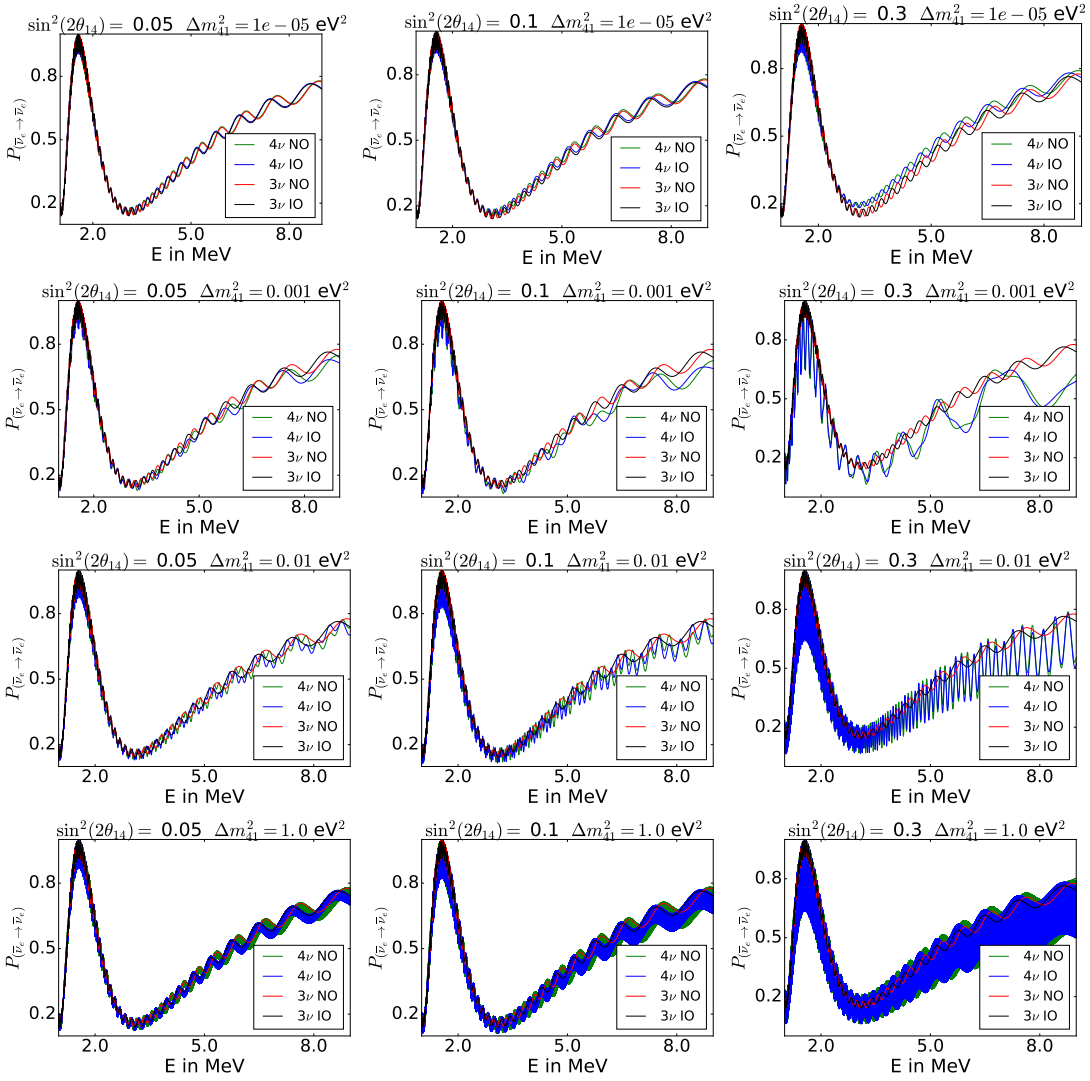

Figure 10.1.: Survival probability $P_{(\overline{\nu}_e \to \overline{\nu}_e)}$ for four neutrinos with different values of $\sin^2(2\theta_{14})$ and Δm^2_{41} in the relevant energy region for Juno and for different orderings for the standard neutrinos (NO in green, IO in blue). For comparison also the probabilities for 3 neutrinos are shown (NO in red and IO in black).

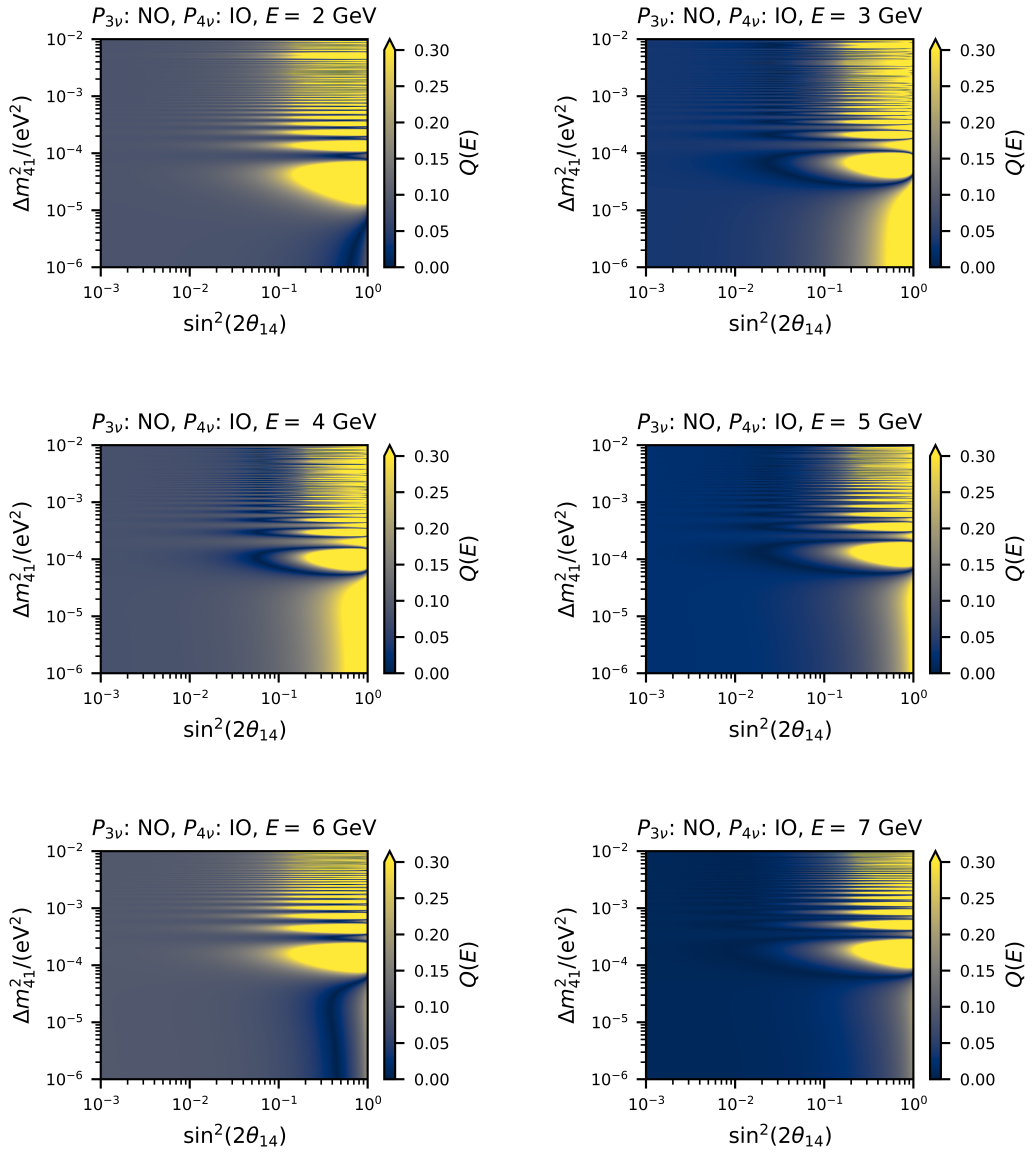

Figure 10.2.: Relative difference $Q(E)$ of the survival probability defined by Equation (10.3) for different energies dependent on the mixing angle $\sin^2 2\theta_{14}$ and the mass squared difference Δm^2_{41}. The three neutrino probability is based on normal ordering, while the four neutrino probability is based on inverted ordering. The dark regions indicate parameter combinations where there is no difference between the two considered probabilities.

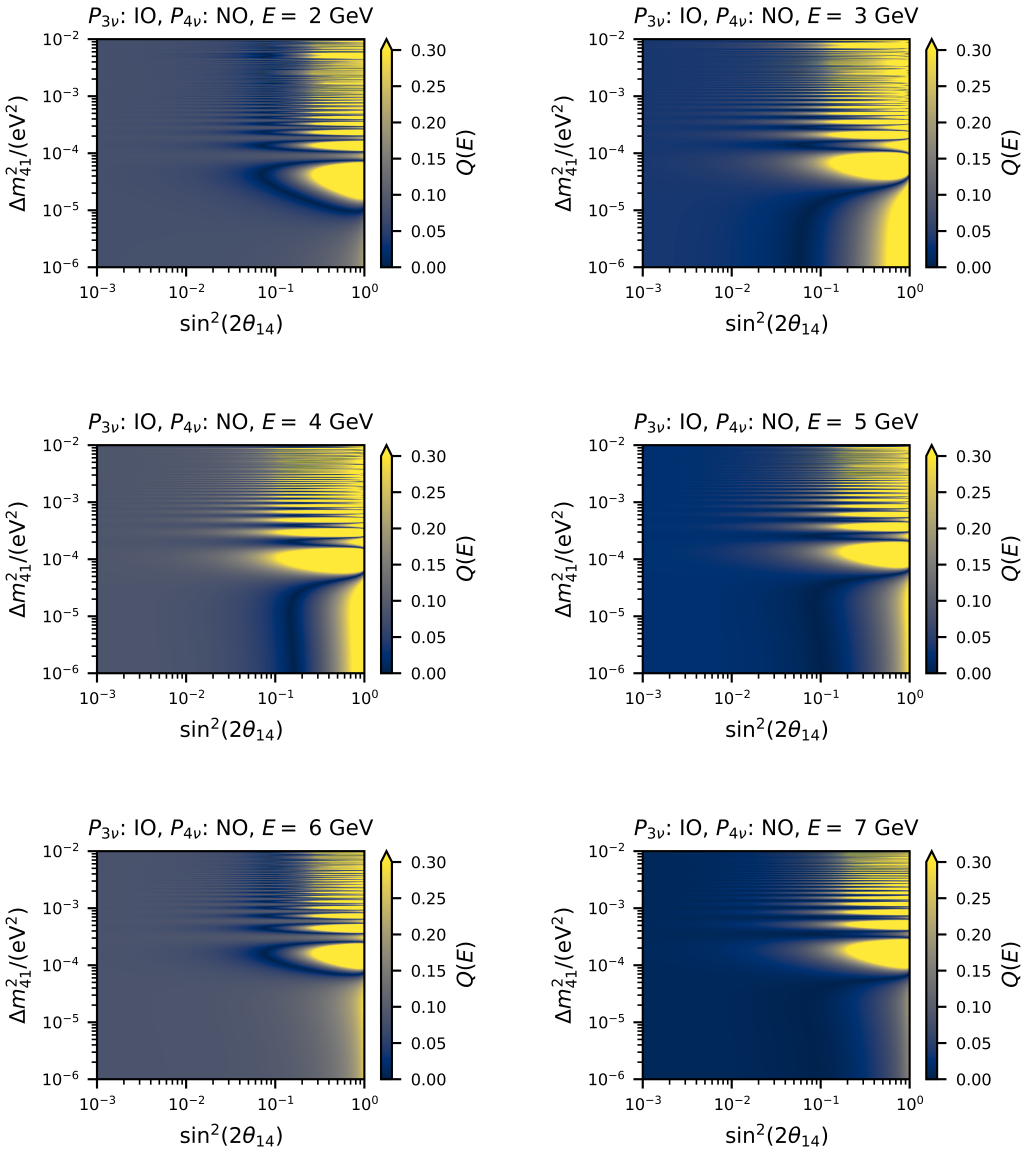

Figure 10.3.: Relative difference of the survival probability defined by Equation (10.3) for different energies dependent on the mixing angle $\sin^2 2\theta_{14}$ and the mass squared difference Δm^2_{41}. The three neutrino probability is based on inverted ordering, while the four neutrino probability is based on normal ordering. The dark regions indicate parameter combinations where there is no difference between the two considered probabilities.

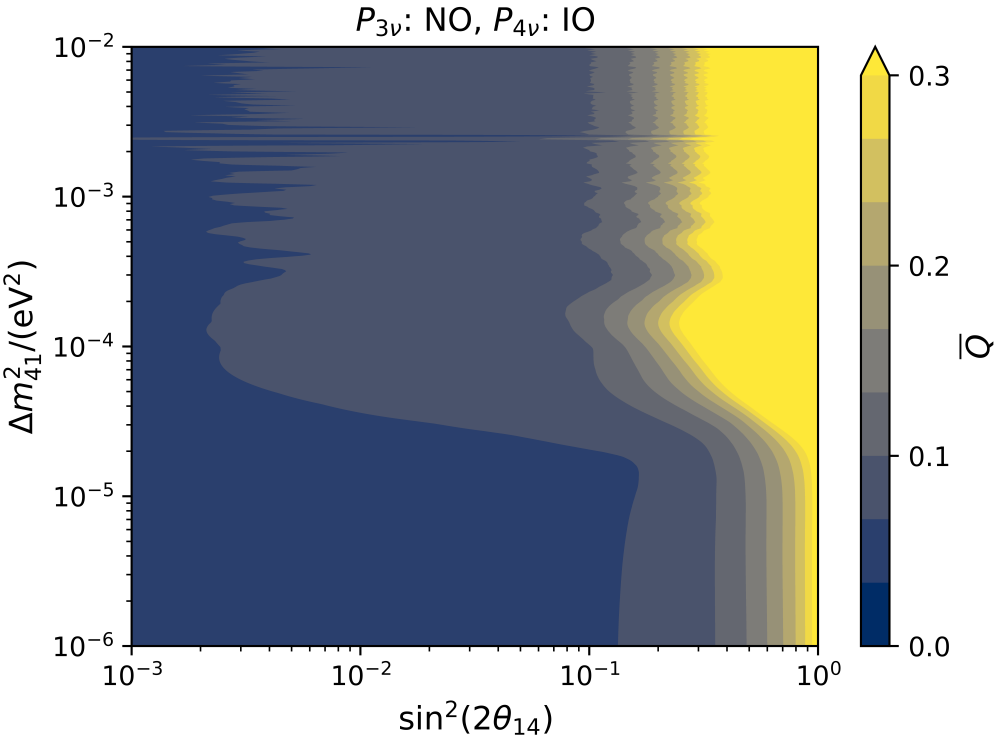

Figure 10.4.: Contours of the averaged relative difference $\overline{Q}$ of the survival probability defined by Equation (10.4) dependent on the mixing angle $\sin^2 2\theta_{14}$ and the mass squared difference Δm^2_{41}. The three neutrino probability is based on normal ordering, while the four neutrino probability is based on inverted ordering. For all considered parameter combinations, the averaged relative difference is larger than 3%.

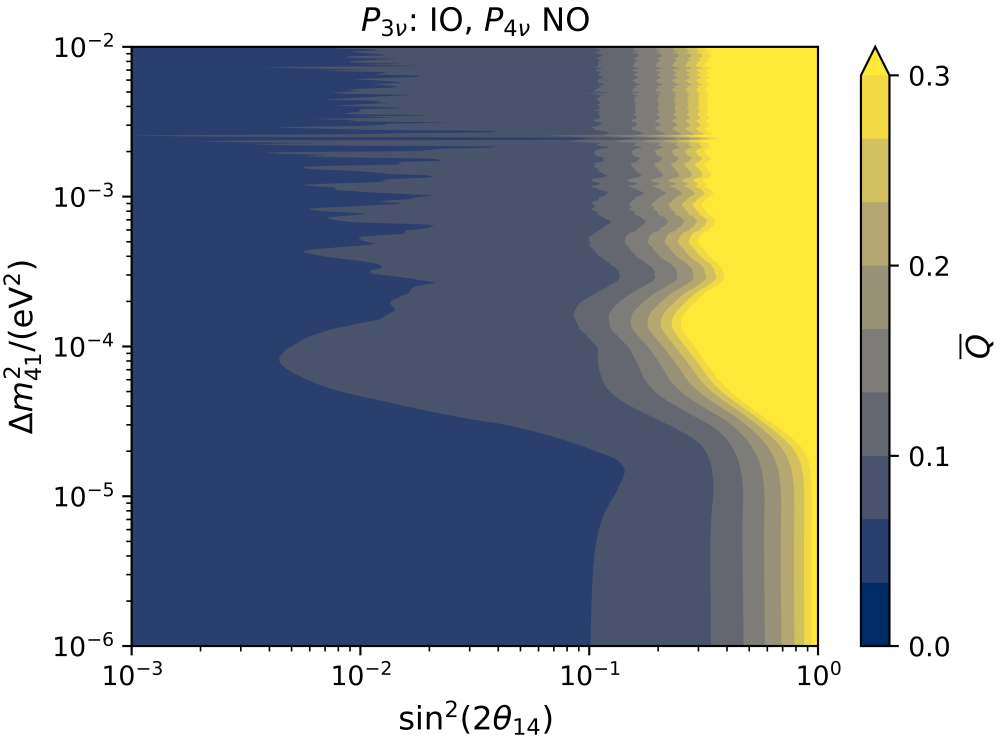

Figure 10.5.: Contours of averaged relative difference $\overline{Q}$ of the survival probability defined by Equation (10.4) dependent on the mixing angle $\sin^2 2\theta_{14}$ and the mass squared difference Δm^2_{41}. The three neutrino probability is based on inverted ordering, while the four neutrino probability is based on normal ordering. For all considered parameter combinations, the averaged relative difference is larger than 3%.

11. Summary

To summarize, we have shown that it is theoretically possible that an additional light sterile neutrino can spoil the determination of the mass ordering at the reactor neutrino experiment JUNO. Due to interference of the terms sensitive to the mass ordering, the additional terms caused by the light sterile neutrino can lead to cancellations. This observation has raised the suspicion whether a $3 + 1\nu$ model can fake the signal of a 3ν model with the opposite mass ordering and therefore lead to a false conclusion by the JUNO collaboration.

We have demonstrated that this cancellation is indeed possible for specific energy values. The relative difference between the survival probability of $3 + 1\nu$ and 3ν can become negligible for specific parameter combinations. Nevertheless, the energy dependence of the survival probabilities is non-trivial and therefore, for each such parameter combination the difference in the survival probability can also become large at other energies. Due to the broad energy spectrum and the high energy resolution of JUNO there is no combination for θ_{14} and Δm^2_{41} where the $3 + 1\nu$ probability fakes a 3ν probability with the opposite mass ordering over the complete energy spectrum. A quantitative determination whether the effect of the additional sterile neutrino is in fact measurable by JUNO has not been done due to the limited information publicly available about the experiment.

Part IV.

A Stringent Model to Explain All Current Anomalies in Neutrino Oscillation Data

12. Introduction to Conflicting Appearance and Disappearance Data

In this part we examine a new model of neutrino oscillations with sterile neutrinos and altered dispersion relations to explain all currently conflicting oscillation data thoroughly. To our knowledge this model is the first and only model based purely on oscillation effects which achieves this task [2].

In this chapter we introduce the current problems of conflicting experimental data, before we show in chapter 13 how simple models fail and eventually in chapter 14 we develop a complete model explaining all current anomalies in neutrino oscillations without spoiling data from different experiments.

As already mentioned in Section 3.4 anomalies in neutrino oscillations are a long standing issue. The excess reported by LSND [49], the deficit in reactor flux [59], and the deficit in Gallium based experiments [51] can all be explained by a short baseline oscillation corresponding to a third mass squared difference $\Delta m_{\mathrm{SB}} \sim 1\mathrm{eV}^2$. Nevertheless, the sterile neutrino hypothesis had a statistically low significance, lacks of theoretical motivation, is in conflict with cosmological data[34] and other oscillation experiments in global fits [104].

To further investigate the LSND anomaly, the MiniBooNE experiment searched for ${}^{(-)}\nu_\mu \to {}^{(-)}\nu_e$ transitions at a different baseline and energy as LSND, but the setup corresponded to the same mass squared difference of $\mathcal{O}(1)\mathrm{eV}^2$. The collaboration recently reported a $4.8\,\sigma$ excess in the low energy region compared to the standard three neutrino hypothesis [50], and combined with the LSND results, the significance rise to $6.1\,\sigma$ for new physics beyond the Standard Model. This anomaly therefore cannot be interpreted as a statistical fluctuation but has to be systematic. It is still possible that this excess stems from an underestimation of the background or a wrong analysis. Several other explanations for the MiniBooNE data has been proposed [105–110] but none of them are able to explain all anomalies. Nevertheless until the follow up experiment MicroBooNE is able to clarify the controversy, we take these results seriously and examine weather this excess might be explained by new oscillation physics corresponding to a new sterile neutrino state.

While all these anomalies hint into the same direction, experiments like atmospheric neutrino experiments [111, 112] or accelerator experiments [113–115] are searching for ν_μ disappearance at these neutrino mass squared difference scales and do not show any deviation from the standard three neutrino model. These experiments provide high statistics and constrain the simplest additional sterile neutrino hypothesis consequently. The global fit in [104] excludes the simplest $3 + 1\nu$ model at the 4.7σ level.

Experiment	E	L	channel	Δm^2_{SB}
LSND	$\sim 20 - 60$ MeV	~ 30 m	$\overset{(-)}{\nu}_\mu \to \overset{(-)}{\nu}_e$	✓
MiniBooNE	$\sim 0.2 - 3$ GeV	~ 541 m	$\overset{(-)}{\nu}_\mu \to \overset{(-)}{\nu}_e$	✓
Gallium	$\sim 400 - 800$ keV	~ 2 m	$\bar{\nu}_e \to \bar{\nu}_e$	✓
Reactor	$\sim 1 - 6$ MeV	$\sim 10 - 100$ m	$\bar{\nu}_e \to \bar{\nu}_e$	✓
MINOS (acc)	~ 7 GeV	~ 735 km	$\overset{(-)}{\nu}_\mu \to \overset{(-)}{\nu}_\mu$	✗
atmospheric	$\sim 0.6 - 100$ GeV	$\sim 15 - 13,000$ km	$\overset{(-)}{\nu}_\mu \to \overset{(-)}{\nu}_\mu$	✗

Table 12.1.: Current status of conflicting neutrino data. The last column indicates whether an additional sterile neutrino is favored (✓) or in conflict (✗) with current data.

A summary of the current conflicting neutrino data is shown in Table 12.1. Since all experiments measure different channels, it needs a closer look why these experiments are excluding each other in the most simple $3 + 1\nu$ model:

As already pointed out in section 3.2, the transition probability of neutrinos from one active flavor α to another flavor β can be written as

$$\begin{aligned} P_{\nu_\alpha \to \nu_\beta} =& \delta_{\alpha\beta} - 4 \sum_{k>j}^{N_{\text{light}}} \text{Re}(\mathbf{U}^*_{\alpha k}\mathbf{U}_{\beta k}\mathbf{U}_{\alpha j}\mathbf{U}^*_{\beta j}) \sin^2\left(\frac{\Delta m^2_{kj} L}{4E}\right) \\ &+ 2 \sum_{k>j}^{N_{\text{light}}} \text{Im}(\mathbf{U}^*_{\alpha k}\mathbf{U}_{\beta k}\mathbf{U}_{\alpha j}\mathbf{U}^*_{\beta j}) \sin\left(\frac{\Delta m^2_{kj} L}{2E}\right), \end{aligned} \tag{12.1}$$

with N_{light} being the total number of active and sterile light neutrinos, $\mathbf{U}$ the $N_{\text{light}} \times N_{\text{light}}$ mixing-matrix. Here we focus solely on BSM extensions with light sterile neutrinos which makes $\mathbf{U}$ unitary. We also neglect possible CP violation due to simplicity which is justified by MiniBooNE data showing almost the same effect in neutrino and antineutrino data. Therefore we consider only real elements of the mixing matrix $\mathbf{U}$, so the last term in Eq. (12.1) vanishes.

The proposed additional mass-squared difference Δm^2_{SB} is in the $\sim 1\,\text{eV}^2$-region and the mass-squared differences Δm^2_{21}, Δm^2_{31} and Δm^2_{32} are experimentally tested to be orders of magnitude smaller (see Table 3.2). Therefore it is possible to neglect Δm^2_{21}, Δm^2_{31} and Δm^2_{32}

at suitable baselength and energies. A common approximation for the transition probability from one active flavor to another at those values of $\frac{L}{E}$ reads

$$\begin{aligned} P_{\nu_\alpha \to \nu_\beta} \approx & \delta_{\alpha\beta} - 4 \sum_j^3 \mathrm{Re}(\mathbf{U}^*_{\alpha 4}\mathbf{U}_{\beta 4}\mathbf{U}_{\alpha j}\mathbf{U}^*_{\beta j}) \sin^2\left(\frac{\Delta m^2_{4j} L}{4E}\right) \\ = & \delta_{\alpha\beta} - 4\sin^2\left(\frac{\Delta m^2_{\mathrm{SB}} L}{4E}\right) \underbrace{\sum_j^3 \mathbf{U}_{\alpha 4}\mathbf{U}_{\beta 4}\mathbf{U}_{\alpha j}\mathbf{U}_{\beta j}}_{-\frac{1}{4}\sin^2 2\theta_{\alpha\beta}\,,\ for\ \alpha\neq\beta} . \end{aligned} \tag{12.2}$$

Here we used the unitarity of $\mathbf{U}$, specifically $\sum_j^3 \mathbf{U}_{\alpha j}\mathbf{U}_{\beta j} = -\mathbf{U}_{\alpha 4}\mathbf{U}_{\beta 4} + \delta_{\alpha\beta}$. This form resembles a simple two neutrino model with an appearance angle $\sin^2 2\theta_{\alpha\beta} = 4|\mathbf{U}_{\alpha 4}|^2|\mathbf{U}_{\beta 4}|^2$ and a disappearance angle $\sin^2 2\theta_{\alpha\alpha} = 4|\mathbf{U}_{\alpha 4}|^2(1-|\mathbf{U}_{\alpha 4}|^2)$, which makes it possible to analyze phenomena of the simplest $3+1\nu$ model as a basic two neutrino model.

The appearance experiments LSND and MiniBooNE show an excess in the $\overset{(-)}{\nu}_\mu \to \overset{(-)}{\nu}_e$ transition, and therefore demand a large value of $\sin^2 2\theta_{\mu e}$ to explain their data. On the other hand, the $\overset{(-)}{\nu}_\mu$ disappearance experiments do not show a significant deficit at this oscillation mode. This leads to a small value of $\sin^2 2\theta_{\mu\mu} = 4\,|\mathbf{U}_{\mu 4}|^2(1-|\mathbf{U}_{\mu 4}|^2) \simeq 4\,|\mathbf{U}_{\mu 4}|^2$ for $|\mathbf{U}_{\mu 4}|^2$ small.

Comparing the different amplitude we end up with the following relationship

$$\begin{aligned} \sin^2 2\theta_{\mu e} = 4\,|\mathbf{U}_{\mu 4}|^2|\mathbf{U}_{e 4}|^2 &= \frac{1}{4}(\sin^2 2\theta_{\mu\mu} + 4\,|\mathbf{U}_{\mu\mu}|^4)(\sin^2 2\theta_{ee} + 4\,|\mathbf{U}_{ee}|^4) \\ &\simeq \frac{1}{4}\sin^2 2\theta_{\mu\mu}\sin^2 2\theta_{ee}. \end{aligned} \tag{12.3}$$

Since the inequality $\sin^2\theta_{\alpha\beta} < 1$ holds for all α, β, both disappearance angles for ν_e *and* ν_μ have to be large, to accomplish a significant appearance probability. Therefore appearance experiments and disappearance experiments contradict each other in the simplest $3+1\nu$ model. This problem is well known and exhibits the basic problem of current short baseline results. It is shown, that it even persists in models adopting more than one additional sterile state [116].

The above relationship holds as long as one considers the elements of the mixing matrix to be constant. If this condition is given up and the elements are allowed to become energy or baseline dependent (as is the case for CP-violating matter vs. antimatter effects), this tension can in principle be avoided.

As shown in Table 12.1 the relevant experiments are indeed all sensitive to a mass-squared difference of $\sim 1\,\mathrm{eV}^2$ due to similar values of $\frac{L}{E}$, but they operate on different energy and baselength scales and so an altered dispersion relation (see the following chapter) could be useful to resolve the above mentioned problem. In this case the energy dependence has to be fairly strong, since the energy regime for MiniBooNE almost overlaps with the low-energy range of atmospheric neutrino experiments.

In summary, to relieve the tension between appearance and disappearance experiments, a model is required which allows for a small $|\mathbf{U}_{\mu 4}|^2$ at high energies (GeV) and a sufficiently large $|\mathbf{U}_{e4}|^2|\mathbf{U}_{\mu 4}|^2$ at low energies (MeV).

13. Altered Dispersion Relations for a Single Sterile Neutrino

Effective potentials in the Hamiltonian in flavor space can generate additional terms in the usual relation between energy E and momentum $\vec{p}$, so that the normal dispersion relation $E^2 = |\vec{p}|^2 + m^2$ is altered. One typical example for such altered dispersion relation (ADR) is the matter effect already covered in Section 7. As mentioned in that section, the matter effect differs for neutrino and antineutrino due to the earth consisting solely of matter. Since MiniBooNE reports anomalies in neutrino and antineutrino mode and such a large signal would require unusually large couplings to matter, the typical matter effect cannot provide a solution of the anomaly. Inspired by matter effects we develop a different formalism to explain the anomaly. Note, that we do not take the standard matter effect into account, since the impact is expected to be small.

One scenario which can be applied to neutrinos and antineutrinos in the same way allows a Lorentz violation of the sterile neutrino. Since Lorentz violation is based on the spacetime itself, there is no difference between particles and antiparticles. In [117, 118] a model is proposed, which adopts one additional sterile neutrino taking a shortcut via an asymmetrically warped extra dimension [119–121] (see also [122–125]). In a semi-classical picture, the sterile neutrino oscillates on its geodesic in the warped bulk surrounding the brane, and thereby a running time difference is generated between active and sterile neutrinos. This running time difference manifests itself as an additional negative potential in the Hamiltonian proportional to the relative time difference $\frac{\delta t}{t} =: \varepsilon$, the so-called shortcut parameter (always entering the Hamiltonian as multiplied by the energy E). Although the semi-classical picture may not be truly accurate, its predictions regarding the form of the potential are correct to leading order in the shortcut parameter [126].

The resulting Hamiltonian in flavor space can be written as

$$H_{(\mathrm{F})} = \frac{1}{2E}\mathbf{U}\begin{pmatrix} m_1^2 & 0 & 0 & 0 \\ 0 & m_2^2 & 0 & 0 \\ 0 & 0 & m_3^2 & 0 \\ 0 & 0 & 0 & m_4^2 \end{pmatrix}\mathbf{U}^\dagger - E\begin{pmatrix} 0 & 0 & 0 & 0 \\ 0 & 0 & 0 & 0 \\ 0 & 0 & 0 & 0 \\ 0 & 0 & 0 & \varepsilon \end{pmatrix} \tag{13.1}$$

Using the aforementioned approximation $m_1^2 = m_2^2 = m_3^2 = 0$ and $m_4^2 = \Delta m^2_{\mathrm{SB}}$ leads to

$$H_{(\mathrm{F})} \approx \begin{pmatrix} & \mathbf{V} & & 0 \\ & & & 0 \\ & & & 0 \\ 0 & 0 & 0 & 1 \end{pmatrix} \left[\frac{1}{2E} \begin{pmatrix} 1 & 0 & 0 & 0 \\ 0 & 1 & 0 & 0 \\ 0 & 0 & & \\ 0 & 0 & & R_{34} \end{pmatrix} \begin{pmatrix} 0 & 0 & 0 & 0 \\ 0 & 0 & 0 & 0 \\ 0 & 0 & 0 & 0 \\ 0 & 0 & 0 & \Delta m^2_{\mathrm{SB}} \end{pmatrix} \begin{pmatrix} 1 & 0 & 0 & 0 \\ 0 & 1 & 0 & 0 \\ 0 & 0 & & \\ 0 & 0 & & R_{34}^T \end{pmatrix} - E\varepsilon \begin{pmatrix} 0 & 0 & 0 & 0 \\ 0 & 0 & 0 & 0 \\ 0 & 0 & 0 & 0 \\ 0 & 0 & 0 & 1 \end{pmatrix} \right] \begin{pmatrix} & \mathbf{V}^\dagger & & 0 \\ & & & 0 \\ & & & 0 \\ 0 & 0 & 0 & 1 \end{pmatrix}, \tag{13.2}$$

with the energy E, shortcut parameter ε, and

$$\mathbf{U} = \begin{pmatrix} & \mathbf{V} & & 0 \\ & & & 0 \\ & & & 0 \\ 0 & 0 & 0 & 1 \end{pmatrix} \times \begin{pmatrix} 1 & 0 & 0 & 0 \\ 0 & 1 & 0 & 0 \\ 0 & 0 & & \\ 0 & 0 & & R_{34} \end{pmatrix}, \tag{13.3}$$

being the full 4×4 unitary mixing matrix. Here, V is the unitary 3×3 mixing matrix corresponding to the standard U_{PMNS} and R_{34} is the rotation in the $3 - 4$ plane generating the sterile admixture of mass eigenstate ν_3 with the mixing angle θ_{34}:

$$R_{34} = \begin{pmatrix} \cos\theta_{34} & \sin\theta_{34} \\ -\sin\theta_{34} & \cos\theta_{34} \end{pmatrix}. \tag{13.4}$$

As already calculated in [118], the eigenvalues of the Hamiltonian become

$$\lambda_1 = 0, \qquad \lambda_2 = 0,$$
$$\lambda_\pm = \frac{\Delta m^2_{\mathrm{SB}}}{4E} \left(1 - \cos 2\theta_{34} \left(\frac{E}{E_R} \right)^2 \pm \sqrt{\sin^2 2\theta_{34} + \cos^2 2\theta_{34} \left[1 - \left(\frac{E}{E_R} \right)^2 \right]^2} \right), \tag{13.5}$$

with the resonance energy

$$E_R = \sqrt{\frac{\Delta m^2_{\mathrm{SB}} \cos 2\theta_{34}}{2\varepsilon}}. \tag{13.6}$$

Below we follow the arguments given by [118] with one exception regarding the reasoning why the probability $P_{\nu_\alpha \to \nu_\alpha}$, with α being an active flavor, should vanish. One has

$$\begin{aligned} P_{\nu_\alpha \to \nu_\alpha} = 1 - 4U^2_{\alpha 3} \cdot \Bigg[& \sin^2 \left(\frac{L(\lambda_+ - \lambda_-)}{2} \right) \sin^2\tilde{\theta} \cos^2\tilde{\theta}\, U^2_{\alpha 3} \\ & + \sin^2 \left(\frac{L(\lambda_+)}{2} \right) \sin^2\tilde{\theta} \left(1 - U^2_{\alpha 3} \right) \\ & + \sin^2 \left(\frac{L(\lambda_-)}{2} \right) \cos^2\tilde{\theta} \left(1 - U^2_{\alpha 3} \right) \Bigg]. \end{aligned} \tag{13.7}$$

Here, $\tilde{\theta}$ denotes the effective mixing angle defined via

$$\sin^2 2\tilde{\theta} = \frac{\sin^2 2\theta_{34}}{\sin^2 2\theta_{34} + \left(\cos 2\theta_{34} - \frac{2E^2\varepsilon}{\Delta m^2_{\mathrm{SB}}}\right)^2} \,. \tag{13.8}$$

According to [118], while $\sin^2\tilde{\theta}$ does not vanish, the eigenvalue λ_+ vanishes and therefore $P_{\nu_\alpha\to\nu_\alpha}$ should vanish as well. Technically, this is a correct statement which applies as long as one considers only a single experiment with a fixed base-length L. However, various experiments now observe neutrinos in a wide energy range above the resonance. For example, for atmospheric experiments not only the energy becomes larger than the energies at LSND or MiniBooNE, but also the base-length can be as large as 15,000 km, which results in a value of $\frac{L}{E}$ which is up to 4 magnitudes larger than the one probed in MiniBooNE.

Therefore, the relevant quantities to be examined are the mass-squared eigenvalues rather than the Hamiltonian eigenvalues. The mass-squared eigenvalues are

$$m^2_\pm = 2E \cdot \lambda_\pm \,, \tag{13.9}$$

which give rise to the oscillatory term $\sin^2\left(m^2_\pm \frac{L}{2E}\right)$ in the probability in Eq. (13.7). Adopting this more familiar form we continue to analyze the oscillations of atmospheric neutrinos. While it is true that $\lambda_+ \propto 1/E$ becomes zero for energies much larger than E_R, m^2_+ as defined herein does not:

$$\lim_{E\to\infty} m^2_+ = \Delta m^2_{\mathrm{SB}} \cdot \frac{1-\cos 2\theta_{34}}{2} \,. \tag{13.10}$$

Note that, although the effective mass-squared eigenvalue m^2_+ can become small for extremely small mixing angles θ_{34}, it is still governed by the vacuum mass squared difference to the 4th eigenvalue, in this case Δm^2_{SB}. This value is still large compared to the standard mass squared differences. Therefore, even above the resonance there is still a non-vanishing oscillation mode, which becomes accessible experimentally if the oscillation length is large enough. Such is the case for atmospheric and astrophysical neutrinos.

For a better understanding we plot the effective masses for this scenario in Fig. 13.1. As can be seen in Fig. 13.1, at the resonance a level crossing occurs and the Hamiltonian eigenstates swap their flavor content. While the predominantly sterile state decouples above the resonance, the now heavier predominantly active state approaches a constant value that due to the level crossing gap is different from its initial value. This behaviour implies a large effective Δm^2_{13} that gives rise to large and fast active-to-sterile oscillations, e.g. in atmospheric neutrinos.

This argument can be generalized to mixing with θ_{14}, θ_{24}, or a combination of the two. Also, the case where all standard mass-squared differences do not vanish can be treated accordingly. For illustration, we show the probabilities at different experiments and different settings in Appendix B.

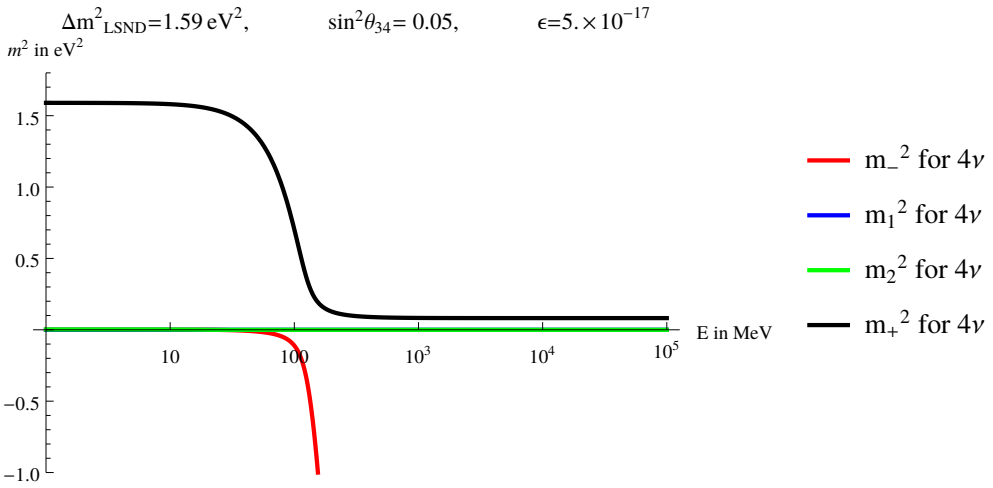

Figure 13.1.: Effective mass-squareds as a function of the energy E in the $3+1\nu$ model including an effective potential due to sterile neutrino shortcuts.

Although the sterile neutrino decouples from the active ones above the resonance, the impact on the disappearance experiments is significant. In any possible mixing pattern the atmospheric experiments or MINOS should notice a deviation from the standard three neutrino case (especially for longer baselines such as the MINOS far detector, or upward going atmospheric neutrinos). One could possibly argue that MINOS might miss the deviation from standard 3 neutrino case due to its narrow energy spectrum at around 7 GeV (see Figures B.4, B.8 and B.12), but atmospheric experiments like IceCube or SuperKamiokaNDE or KM3NeT have not only high statistics but also a wide energy spectrum and high resolution for the azimuth angle and the energy (see Figures B.3, B.7 and B.11). Therefore, these experiments should be highly sensitive to this significant deviation. Atmospheric neutrino experiments also tested the $\frac{L}{E}$-dependence of the oscillation probability, finding no observable deviations from the 3ν case. A simple $3+1\nu$ model even with an altered dispersion relation for the sterile neutrino is therefore ruled out by current data.

14. A Realistic 3+3 Model

14.1. $3 + 3\nu$ with a Common Sterile Neutrino Potential

The emergence of a large mass-squared difference in the energy regime far above the resonance described above can be avoided by adding three sterile neutrinos instead of a single sterile neutrino. In the following we assume that each sterile state mixes with exactly one of the predominantly active mass eigenstates, respectively. Therefore all mass eigenstates become affected by the common sterile potential. If all sterile neutrinos are affected by the same potentials, the mass differences among the predominantly active states will not be altered even though their masses change as the E-dependent potential and mixing change. This mechanism removes the 'unwanted' mass difference which spoiled atmospheric neutrino oscillations in the $3 + 1\nu$ case.

The resulting 6×6 mixing matrix is parametrized as

$$\mathbf{U}^{6\times 6} = \mathbf{U}_{23}\mathbf{U}_{13}\mathbf{U}_{12}\mathbf{U}_{14}\mathbf{U}_{25}\mathbf{U}_{36}\,. \tag{14.1}$$

The vacuum masses read

$$\Delta m^2_{41} = \Delta m^2_{\rm SB}\,, \tag{14.2}$$

$$\Delta m^2_{51} = \Delta m^2_{\rm SB} + \Delta m^2_{21} \quad \rightarrow \quad \Delta m^2_{52} = \Delta m^2_{\rm SB}\,, \tag{14.3}$$

$$\Delta m^2_{61} = \Delta m^2_{\rm SB} + \Delta m^2_{31} \quad \rightarrow \quad \Delta m^2_{63} = \Delta m^2_{\rm SB}\,. \tag{14.4}$$

Assuming universal shortcut parameters (ε) for the three sterile neutrinos the effective potential becomes

$$V_{\rm eff} = \begin{pmatrix} 0 & 0 & 0 & 0 & 0 & 0 \\ 0 & 0 & 0 & 0 & 0 & 0 \\ 0 & 0 & 0 & 0 & 0 & 0 \\ 0 & 0 & 0 & \varepsilon E & 0 & 0 \\ 0 & 0 & 0 & 0 & \varepsilon E & 0 \\ 0 & 0 & 0 & 0 & 0 & \varepsilon E \end{pmatrix}. \tag{14.5}$$

Every mass eigenstate $\nu_{1,2,3}$ has its own sterile state admixture. Therefore, the results from [118] remain applicable. The resulting mass eigenvalues are denoted by $m^2_{1\pm}, m^2_{2\pm}, m^2_{3\pm}$, which

correspond to the $m^2_\pm$ mass eigenstates in the previous section. Considering also the non-vanishing small masses m^2_1, m^2_2 and m^2_3, the eigenvalues read

$$\begin{aligned} m^2_{1\pm} =& \frac{m^2_1+m^2_4}{2} - \frac{\Delta m^2_{\rm SB}}{2} \\ & \times \left(\cos 2\theta_{14} \left(\frac{E}{E_{R,1}}\right)^2 \mp \sqrt{\sin^2 2\theta_{14} + \cos^2 2\theta_{14} \left[1 - \left(\frac{E}{E_{R,1}}\right)^2\right]^2} \right) , \end{aligned} \tag{14.6}$$

$$\begin{aligned} m^2_{2\pm} =& \frac{m^2_2+m^2_5}{2} - \frac{\Delta m^2_{\rm SB}}{2} \\ & \times \left(\cos 2\theta_{25} \left(\frac{E}{E_{R,2}}\right)^2 \mp \sqrt{\sin^2 2\theta_{25} + \cos^2 2\theta_{25} \left[1 - \left(\frac{E}{E_{R,2}}\right)^2\right]^2} \right) , \end{aligned} \tag{14.7}$$

$$\begin{aligned} m^2_{3\pm} =& \frac{m^2_3+m^2_6}{2} - \frac{\Delta m^2_{\rm SB}}{2} \\ & \times \left(\cos 2\theta_{36} \left(\frac{E}{E_{R,3}}\right)^2 \mp \sqrt{\sin^2 2\theta_{36} + \cos^2 2\theta_{36} \left[1 - \left(\frac{E}{E_{R,3}}\right)^2\right]^2} \right) , \end{aligned} \tag{14.8}$$

with the corresponding resonance energies

$$E_{R,1} = \sqrt{\frac{\Delta m^2_{\rm SB} \cos 2\theta_{14}}{2\varepsilon}} , \quad E_{R,2} = \sqrt{\frac{\Delta m^2_{\rm SB} \cos 2\theta_{25}}{2\varepsilon}} , \quad E_{R,3} = \sqrt{\frac{\Delta m^2_{\rm SB} \cos 2\theta_{36}}{2\varepsilon}} . \tag{14.9}$$

All mass-squareds m^2_{i-} approach minus infinity and decouple in the limit $E \gg E_{R,i}$. The mass-squared eigenvalues of interest are again m^2_{i+}, whose values in the limit $E \gg E_{R,i}$ are

$$\lim_{E\to\infty} m^2_{1+} = \frac{1}{2}\left(m^2_1 + m^2_4 + \Delta m^2_{\rm SB} \cdot \cos 2\theta_{14}\right) , \tag{14.10}$$

$$\lim_{E\to\infty} m^2_{2+} = \frac{1}{2}\left(m^2_2 + m^2_5 + \Delta m^2_{\rm SB} \cdot \cos 2\theta_{25}\right) , \tag{14.11}$$

$$\lim_{E\to\infty} m^2_{3+} = \frac{1}{2}\left(m^2_3 + m^2_6 + \Delta m^2_{\rm SB} \cdot \cos 2\theta_{36}\right) , \tag{14.12}$$

while the relevant mass-squared differences far above the resonance become

$$m^2_{2+} - m^2_{1+} = \Delta m^2_{21} + \frac{\Delta m^2_{\rm SB}}{2}\left(\cos 2\theta_{14} - \cos 2\theta_{25}\right) , \tag{14.13}$$

$$m^2_{3+} - m^2_{1+} = \Delta m^2_{31} + \frac{\Delta m^2_{\rm SB}}{2}\left(\cos 2\theta_{14} - \cos 2\theta_{36}\right) , \tag{14.14}$$

$$m^2_{3+} - m^2_{2+} = \Delta m^2_{32} + \frac{\Delta m^2_{\rm SB}}{2}\left(\cos 2\theta_{25} - \cos 2\theta_{36}\right) , \tag{14.15}$$

If these mass-squared differences are all assumed to lie in the same region as the mass-squared difference in the $3 + 1\nu$ case, a corresponding oscillation should be measurable in atmospheric neutrino experiments. Such an “extra" oscillation is not seen.

The only way to avoid the generation of such a mass-squared difference, is by imposing a common mixing in addition to the common potential, i.e. by setting all new mixing angles to the same value: $\theta_{14} = \theta_{25} = \theta_{36} \equiv \theta$. In this case the second terms in Equations (14.13)-(14.15) vanish for all mass-squared differences, and one ends up with the same mass-squared differences as in a standard three neutrino scenario (see Fig. 14.1). Consequently, it is possible to avoid the constraints by atmospheric neutrino experiments. However, as long as the resonance energies for the three sterile neutrinos are assumed to be universal, a new problem arises in the form of a vanishing amplitude for the MiniBooNE experiment in the resonant region.

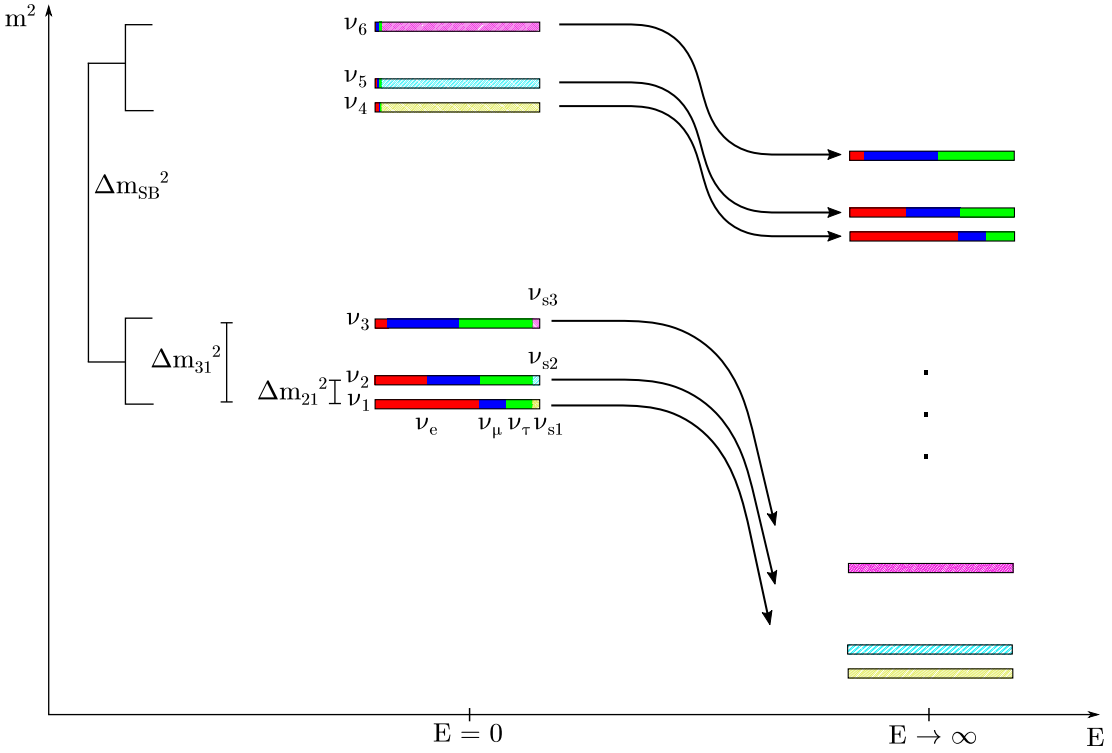

Figure 14.1.: Schematic overview of mass eigenstates and their flavor content depending on the Energy E.

At MiniBooNE or LSND the oscillation probability is governed by the terms where the mass-squared difference is in the Δm^2_{SB} region. These are the mass-squared differences ($\Delta\tilde{m}^2_{41}$, $\Delta\tilde{m}^2_{42}$, $\Delta\tilde{m}^2_{43}$), ($\Delta\tilde{m}^2_{51}$, $\Delta\tilde{m}^2_{52}$, $\Delta\tilde{m}^2_{53}$), and ($\Delta\tilde{m}^2_{61}$, $\Delta\tilde{m}^2_{62}$, $\Delta\tilde{m}^2_{63}$). Approximating these effec-

tive mass squared differences to be equal to Δm_{SB} The transition probability can be factorized as:

$$P_{\nu_\mu \to \nu_e} \sim -4 \sin^2 \left(\Delta m^2_{\mathrm{SB}} \frac{L}{2E} \right) \left(\sum_{j=1,2,3} \tilde{\mathbf{U}}_{\mu j} \tilde{\mathbf{U}}_{ej} \right) \left(\sum_{j=4,5,6} \tilde{\mathbf{U}}_{\mu j} \tilde{\mathbf{U}}_{ej} \right) , \tag{14.16}$$

where $\tilde{\mathbf{U}}$ and $\Delta \tilde{m}^2_{ij}$ indicate the effective mixing matrix and effective mass squared differences diagonalizing the effective Hamiltonian with the additional potential. For simplicity, we define the mixing matrix as

$$\begin{aligned}
\tilde{\mathbf{U}}^{6\times 6} &= \underbrace{(\tilde{\mathbf{U}}_{23}\tilde{\mathbf{U}}_{13}\tilde{\mathbf{U}}_{12})}_{\tilde{\mathbf{U}}_0}(\tilde{\mathbf{U}}_{14}\tilde{\mathbf{U}}_{25}\tilde{\mathbf{U}}_{36}) \\
&= \tilde{\mathbf{U}}_0 \cdot \begin{pmatrix} c_{\tilde\theta} & 0 & 0 & s_{\tilde\theta} & 0 & 0 \\ 0 & 1 & 0 & 0 & 0 & 0 \\ 0 & 0 & 1 & 0 & 0 & 0 \\ -s_{\tilde\theta} & 0 & 0 & c_{\tilde\theta} & 0 & 0 \\ 0 & 0 & 0 & 0 & 1 & 0 \\ 0 & 0 & 0 & 0 & 0 & 1 \end{pmatrix} \begin{pmatrix} 1 & 0 & 0 & 0 & 0 & 0 \\ 0 & c_{\tilde\theta} & 0 & 0 & s_{\tilde\theta} & 0 \\ 0 & 0 & 1 & 0 & 0 & 0 \\ 0 & 0 & 0 & 1 & 0 & 0 \\ 0 & -s_{\tilde\theta} & 0 & 0 & c_{\tilde\theta} & 0 \\ 0 & 0 & 0 & 0 & 0 & 1 \end{pmatrix} \begin{pmatrix} 1 & 0 & 0 & 0 & 0 & 0 \\ 0 & 1 & 0 & 0 & 0 & 0 \\ 0 & 0 & c_{\tilde\theta} & 0 & 0 & s_{\tilde\theta} \\ 0 & 0 & 0 & 1 & 0 & 0 \\ 0 & 0 & 0 & 0 & 1 & 0 \\ 0 & 0 & -s_{\tilde\theta} & 0 & 0 & c_{\tilde\theta} \end{pmatrix} \\
&= \tilde{\mathbf{U}}_0 \cdot \begin{pmatrix} c_{\tilde\theta} \cdot \mathbb{1}_{3\times 3} & s_{\tilde\theta} \cdot \mathbb{1}_{3\times 3} \\ -s_{\tilde\theta} \cdot \mathbb{1}_{3\times 3} & c_{\tilde\theta} \cdot \mathbb{1}_{3\times 3} \end{pmatrix} .
\end{aligned} \tag{14.17}$$

Democratic mixing in vacuum with θ and the same potential for each sterile state also leads to a common effective mixing angle $\tilde\theta = \tilde\theta_{14} = \tilde\theta_{25} = \tilde\theta_{36}$. Since $\tilde{\mathbf{U}}_0$ only describes a rotation in the upper left corner, it can be written as

$$\tilde{\mathbf{U}}_0 = \begin{pmatrix} \tilde{\mathbf{A}}_{3\times 3} & 0_{3\times 3} \\ 0_{3\times 3} & \mathbb{1}_{3\times 3} \end{pmatrix} . \tag{14.18}$$

Any submatrix formed from rotations alone is orthogonal, and therefore unitary. So the submatrix $\tilde{\mathbf{A}}_{3\times 3}$ is *unitary*. The Equations (14.17) (14.18) lead to the full mixing matrix

$$\tilde{\mathbf{U}}^{6\times 6} = \begin{pmatrix} c_\theta \cdot \tilde{\mathbf{A}}_{3\times 3} & s_\theta \cdot \tilde{\mathbf{A}}_{3\times 3} \\ -s_\theta \cdot \mathbb{1}_{3\times 3} & c_\theta \cdot \mathbb{1}_{3\times 3} \end{pmatrix} . \tag{14.19}$$

The oscillation probabilities for LSND and MiniBooNE then reads

$$\begin{aligned}
P_{\nu_\mu \to \nu_e} \sim & -4 \sin^2 \left(\Delta m^2_{\mathrm{SB}} \frac{L}{2E} \right) \times \\
& \times \left(\tilde{\mathbf{U}}_{\mu 1}\tilde{\mathbf{U}}_{e1} + \tilde{\mathbf{U}}_{\mu 2}\tilde{\mathbf{U}}_{e2} + \tilde{\mathbf{U}}_{\mu 3}\tilde{\mathbf{U}}_{e3} \right) \left(\tilde{\mathbf{U}}_{\mu 4}\tilde{\mathbf{U}}_{e4} + \tilde{\mathbf{U}}_{\mu 5}\tilde{\mathbf{U}}_{e5} + \tilde{\mathbf{U}}_{\mu 6}\tilde{\mathbf{U}}_{e6} \right) .
\end{aligned} \tag{14.20}$$

Since the submatrix $\tilde{\mathbf{A}}_{3\times3}$ itself is unitary and the unitarity conditions $\sum_k^6 \tilde{\mathbf{U}}_{\mu k}\tilde{\mathbf{U}}_{ek} = 0$ as well as $\sum_k^3 \tilde{\mathbf{A}}_{\mu k}\tilde{\mathbf{A}}_{ek} = 0$ hold, it is readily seen that both brackets have to vanish when all new mixing angles θ_{ij} are the same. Consequently, a $3+3\nu$ model with three additional sterile neutrinos and a common resonance energy also fails. On the one hand it is indeed possible to avoid the constraints from atmospheric neutrinos above the resonance, if all three sterile neutrinos mix with the same mixing angle. This democratic mixing removes the additional mass-squared differences in the considered region and thereby immunizes the model against constraints from high energy atmospheric neutrinos. On the other hand, however, the democratic mixing simultaneously implies a vanishing transition amplitude for ${}^{(-)}\nu_\mu \to {}^{(-)}\nu_e$ oscillations at MiniBooNE or LSND and consequently invalidates the desired main feature of the model. As we show next, the issue can be resolved by assigning different resonance energies to the different sterile neutrinos.

14.2. Different Effective Potentials for Different Sterile Neutrinos

14.2.1. Treatment of Short Baseline and Atmospheric/Accelerator Experiments

From the previous discussion it becomes clear that both the low energy limit $E \to 0$ and the high energy limit $E \to \infty$ are independent of the specific values of the effective potentials of the different sterile neutrinos. What matters is only that the energy is well below or well above the respective resonance energy. However, there exists the possibility of assigning different resonance energies to the sterile neutrinos (e.g. by tying each sterile neutrino to its own extra dimension). The potentials for the neutrinos do not necessarily have to be the same for each sterile neutrino. If the effective potentials differ, we still expect a resonant behavior around the resonance energy also for ${}^{(-)}\nu_\mu \to {}^{(-)}\nu_e$ transitions: In the intermediate energy region the arguments made in the previous chapter no longer hold since the effective mixing angles differ for the different sterile neutrinos as a consequence of to the different effective potentials. As long as the vacuum mixing angle is the same for all sterile neutrinos, we nevertheless end up with the aforementioned low and high energy behavior.

According to the current best-fit reported by MiniBooNE, we adopt the new mass-squared difference to be $\Delta m^2_{\text{LSND}} = \Delta m^2_{41} = 1.59\,\text{eV}^2$, the vacuum mixing angle to $\sin^2\theta \sim 0.0063$

and the shortcut parameter to $\varepsilon = 5 \cdot 10^{-17}$, resulting in a resonance energy of roughly $E_R \sim 120$ MeV. The effective potential with different shortcut parameters can be written as

$$V_{\text{eff}} = \begin{pmatrix} 0 & 0 & 0 & 0 & 0 & 0 \\ 0 & 0 & 0 & 0 & 0 & 0 \\ 0 & 0 & 0 & 0 & 0 & 0 \\ 0 & 0 & 0 & \varepsilon E & 0 & 0 \\ 0 & 0 & 0 & 0 & \kappa \cdot \varepsilon E & 0 \\ 0 & 0 & 0 & 0 & 0 & \xi \cdot \varepsilon E \end{pmatrix}. \tag{14.21}$$

Due to the larger effective potential for the sterile states $\nu_{s,2}$ and $\nu_{s,3}$ states, the resonance energy becomes smaller and the decoupling of these states happens at lower energies. We chose a rather large factor of $\kappa = \xi = 100$ to generate a resonance not only at MiniBooNE but also at LSND in the energy region of $\sim 20 - 50$ GeV to explain also the excess reported for LSND [49].

In the numerical analysis we adopt the best-fit values from [20] for the standard 3ν mixing angles and mass-squared differences, and assume normal ordering and vanishing CP violation. We also neglect matter effects, since they do not solve the problem we intend to address. Such matter effects are known to exist, and they make a significant difference in the few GeV realm, but the sterile neutrino is already completely decoupled above the highest $E_R \propto 1/\sqrt{\varepsilon}$, due to the ADR potential. The best-fit values for the SM parameters are taken from Table 3.2. Numerical calculations for the oscillation probabilities are shown in Figures 14.2 - 14.6 and the effective squared masses are shown in Fig. 14.7. As can clearly be seen, we can achieve resonant behavior in the ${}^{(-)}\nu_\mu \to {}^{(-)}\nu_e$ channel at MiniBooNE with no significant deviation from three neutrino mixing in atmospheric data: The oscillations amplitudes for ${}^{(-)}\nu_\mu \to {}^{(-)}\nu_{e/\tau}$ at MiniBooNE (Fig. 14.2 (a)/(c)) feature the same resonance pattern. One observes a resonant enhancement of the transition probability in the sub ~ 120 MeV region, combined with a suppression in the energy region above ~ 120 MeV. The latter behavior results from the decoupling of the sterile neutrinos, as can be seen in the oscillations amplitudes for the individual sterile flavors, ${}^{(-)}\nu_\mu \to {}^{(-)}\nu_{s1,2,3}$ (Fig. 14.4 (d)-(f)). The disappearance oscillation probability ${}^{(-)}\nu_\mu \to {}^{(-)}\nu_\mu$ at MiniBooNE (Fig. 14.2 (b)) exhibits a characteristic behavior at the resonance, since the transition into sterile neutrinos dominates in this energy region. A measurement of the survival probability ${}^{(-)}\nu_\mu \to {}^{(-)}\nu_\mu$ at energies at MiniBooNE could thus provide a good test for this model: a depletion of the survival probability significantly higher than the transition to ${}^{(-)}\nu_e$ or ${}^{(-)}\nu_\tau$, would be a clear sign for a transition into sterile neutrinos (i.e. $P_{\nu_\mu \to \nu_s} \neq 0$).

Taking a look at atmospheric experiments in Fig. 14.5, one can observe that in the realm $E >$ GeV, the predictions of this model are exactly the same as in the standard 3ν paradigm, due to the complete decoupling of the sterile states above the highest $E_R \sim 120$ MeV. This decoupling leads to perfect satisfaction of the current fits at these kind of experiments, in contrast to the standard $3+1\nu$ models. A discussion of the sub-GeV region is presented in section 14.2.3.

The same high energy properties as in atmospheric experiments can also be found at MINOS, where one can see the same strong convergence to the 3ν probabilities. MINOS, however, has a neutrino beam with a distinct peak energy at about 7 GeV, and so is blind to the low energy effects to be discussed in Sec. 14.2.3.

14.2.2. Behavior Below the Resonance

Although the transition $\overset{(-)}{\nu}_\mu \to \overset{(-)}{\nu}_{e/\tau}$ vanishes far below the resonance, $\overset{(-)}{\nu}_\mu \to \overset{(-)}{\nu}_{s1,2,3}$ does not vanish due to the vacuum mixing. The same is also true for $\overset{(-)}{\nu}_e \to \overset{(-)}{\nu}_{s1,2,3}$ and $\overset{(-)}{\nu}_\tau \to \overset{(-)}{\nu}_{s1,2,3}$, which is particularly interesting for reactor experiments, which usually operate in the MeV-region, since this model predicts a deviation in the $\bar{\nu}_e \to \bar{\nu}_e$ channel. A good approximation for $\overset{(-)}{\nu}_e \to \overset{(-)}{\nu}_e$ in the low energy region well below the resonances is given by (compare Eq. (14.20)):

$$\begin{aligned} P_{\nu_e \to \nu_e} \sim & 1 - 4 \sin^2 \left(\Delta m^2_{\mathrm{SB}} \frac{L}{2E} \right) \left(U^2_{e1} + U^2_{e2} + U^2_{e3} \right) \left(U^2_{e4} + U^2_{e5} + U^2_{e6} \right) \\ = & 1 - 4 \sin^2 \left(\Delta m^2_{\mathrm{SB}} \frac{L}{2E} \right) \cos^2 \theta \sin^2 \theta \\ = & 1 - \sin^2 \left(\Delta m^2_{\mathrm{SB}} \frac{L}{2E} \right) \sin^2 2\theta \,, \end{aligned} \tag{14.22}$$

where again the unitarity conditions are used. This expression resembles a simple $3 + 1\nu$ model for disappearance experiments in the low energy region, which is actually favored by the Reactor- or Gallium anomalies.

14.2.3. Open Questions

As can be seen in Fig. 14.5, the proposed model resembles three neutrino oscillations far above the resonance (in this case above the GeV region). However, due to the desired resonance at around 120 MeV for explaining the MiniBooNE data, this resonance will also have impact on the sub-GeV neutrinos at atmospheric experiments. The corresponding oscillations in this energy region are plotted in Fig. 14.8. As expected, the model predicts a significant deviation from the simple three neutrino model. Nevertheless, without access to the actual data it is hard to judge whether these oscillation patterns are excluded by current experiments. Previous analyses [111, 112] searched for sterile neutrinos without altered dispersion relations. Oscillation probabilities within the standard 3 neutrino scenario for the range of these searches are also shown in Fig. 14.8 for comparison. While the difference to the probability for the proposed model is obvious, exclusion limits in the literature cannot be adopted for the present case. To either exclude or confirm the model proposed in this article, we recommend a reanalysis of the current sub-GeV data in atmospheric experiments.

In addition, this model can be constrained by cosmology which is addressed in [2] based on previous calculations in [117, 125, 127].

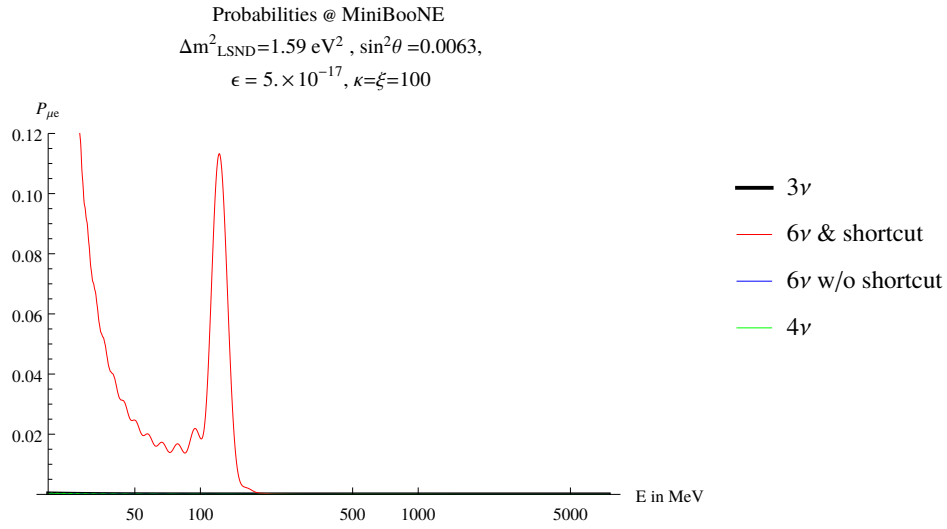

(a) $P_{\nu_\mu \to \nu_e}$

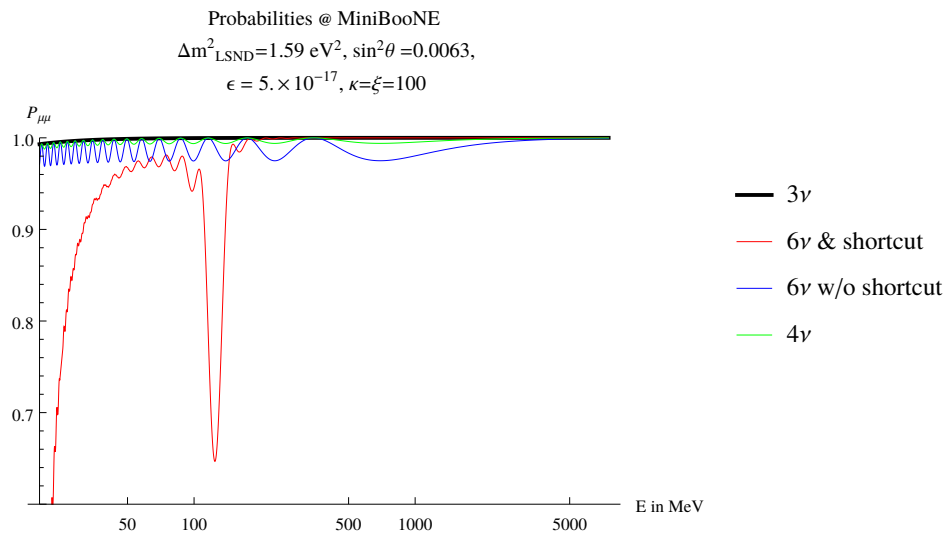

(b) $P_{\nu_\mu \to \nu_\mu}$

Figure 14.2.: Probabilities $P_{\mu e}$ and $P_{\mu\mu}$ at MiniBooNE for different scenarios: The standard three neutrino case (black), the proposed scenario with three additional light sterile neutrinos, democratic mixing and effective potential due to shortcut effects (red), a scenario with three light sterile neutrinos and democratic mixing without effective potential (blue), and a simple 4ν scenario with one additional light sterile neutrino (green).

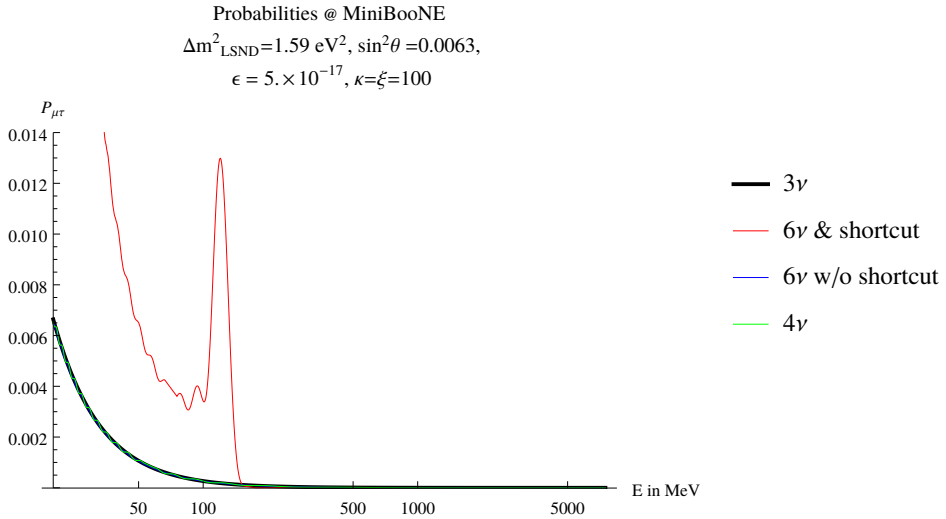

(a) $P_{\nu_\mu \to \nu_\tau}$

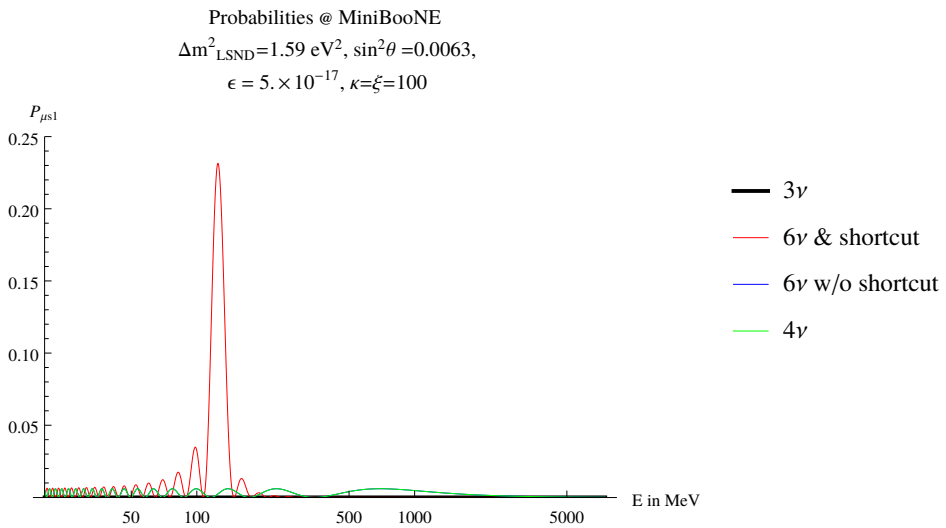

(b) $P_{\nu_\mu \to \nu_{s1}}$

Figure 14.3.: Probabilities $P_{\mu\tau}$ and $P_{\mu s1}$ at MiniBooNE for different scenarios: The standard three neutrino case (black), the proposed scenario with three additional light sterile neutrinos, democratic mixing and effective potential due to shortcut effects (red), a scenario with three light sterile neutrinos and democratic mixing without effective potential (blue), and a simple 4ν scenario with one additional light sterile neutrino (green).

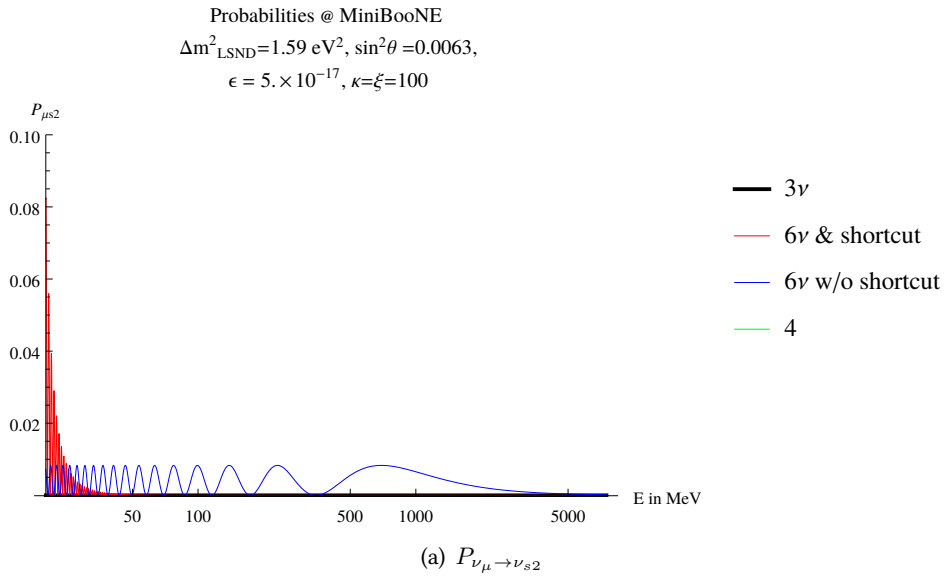

(a) $P_{\nu_\mu \to \nu_{s2}}$

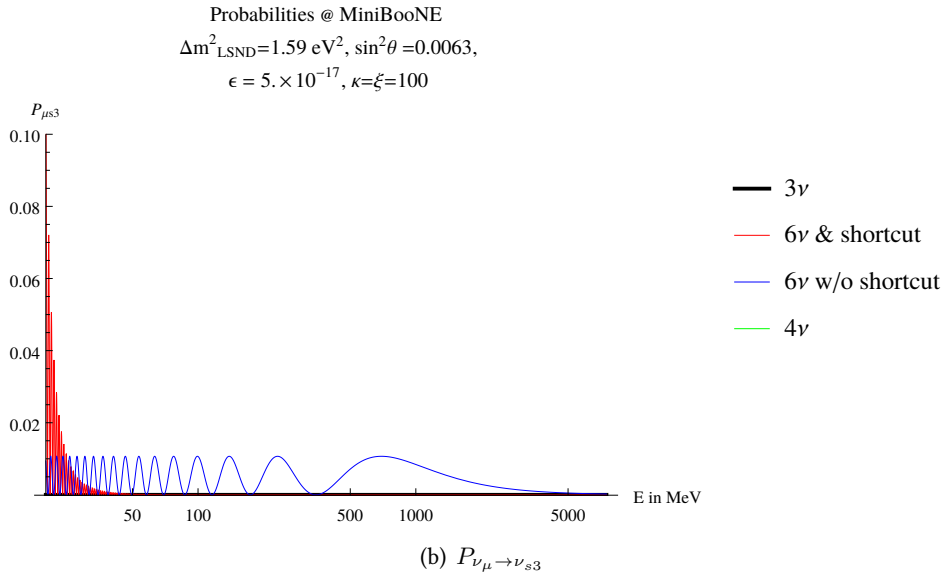

(b) $P_{\nu_\mu \to \nu_{s3}}$

Figure 14.4.: Probabilities $P_{\mu s2}$ and $P_{\mu s3}$ at MiniBooNE for different scenarios: The standard three neutrino case (black), the proposed scenario with three additional light sterile neutrinos, democratic mixing and effective potential due to shortcut effects (red), a scenario with three light sterile neutrinos and democratic mixing without effective potential (blue), and a simple 4ν scenario with one additional light sterile neutrino (green).

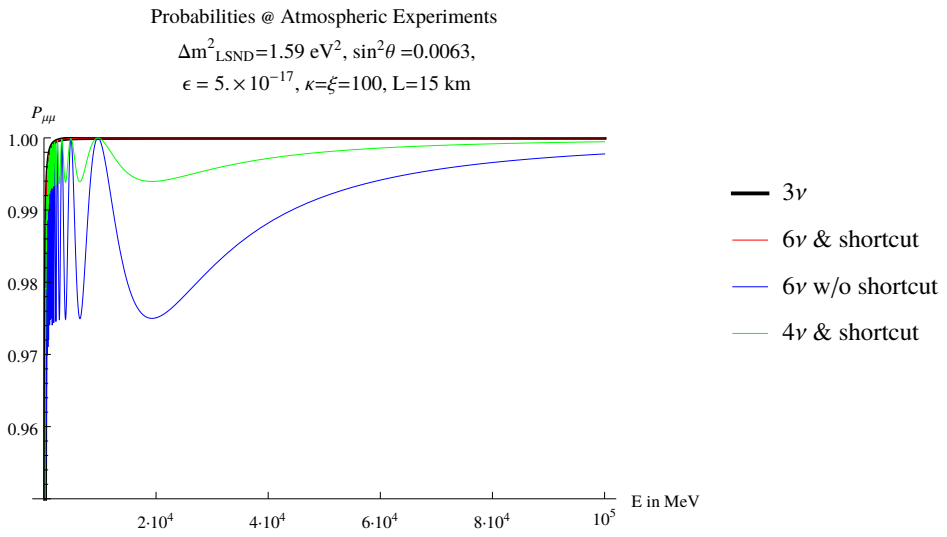

(a) Downward going neutrinos

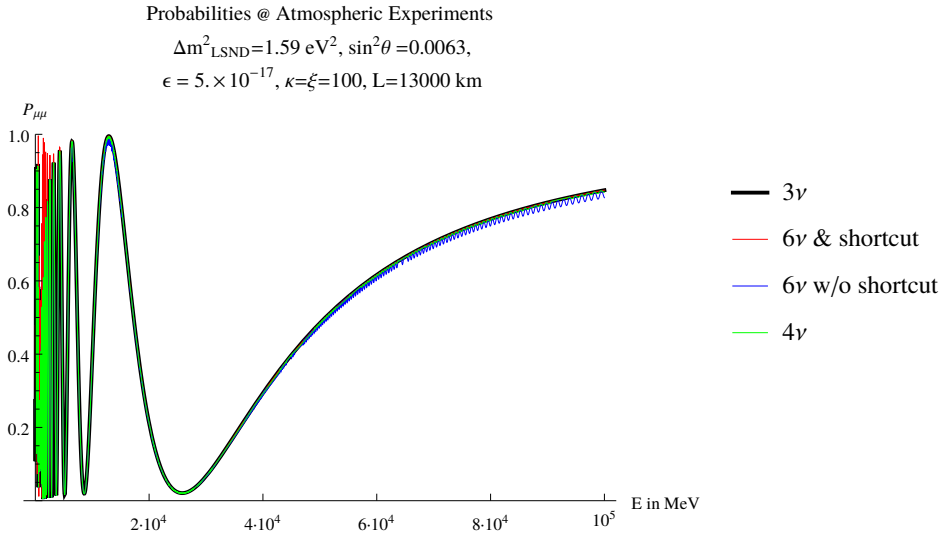

(b) Upward going neutrinos

Figure 14.5.: Different Probabilities at atmospheric neutrino experiments for different scenarios: The standard three neutrino case (black), the proposed scenario with three additional light sterile neutrinos, democratic mixing and effective potential due to shortcut effects (red), a scenario with three light sterile neutrinos and democratic mixing without effective potential (blue), and a simple 4ν scenario with one additional light sterile neutrino (green)

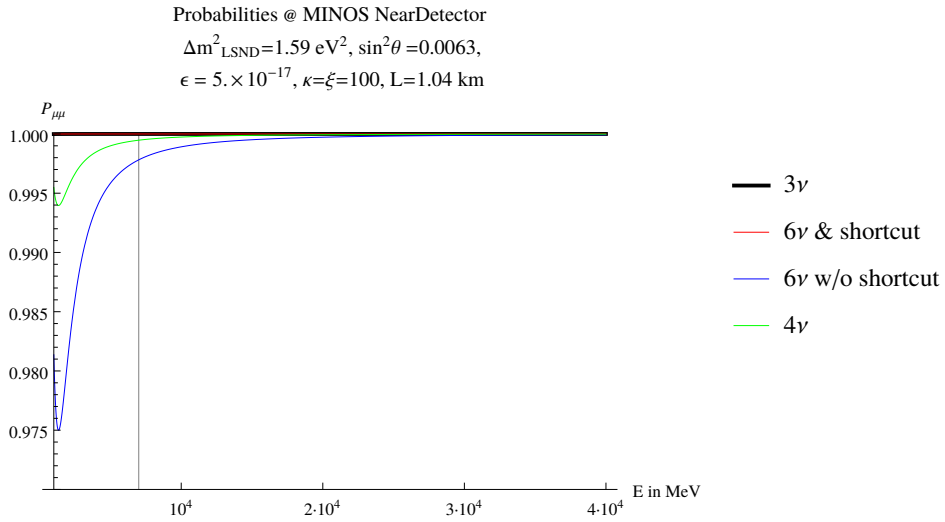

(a) Near Detector

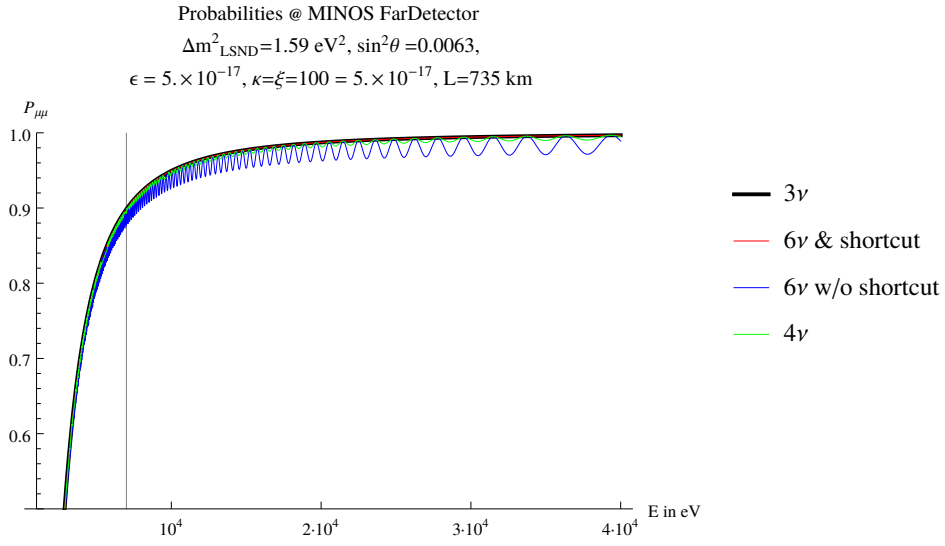

(b) Far Detector

Figure 14.6.: Different Probabilities at MINOS for different scenarios: The standard three neutrino case (black), the proposed scenario with three additional light sterile neutrinos, democratic mixing and effective potential due to shortcut effects (red), a scenario with three light sterile neutrinos and democratic mixing without effective potential (blue), and a simple 4ν scenario with one additional light sterile neutrino (green). The vertical line indicates the peak energy in the spectrum.

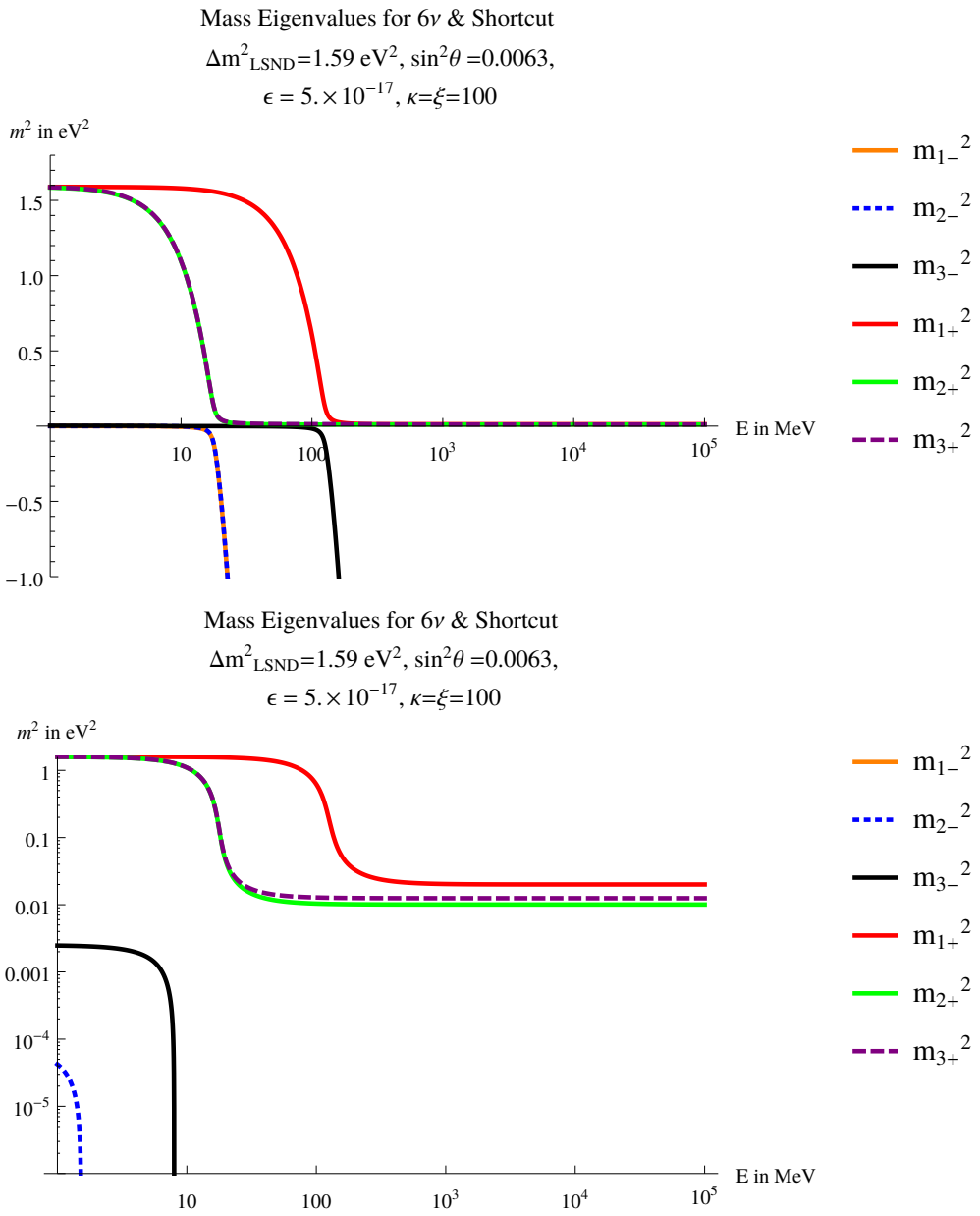

Figure 14.7.: Effective masses squared m^2 depending on the energy E in with linear (top) and logarithmic (bottom) vertical-axis. The effective mass squared m^2_{1-} is not visible in the bottom plot due to its vacuum value $m^2_1 = 0$.

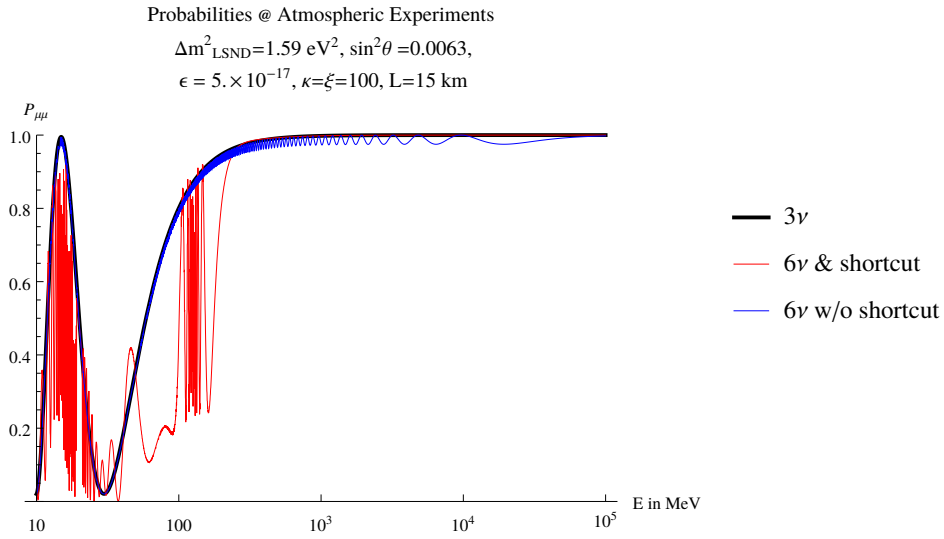

(a) Downward going neutrinos

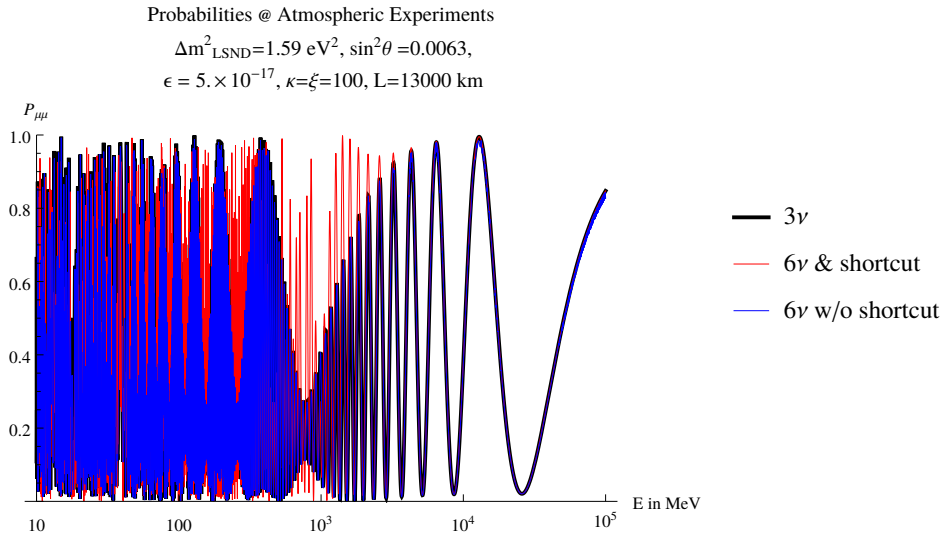

(b) Upward going neutrinos

Figure 14.8.: Different Probabilities at atmospheric neutrino experiments: The standard three neutrino case (black), the proposed scenario with three additional light sterile neutrinos, democratic mixing and effective potential due to shortcut effects (red) and a scenario with three light sterile neutrinos and democratic mixing without effective potential (blue). In contrast to Figure 14.5 here we highlight the Sub-GeV to 10 GeV region.

15. Summary

In this part we have examined in detail the recently reported MiniBooNE anomaly and the discrepancies with other high sensitivity atmospheric and accelerator based neutrino experiments. We have shown that the simplest $3 + 1\nu$ model fails to explain all current data, and also an additional effective potential is not sufficient to explain the high experimental data at experiments with higher energy than MiniBooNE.

Eventually we have developed a $3 + 3\nu$ framework with an altered dispersion relation that indeed is able to explain not only the MiniBooNE anomaly but also the LSND, reactor and Gallium anomaly while not being in conflict with atmospheric or accelerator neutrino experiments. To our best knowledge this is the first framework which successfully can explain all current neutrino oscillation data.

The altered dispersion relation in the presented framework can be caused by shortcuts of the extra sterile neutrinos via extra-dimensions as pointed out in [126], but it is also possible to generate a similar effect by other new physics involved. The key feature in this approach is the democratic vacuum mixing of each of the three sterile states with one of the predominantly active mass eigenstate and the equality of the corresponding mass difference Δm^2_{41}, Δm^2_{52} and Δm^2_{63}. This setup leads directly to to the possibility of describing the oscillation phenomena of disappearing experiments like reactor experiments or GALLEX and SAGE in the low energy region with an effective $1 + 1\nu$ model, explaining the reactor and Gallium anomalies. Simultaneously, in the high energy region of atmospheric and accelerator experiments, the sterile neutrinos affected by the altered dispersion relation decouple completely without changing the standard mass squared differences or mixing angles among the active neutrinos, resembling the standard 3ν model.

In intermediate energy regions the altered dispersion relations cause level crossings among the active and sterile states, implying resonance energies. Due to different effective potentials for the different sterile states, also the resonance energies differ. Therefore, despite democratic vacuum mixing, the transition probability $P_{\nu_\mu \to \nu_e}$ can be enhanced, explaining the resonant feature in MiniBooNE data. The second resonance energy causes the excess in the LSND experiment. Currently the MiniBooNE collaboration is working on a fit of the proposed model to their current data.

Albeit being speculative and inevitably introducing new parameters via the sterile neutrino sector, the proposed approach is capable of solving all current neutrino anomalies at once. While it is possible that these anomalies are due to our limited understanding of experimental backgrounds, the proposed data by the MicroBooNE experiment will clarify this issue at least

for the MiniBooNE data. Additionally, the presented framework is testable by the MicroBooNE and ICARUS experiments and may reveal itself also in sub-GeV atmospheric neutrino data.

Part V.

Conclusion

16. Conclusion and Outlook

In this thesis we have addressed several issues in neutrino oscillation physics. After reviewing the current status of the standard model and the derivation of neutrino oscillations in part I, we have developed a new method to analyze the CP violation in neutrino oscillations in part II. Since current experiments have reached the sensitivity to measure CP violation generated by the CP phase in the leptonic mixing matrix, we have investigated the effect of new physics models on these measurements. The new model independent approach is not bound to unitarity of the 3×3 leptonic mixing matrix and therefore more general than the standard approach. We have focussed on the observable CP violating amplitudes $\mathcal{A}^{kj}_{\alpha\beta}$ and have determined specific analytic relations among them. We have stressed, that in the standard three neutrino scheme a uniform value of all amplitudes $\mathcal{A}^{kj}_{\alpha\beta}$ is predicted, and that any deviation from that will be a sign for new physics. With the presented numerical analysis it is also possible to discriminate between different sources of new physics, i.e. direct or indirect unitarity violation. With the help of the GLoBES package we have performed different analyses for the accelerator experiments T2K and NOvA. We have assumed a large unitarity violation to generate the data and analyzed it within this approach. We have shown that NOvA can constrain the combination $\mathcal{A}^{31}_{e\mu} + \mathcal{A}^{32}_{e\mu}$ significantly and, for suitable parameter settings, may exclude the standard prediction of a uniform amplitude as well as direct unitarity violation. Due to the different setup, T2K is not able to determine this combination. We have also shown, that by using a similar experiment with larger baseline, so that the oscillation driven by Δm^2_{21} can be measured, it is be possible to determine the value of the amplitude $\mathcal{A}^{21}_{e\mu}$. We have also analyzed the role of matter effects and have discussed the challenges arising due to the different potentials for neutrinos and antineutrinos. The matter effect not only leads to energy dependent amplitudes, but also to a non-cancellation of different terms in the probabilities. We have investigated the energy dependence of the amplitudes and provide perspectives for further research. If current experiments come to contradicting conclusions concerning CP violation, we are confident, that the proposed model independent method will provide a powerful tool to determine the source of this effect.

In part III we have investigated the impact of a light sterile neutrino on the determination of the mass ordering at the reactor experiment JUNO. The additional light sterile neutrino generates additional terms in the oscillation probability that influence the sensitivity to the mass ordering. For specific energies it is possible, that the additional terms not only cancel the standard terms sensitive to mass ordering but mimics a term with the opposite mass ordering. This effect requires specific parameter settings which differ depending on the energy. Since the JUNO experiment has a broad energy spectrum and a high energy resolution we have deduced,

that there is no combination of the mixing angle θ_{14} and the mass squared difference Δm^2_{41} that can fake a false mass ordering without generally being detectable by JUNO.

In Part IV we have examined the long existing short baseline anomalies and the currently reported results of a low-energy excess in the MiniBooNE data. It is well known that the simplest explanation for these anomalies, the addition of a single sterile neutrino, is not in agreement with the negative results of accelerator and atmospheric neutrino experiments. We have shown that this disagreement can not be solved by adding an effective MSW-like potential for the sterile state, since it induces additional oscillations in the high energy region. Based on these findings we have developed a model with three additional sterile neutrinos each mixing exclusively with one of the predominantly active mass eigenstates. The angles generating this mixing have same value and the new mass eigenstates are separated from the corresponding predominantly active mass eigenstates by same mass squared difference. If the additional sterile states experience an effective potential, e.g. by extradimensional shortcuts, the sterile states will completely decouple in the high energy limit and the standard three neutrino oscillation is regained, explaining data from atmospheric and accelerator experiments. In the very low energy region, the disappearance probability mimics a $1 + 1$ neutrino scenario, which is favored by the Gallium- and reactor anomalies. In the intermediate energy region, at LSND and MiniBooNE, resonant amplification of the oscillation probability can explain the reported excess of electron neutrino events. The resonances are generated by different effective potentials for the different sterile states. Currently, the MiniBooNE collaboration is working on a fit of this model to their data. This model can be falsified by investigating the low energy data of atmospheric experiments, since the resonances generating the excess at MiniBooNE, also impacts the disappearance probability in this energy region. The upcoming data release of MicroBooNE will also be a test for the MiniBooNE anomaly and for this model as well.

In general current neutrino oscillation experiments will provide a significant increase in data and therefore new possibilities to search for new physics. With the work done in this thesis we provide new testable models and new tools to examine these data.

Part VI.

Appendix

A. Analytic relations of CP violating amplitudes

The following analytic relations have been taken from [78] and translated into the notations used for this paper. All 36 amplitudes can be reduced to a linear combination of the nine amplitudes $\mathcal{A}^{21}_{e\mu}$, $\mathcal{A}^{32}_{e\mu}$, $\mathcal{A}^{43}_{e\mu}$, $\mathcal{A}^{21}_{\mu\tau}$, $\mathcal{A}^{32}_{\mu\tau}$, $\mathcal{A}^{43}_{\mu\tau}$, $\mathcal{A}^{21}_{\tau s}$, $\mathcal{A}^{32}_{\tau s}$ and $\mathcal{A}^{43}_{\tau s}$.

$$
\begin{aligned}
\mathcal{A}^{31}_{e\mu} &= -\mathcal{A}^{32}_{e\mu} + \mathcal{A}^{43}_{e\mu},\\
\mathcal{A}^{41}_{e\mu} &= -\mathcal{A}^{21}_{e\mu} + \mathcal{A}^{32}_{e\mu} - \mathcal{A}^{43}_{e\mu},\\
\mathcal{A}^{42}_{e\mu} &= \mathcal{A}^{21}_{e\mu} - \mathcal{A}^{32}_{e\mu},\\
\mathcal{A}^{21}_{e\tau} &= -\mathcal{A}^{21}_{\mu\tau} + \mathcal{A}^{21}_{\tau s},\\
\mathcal{A}^{31}_{e\tau} &= \mathcal{A}^{32}_{\mu\tau} - \mathcal{A}^{43}_{\mu\tau} - \mathcal{A}^{32}_{\tau s} + \mathcal{A}^{43}_{\tau s},\\
\mathcal{A}^{41}_{e\tau} &= \mathcal{A}^{21}_{\mu\tau} - \mathcal{A}^{32}_{\mu\tau} + \mathcal{A}^{43}_{\mu\tau} - \mathcal{A}^{21}_{\tau s} + \mathcal{A}^{32}_{\tau s} - \mathcal{A}^{43}_{\tau s},\\
\mathcal{A}^{32}_{e\tau} &= -\mathcal{A}^{32}_{\mu\tau} + \mathcal{A}^{32}_{\tau s},\\
\mathcal{A}^{42}_{e\tau} &= -\mathcal{A}^{21}_{\mu\tau} + \mathcal{A}^{32}_{\mu\tau} + \mathcal{A}^{21}_{\tau s} - \mathcal{A}^{32}_{\tau s},\\
\mathcal{A}^{43}_{e\tau} &= -\mathcal{A}^{43}_{\mu\tau} + \mathcal{A}^{43}_{\tau s},\\
\mathcal{A}^{21}_{es} &= -\mathcal{A}^{21}_{e\mu} + \mathcal{A}^{21}_{\mu\tau} - \mathcal{A}^{21}_{\tau s},\\
\mathcal{A}^{31}_{es} &= \mathcal{A}^{32}_{e\mu} - \mathcal{A}^{43}_{e\mu} - \mathcal{A}^{32}_{\mu\tau} + \mathcal{A}^{43}_{\mu\tau} + \mathcal{A}^{32}_{\tau s} - \mathcal{A}^{43}_{\tau s},\\
\mathcal{A}^{41}_{es} &= \mathcal{A}^{21}_{e\mu} - \mathcal{A}^{32}_{e\mu} + \mathcal{A}^{43}_{e\mu} - \mathcal{A}^{21}_{\mu\tau} + \mathcal{A}^{32}_{\mu\tau} - \mathcal{A}^{43}_{\mu\tau} + \mathcal{A}^{21}_{\tau s} - \mathcal{A}^{32}_{\tau s} + \mathcal{A}^{43}_{\tau s},\\
\mathcal{A}^{32}_{es} &= -\mathcal{A}^{32}_{e\mu} + \mathcal{A}^{32}_{\mu\tau} - \mathcal{A}^{32}_{\tau s},\\
\mathcal{A}^{42}_{es} &= -\mathcal{A}^{21}_{e\mu} + \mathcal{A}^{32}_{e\mu} + \mathcal{A}^{21}_{\mu\tau} - \mathcal{A}^{32}_{\mu\tau} - \mathcal{A}^{21}_{\tau s} + \mathcal{A}^{32}_{\tau s}\\
\mathcal{A}^{43}_{es} &= -\mathcal{A}^{43}_{e\tau} + \mathcal{A}^{43}_{\mu\tau} - \mathcal{A}^{43}_{\tau s},\\
\mathcal{A}^{31}_{\mu\tau} &= -\mathcal{A}^{32}_{\mu\tau} + \mathcal{A}^{43}_{\mu\tau},\\
\mathcal{A}^{41}_{\mu\tau} &= -\mathcal{A}^{21}_{\mu\tau} + \mathcal{A}^{32}_{\mu\tau} - \mathcal{A}^{43}_{\mu\tau},\\
\mathcal{A}^{42}_{\mu\tau} &= \mathcal{A}^{21}_{\mu\tau} - \mathcal{A}^{32}_{\mu\tau},\\
\mathcal{A}^{21}_{\mu s} &= \mathcal{A}^{21}_{e\mu} - \mathcal{A}^{21}_{\mu\tau},\\
\mathcal{A}^{31}_{\mu s} &= -\mathcal{A}^{32}_{e\mu} + \mathcal{A}^{43}_{e\mu} + \mathcal{A}^{32}_{\mu\tau} - \mathcal{A}^{43}_{\mu\tau},\\
\mathcal{A}^{41}_{\mu s} &= -\mathcal{A}^{21}_{e\mu} + \mathcal{A}^{32}_{e\mu} - \mathcal{A}^{43}_{e\mu} + \mathcal{A}^{21}_{\mu\tau} - \mathcal{A}^{32}_{\mu\tau} + \mathcal{A}^{43}_{\mu\tau},\\
\mathcal{A}^{32}_{\mu s} &= \mathcal{A}^{32}_{e\mu} - \mathcal{A}^{32}_{\mu\tau},\\
\mathcal{A}^{42}_{\mu s} &= \mathcal{A}^{21}_{e\mu} - \mathcal{A}^{32}_{e\mu} - \mathcal{A}^{21}_{\mu\tau} + \mathcal{A}^{32}_{\mu\tau},\\
\mathcal{A}^{43}_{\mu s} &= \mathcal{A}^{43}_{e\mu} - \mathcal{A}^{43}_{\mu\tau},\\
\mathcal{A}^{31}_{\tau s} &= -\mathcal{A}^{32}_{\tau s} + \mathcal{A}^{43}_{\tau s},\\
\mathcal{A}^{41}_{\tau s} &= -\mathcal{A}^{21}_{\tau s} + \mathcal{A}^{32}_{\tau s} - \mathcal{A}^{43}_{\tau s},\\
\mathcal{A}^{42}_{\tau s} &= \mathcal{A}^{21}_{\tau s} - \mathcal{A}^{32}_{\tau s}.
\end{aligned}
$$

B. Probabilities for $3+1\nu$ with Altered Dispersion Relation.

For illustration we show different probabilities at different energies and baselines in the model with altered dispersion relation and one additional sterile neutrino explained in Section 13.

We consider different mixing schemes of the sterile neutrino, either only via the mixing angle θ_{14} (Figures B.1-B.4), θ_{24} (Figures B.5-B.8) or θ_{34} (Figures B.9-B.12).

The considered experimental setups correspond to MiniBooNE (Figures B.1, B.2, B.5, B.6, B.9 and B.10), atmospheric neutrino oscillation experiments (Figures B.3, B.7 and B.11) and the accelerator experiment MINOS (Figures B.4, B.8 and B.12). While the probabilities at MiniBooNE show a significant resonant feature as reported by the collaboration, the deviations at atmospheric and accelerator experiments are large compared to the three neutrino case for each mixing.

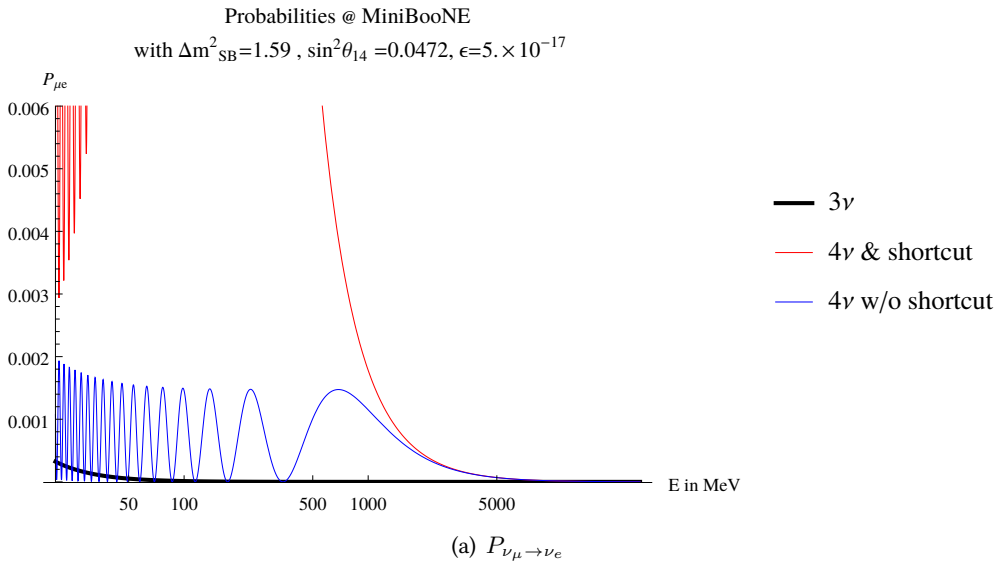

(a) $P_{\nu_\mu \to \nu_e}$

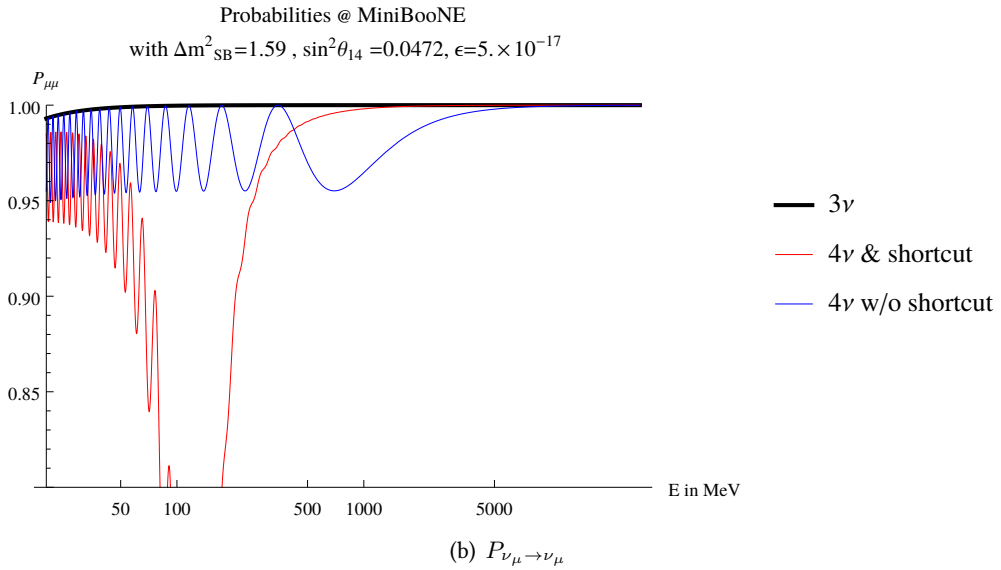

(b) $P_{\nu_\mu \to \nu_\mu}$

Figure B.1.: Probabilities at $P_{\mu e}$ and $P_{\mu\mu}$ MiniBoone for only θ_{14}-mixing

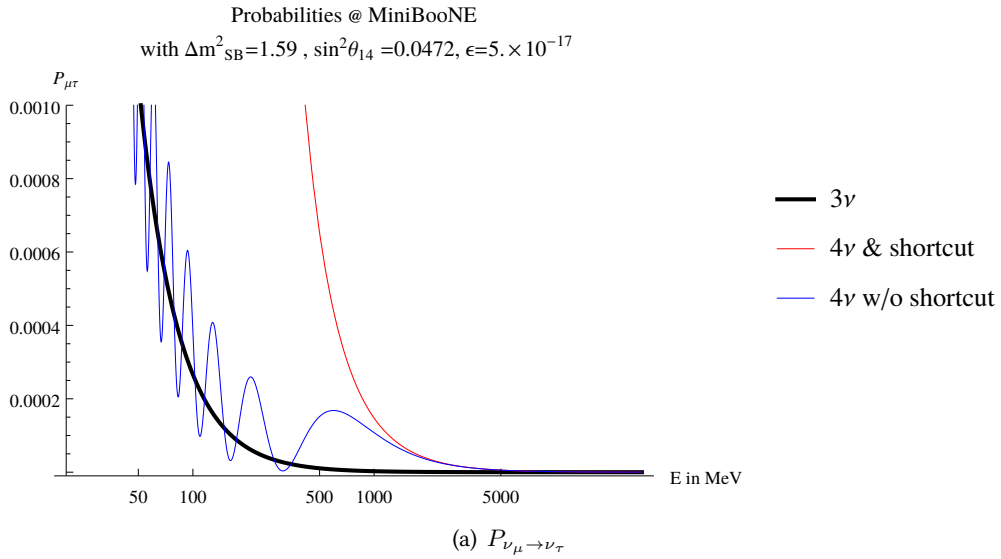

(a) $P_{\nu_\mu \to \nu_\tau}$

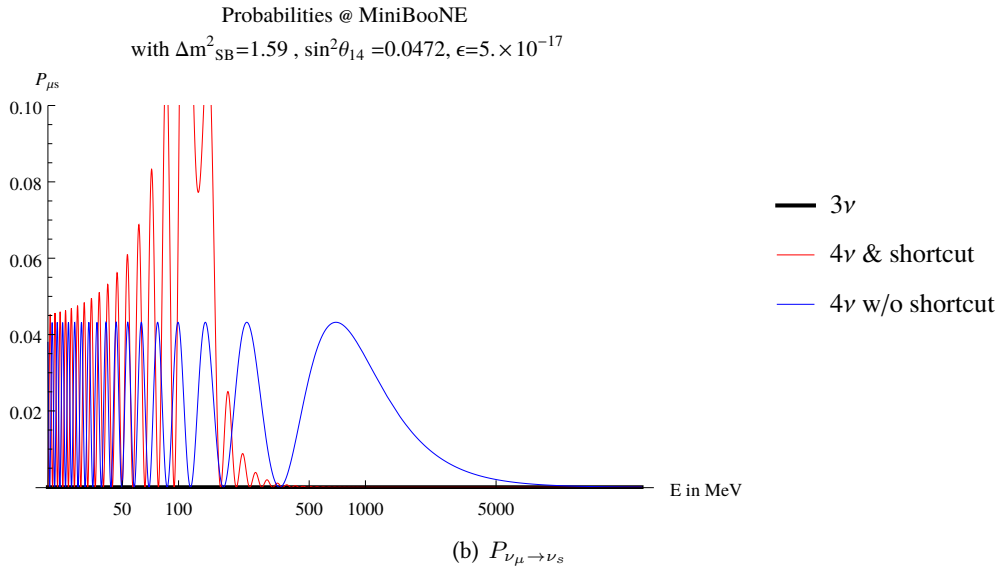

(b) $P_{\nu_\mu \to \nu_s}$

Figure B.2.: Probabilities at $P_{\mu\tau}$ and $P_{\mu s}$ MiniBoone for only θ_{14}-mixing

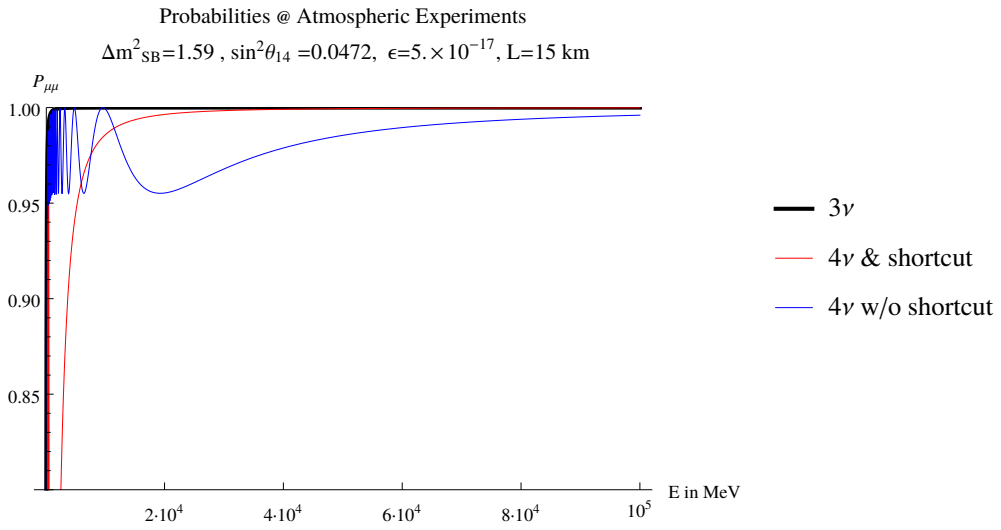

(a) Downward going neutrinos

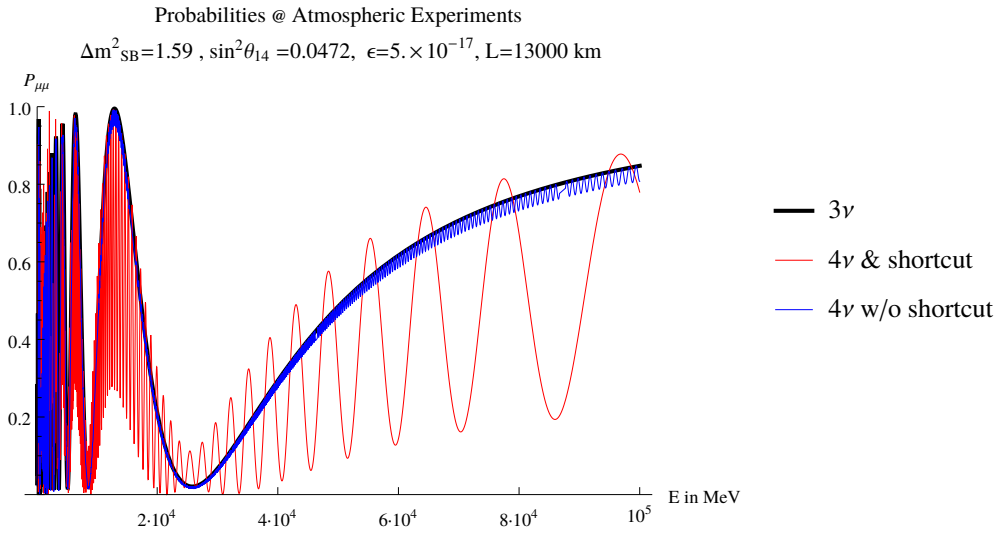

(b) Upward going neutrinos

Figure B.3.: Probability $P_{\mu\mu}$ at atmospheric neutrino experiments for downward and upward going neutrinos for only θ_{14}-mixing

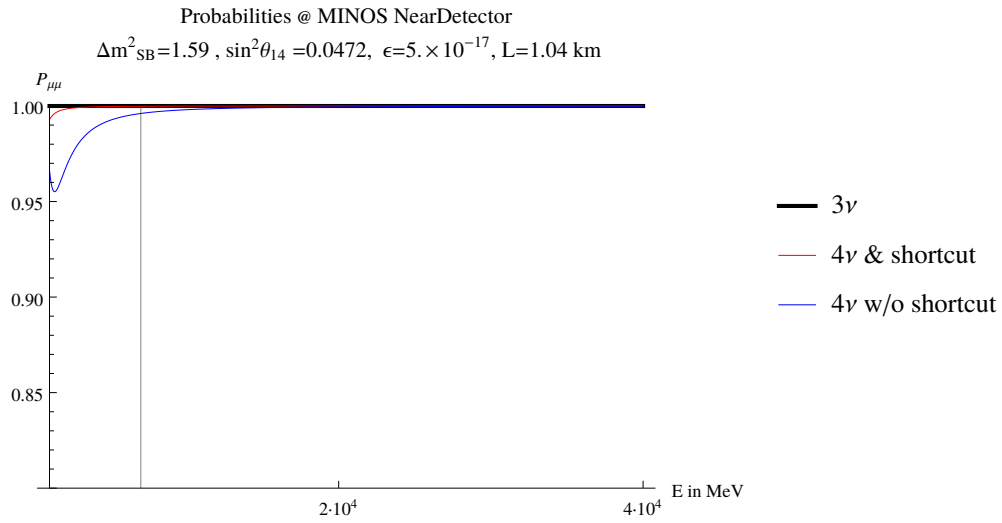

(a) Near Detector

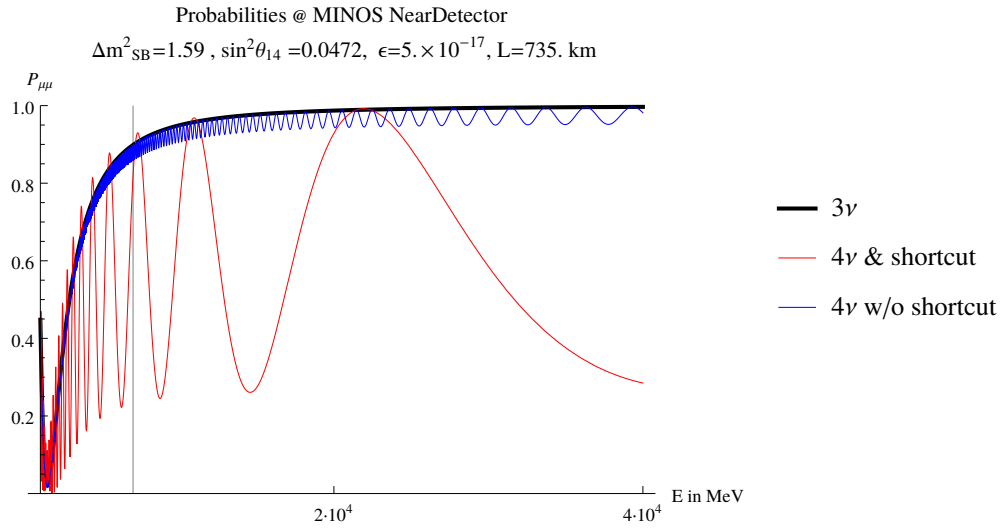

(b) Far Detector

Figure B.4.: Probability $P_{\mu\mu}$ at MINOS for only θ_{14}-mixing, the vertical line indicates the peak energy in the spectrum.

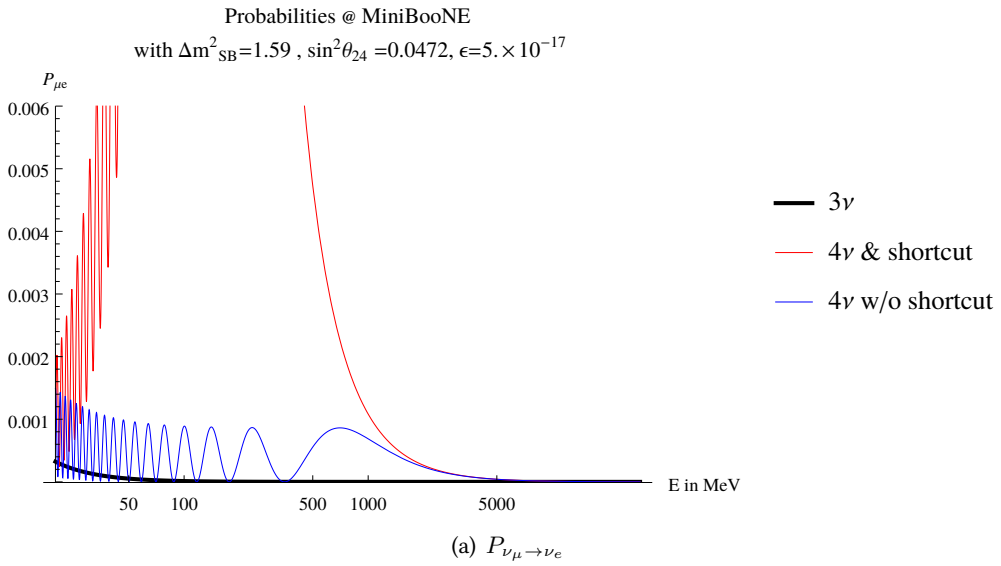

(a) $P_{\nu_\mu \to \nu_e}$

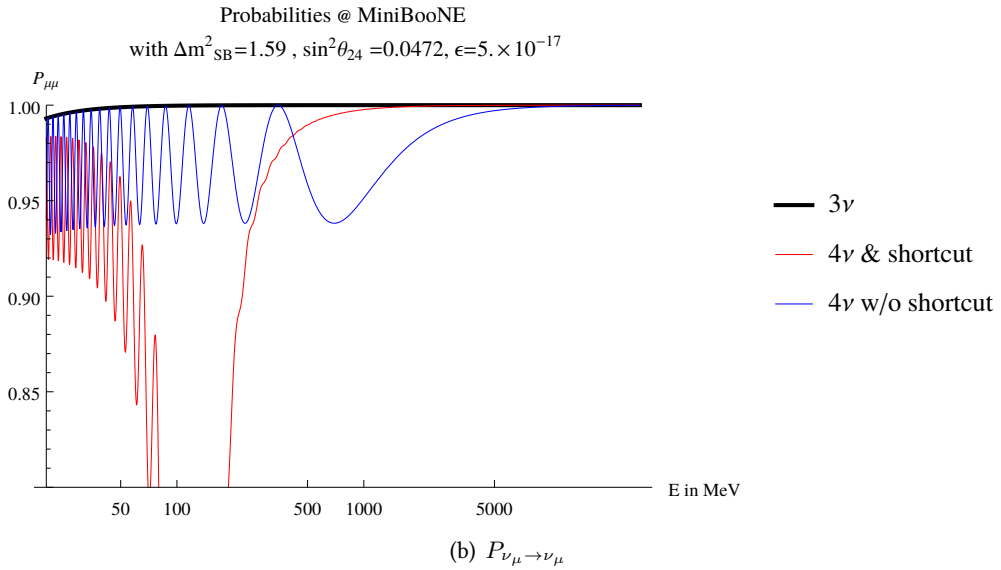

(b) $P_{\nu_\mu \to \nu_\mu}$

Figure B.5.: Probabilities at $P_{\mu e}$ and $P_{\mu\mu}$ MiniBoone for only θ_{24}-mixing

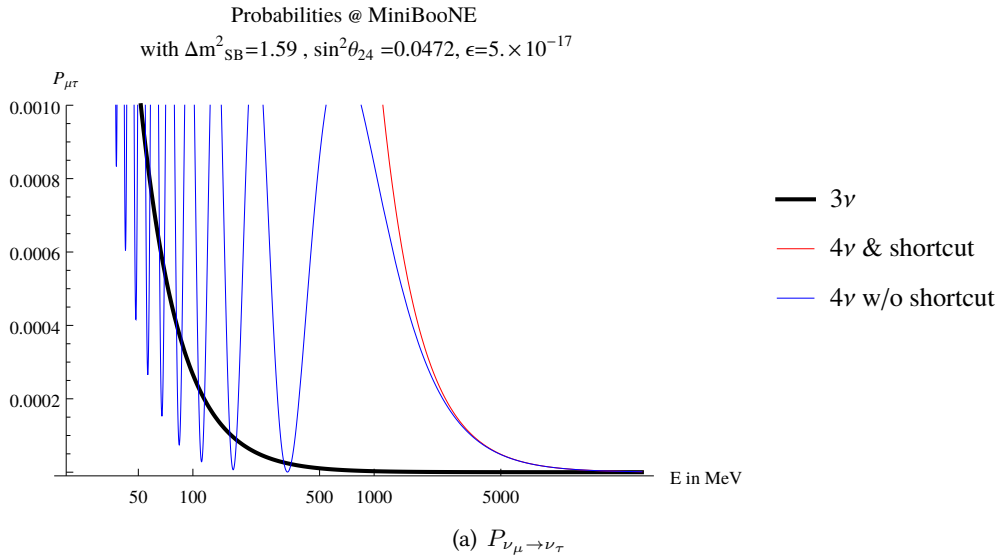

(a) $P_{\nu_\mu \to \nu_\tau}$

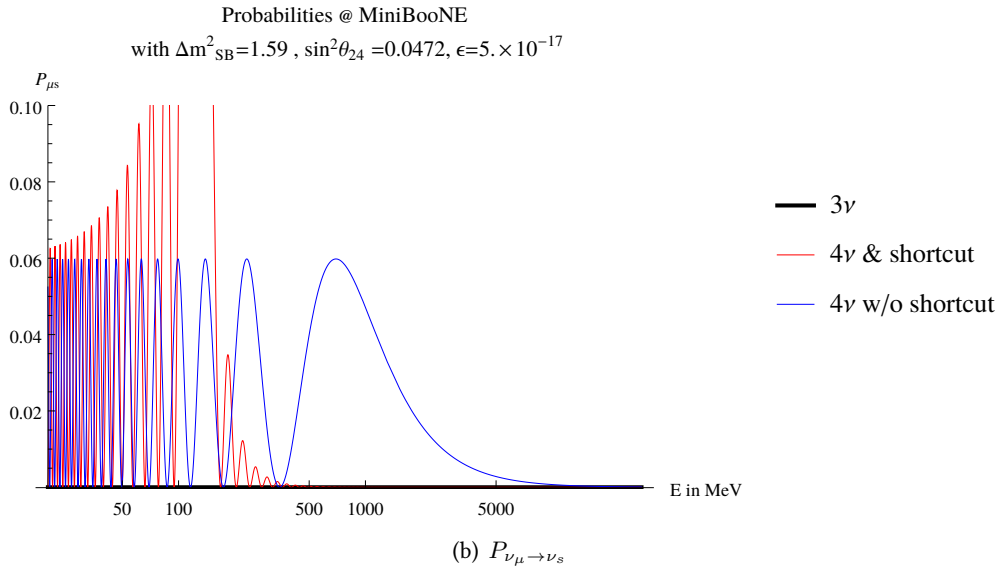

(b) $P_{\nu_\mu \to \nu_s}$

Figure B.6.: Probabilities at $P_{\mu\tau}$ and $P_{\mu s}$ MiniBoone for only θ_{24}-mixing

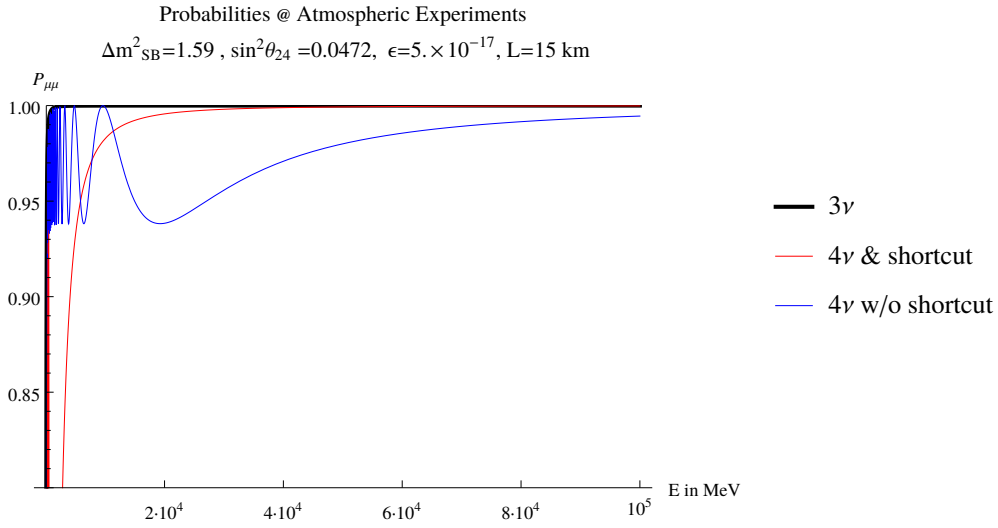

(a) Downward going neutrinos

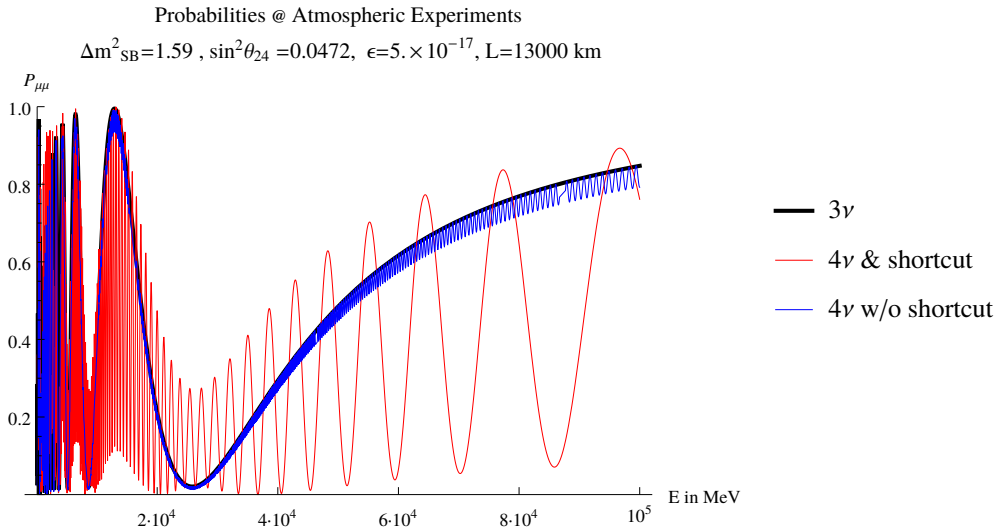

(b) Upward going neutrinos

Figure B.7.: Probability $P_{\mu\mu}$ at atmospheric neutrino experiments for downward and upward going neutrinos for only θ_{24}-mixing

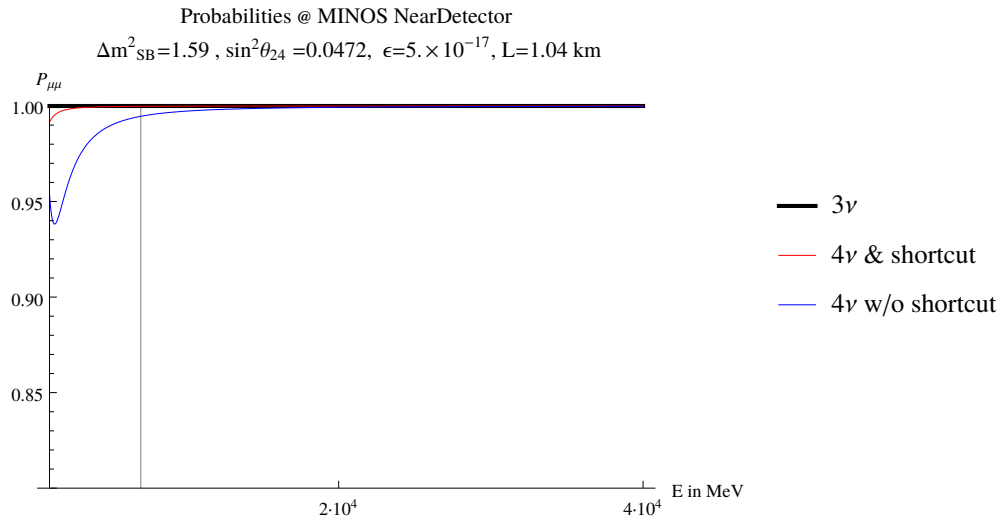

(a) Near Detector

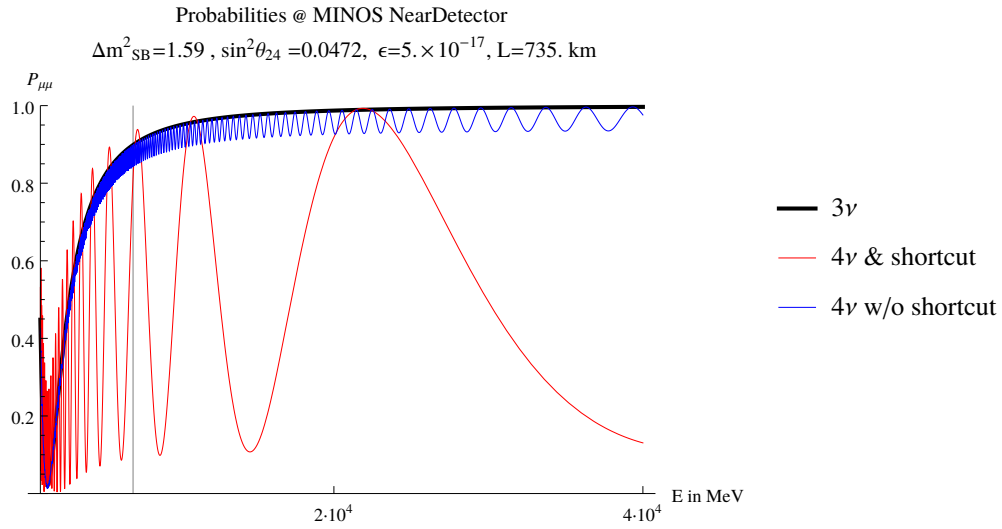

(b) Far Detector

Figure B.8.: Probability $P_{\mu\mu}$ at MINOS for only θ_{24}-mixing, the vertical line indicates the peak energy in the spectrum.

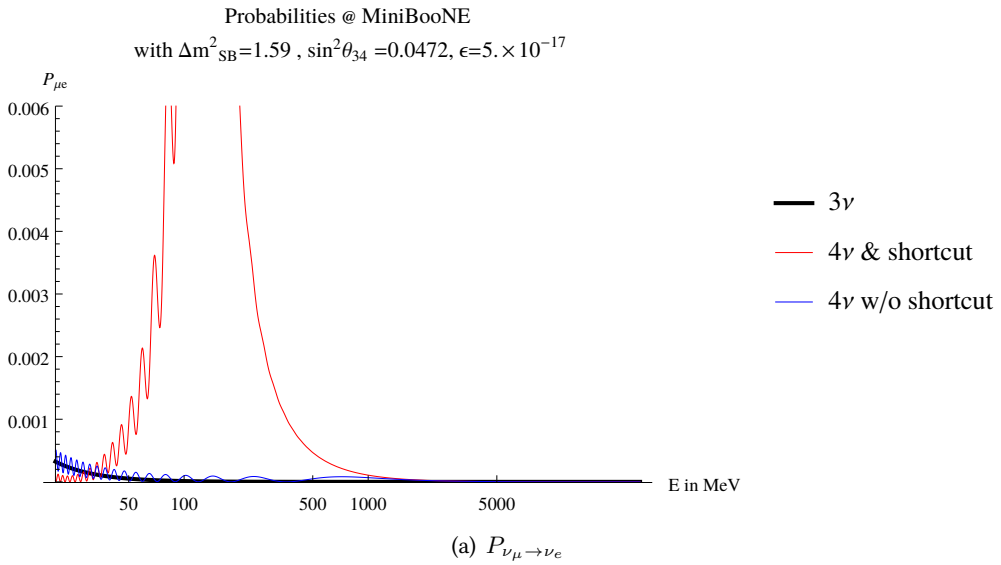

(a) $P_{\nu_\mu \to \nu_e}$

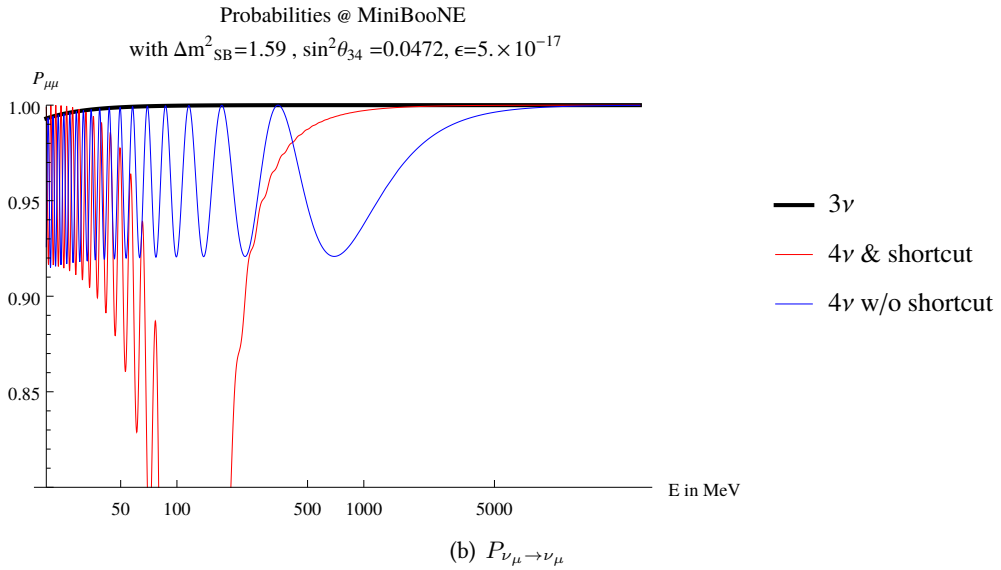

(b) $P_{\nu_\mu \to \nu_\mu}$

Figure B.9.: Probabilities at $P_{\mu e}$ and $P_{\mu\mu}$ MiniBoone for only θ_{34}-mixing

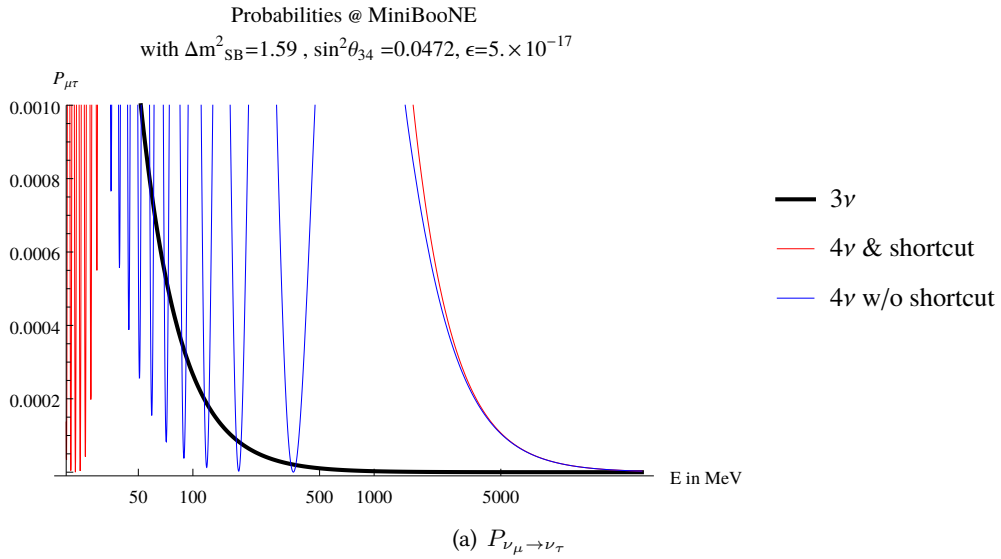

(a) $P_{\nu_\mu \to \nu_\tau}$

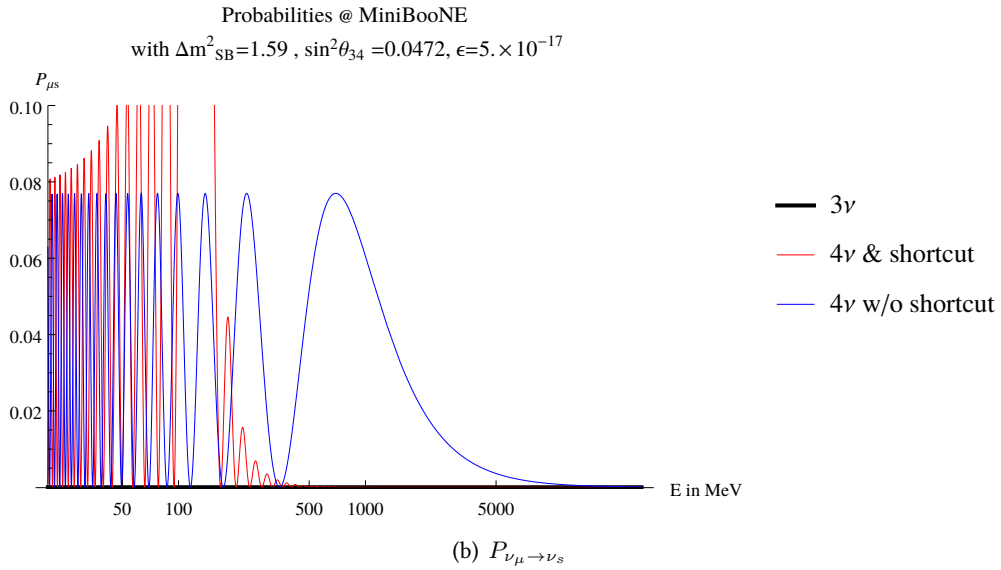

(b) $P_{\nu_\mu \to \nu_s}$

Figure B.10.: Probabilities at $P_{\mu\tau}$ and $P_{\mu s}$ MiniBoone for only θ_{34}-mixing

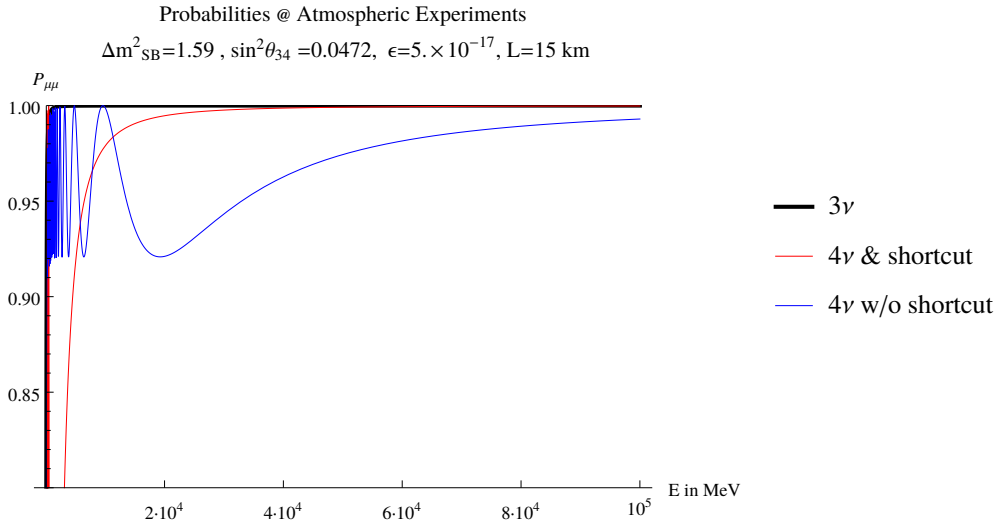

(a) Downward going neutrinos

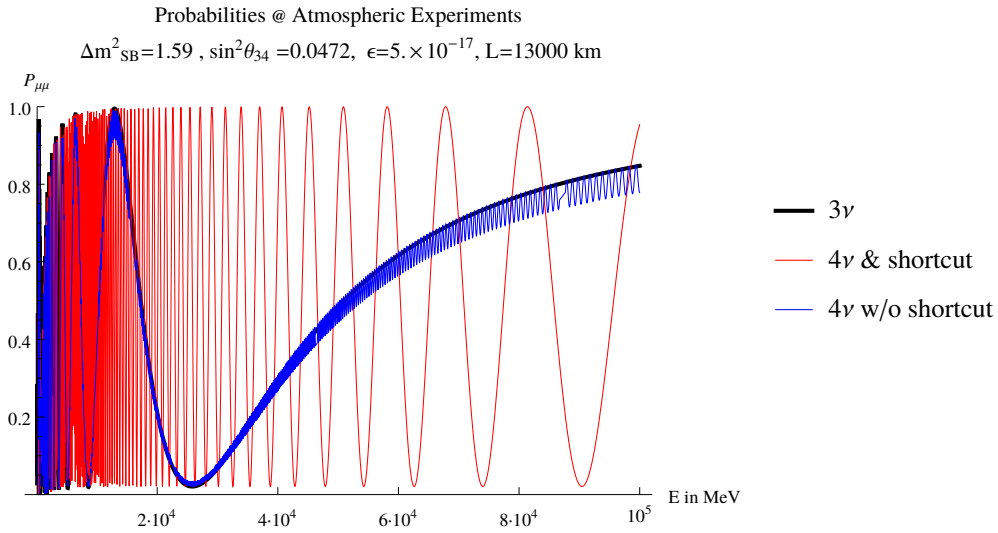

(b) Upward going neutrinos

Figure B.11.: Probability $P_{\mu\mu}$ at atmospheric neutrino experiments for downward and upward going neutrinos for only θ_{34}-mixing

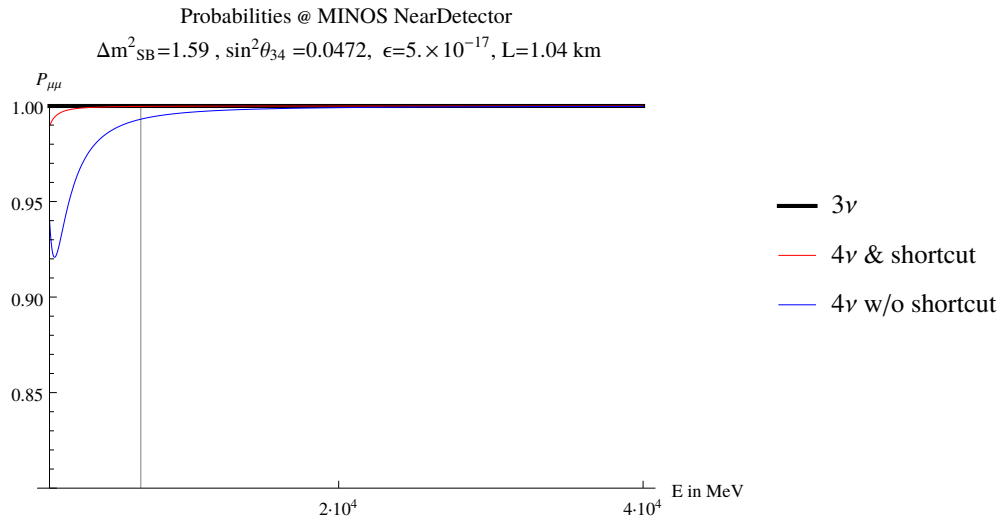

(a) Near Detector

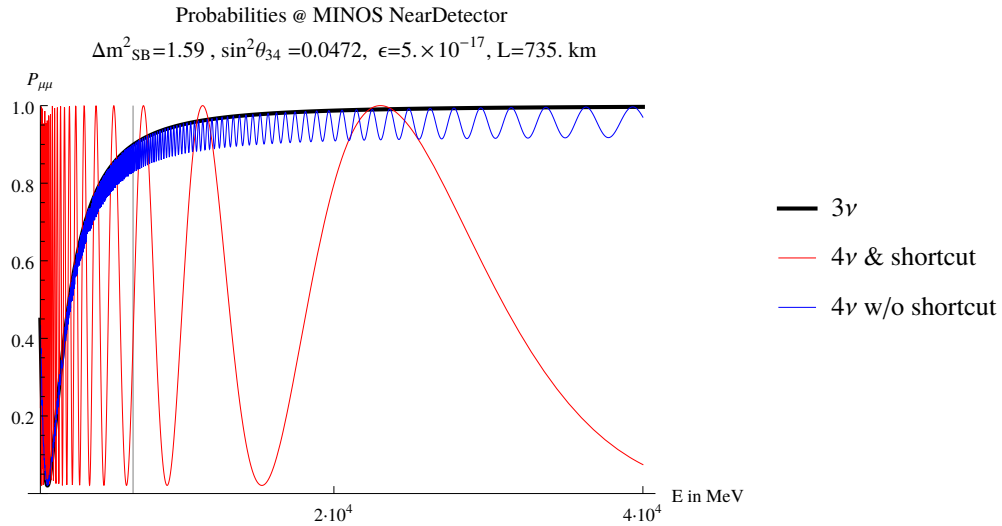

(b) Far Detector

Figure B.12.: Probability $P_{\mu\mu}$ at MINOS for only θ_{34}-mixing, the vertical line indicates the peak energy in the spectrum.

Bibliography

[1] Heinrich Päs and Philipp Sicking. "Discriminating sterile neutrinos and unitarity violation with CP invariants". In: *Phys. Rev.* D95.7 (2017), p. 075004. DOI: 10.1103/PhysRevD.95.075004. arXiv: 1611.08450 [hep-ph].

[2] Dominik Döring et al. "Sterile Neutrinos with Altered Dispersion Relations as an Explanation for the MiniBooNE, LSND, Gallium and Reactor Anomalies". In: (2018). arXiv: 1808.07460 [hep-ph].

[3] W. Pauli. "Dear radioactive ladies and gentlemen". In: *Phys. Today* 31N9 (1978), p. 27.

[4] Wolfgang Pauli. *Fünf Arbeiten Zum Ausschliessungsprinzip Und Zum Neutrino. (German) [Five works on the Exclusion Principle and the neutrino]*. German. Vol. 27. Texte zur Forschung. Wissenschaftliche Buchgesellschaft, 1977, p. 121. ISBN: 3-534-06733-9.

[5] C. L. Cowan et al. "Detection of the free neutrino: A Confirmation". In: *Science* 124 (1956), pp. 103–104. DOI: 10.1126/science.124.3212.103.

[6] G. Danby et al. "Observation of High-Energy Neutrino Reactions and the Existence of Two Kinds of Neutrinos". In: *Phys. Rev. Lett.* 9 (1962), pp. 36–44. DOI: 10.1103/PhysRevLett.9.36.

[7] K. Kodama et al. "Observation of tau neutrino interactions". In: *Phys. Lett.* B504 (2001), pp. 218–224. DOI: 10.1016/S0370-2693(01)00307-0. arXiv: hep-ex/0012035 [hep-ex].

[8] B. T. Cleveland et al. "Measurement of the solar electron neutrino flux with the Homestake chlorine detector". In: *Astrophys. J.* 496 (1998), pp. 505–526. DOI: 10.1086/305343.

[9] S. P. Mikheev and A. Yu. Smirnov. "Resonant amplification of neutrino oscillations in matter and solar neutrino spectroscopy". In: *Nuovo Cim.* C9 (1986), pp. 17–26. DOI: 10.1007/BF02508049.

[10] L. Wolfenstein. "Neutrino Oscillations in Matter". In: *Phys. Rev.* D17 (1978). [,294(1977)], pp. 2369–2374. DOI: 10.1103/PhysRevD.17.2369.

[11] Q. R. Ahmad et al. "Direct evidence for neutrino flavor transformation from neutral current interactions in the Sudbury Neutrino Observatory". In: *Phys. Rev. Lett.* 89 (2002), p. 011301. DOI: 10.1103/PhysRevLett.89.011301. arXiv: nucl-ex/0204008 [nucl-ex].

[12] Y. Fukuda et al. "Evidence for oscillation of atmospheric neutrinos". In: *Phys. Rev. Lett.* 81 (1998), pp. 1562–1567. DOI: 10.1103/PhysRevLett.81.1562. arXiv: hep-ex/9807003 [hep-ex].

[13] Joshua Ellis. "TikZ-Feynman: Feynman diagrams with TikZ". In: *Comput. Phys. Commun.* 210 (2017), pp. 103–123. DOI: 10.1016/j.cpc.2016.08.019. arXiv: 1601.05437 [hep-ph].

[14] B. Pontecorvo. "Inverse beta processes and nonconservation of lepton charge". In: *Sov. Phys. JETP* 7 (1958). [Zh. Eksp. Teor. Fiz.34,247(1957)], pp. 172–173.

[15] Ziro Maki, Masami Nakagawa, and Shoichi Sakata. "Remarks on the unified model of elementary particles". In: *Prog. Theor. Phys.* 28 (1962). [,34(1962)], pp. 870–880. DOI: 10.1143/PTP.28.870.

[16] Vadim O. Egorov and Igor P. Volobuev. "Neutrino oscillation processes in a quantum-field-theoretical approach". In: *Phys. Rev.* D97.9 (2018), p. 093002. DOI: 10.1103/PhysRevD.97.093002. arXiv: 1709.09915 [hep-ph].

[17] P. F. de Salas et al. "Status of neutrino oscillations 2018: 3σ hint for normal mass ordering and improved CP sensitivity". In: *Phys. Lett.* B782 (2018), pp. 633–640. DOI: 10.1016/j.physletb.2018.06.019. arXiv: 1708.01186 [hep-ph].

[18] P. F. De Salas et al. "Neutrino Mass Ordering from Oscillations and Beyond: 2018 Status and Future Prospects". In: (2018). DOI: 10.3389/fspas.2018.00036. arXiv: 1806.11051 [hep-ph].

[19] F. Capozzi et al. "Current unknowns in the three neutrino framework". In: *Prog. Part. Nucl. Phys.* 102 (2018), pp. 48–72. DOI: 10.1016/j.ppnp.2018.05.005. arXiv: 1804.09678 [hep-ph].

[20] C. Patrignani et al. "Review of Particle Physics". In: *Chin. Phys.* C40.10 (2016), p. 100001. DOI: 10.1088/1674-1137/40/10/100001.

[21] André de Gouvêa. "Neutrino Mass Models". In: *Ann. Rev. Nucl. Part. Sci.* 66 (2016), pp. 197–217. DOI: 10.1146/annurev-nucl-102115-044600.

[22] S. F. King. "Neutrino mass models". In: *Rept. Prog. Phys.* 67 (2004), pp. 107–158. DOI: 10.1088/0034-4885/67/2/R01. arXiv: hep-ph/0310204 [hep-ph].

[23] Heinrich Päs and Werner Rodejohann. "Neutrinoless Double Beta Decay". In: *New J. Phys.* 17.11 (2015), p. 115010. DOI: 10.1088/1367-2630/17/11/115010. arXiv: 1507.00170 [hep-ph].

[24] Stefano Dell'Oro et al. "Neutrinoless double beta decay: 2015 review". In: *Adv. High Energy Phys.* 2016 (2016), p. 2162659. DOI: 10.1155/2016/2162659. arXiv: 1601.07512 [hep-ph].

[25] J. Schechter and J. W. F. Valle. "Neutrinoless Double beta Decay in SU(2) x U(1) Theories". In: *Phys. Rev.* D25 (1982). [,289(1981)], p. 2951. DOI: 10.1103/PhysRevD.25.2951.

[26] Jose F. Nieves. "Dirac and Pseudodirac Neutrinos and Neutrinoless Double Beta Decay". In: *Phys. Lett.* 147B (1984), pp. 375–379. DOI: 10.1016/0370-2693(84)90136-9.

[27] Eiichi Takasugi. "Can the Neutrinoless Double Beta Decay Take Place in the Case of Dirac Neutrinos?" In: *Phys. Lett.* 149B (1984), pp. 372–376. DOI: 10.1016/0370-2693(84)90426-X.

[28] T. Bloxham et al. "First results on double beta decay modes of Cd, Te and Zn isotopes with the COBRA experiment". In: *Phys. Rev.* C76 (2007), p. 025501. DOI: 10.1103/PhysRevC.76.025501. arXiv: 0707.2756 [nucl-ex].

[29] K. Alfonso et al. "Search for Neutrinoless Double-Beta Decay of ^{130}Te with CUORE-0". In: *Phys. Rev. Lett.* 115.10 (2015), p. 102502. DOI: 10.1103/PhysRevLett.115.102502. arXiv: 1504.02454 [nucl-ex].

[30] M. Auger et al. "Search for Neutrinoless Double-Beta Decay in ^{136}Xe with EXO-200". In: *Phys. Rev. Lett.* 109 (2012), p. 032505. DOI: 10.1103/PhysRevLett.109.032505. arXiv: 1205.5608 [hep-ex].

[31] M. Agostini et al. "Improved Limit on Neutrinoless Double-β Decay of ^{76}Ge from GERDA Phase II". In: *Phys. Rev. Lett.* 120.13 (2018), p. 132503. DOI: 10.1103/PhysRevLett.120.132503. arXiv: 1803.11100 [nucl-ex].

[32] A. Gando et al. "Limit on Neutrinoless $\beta\beta$ Decay of ^{136}Xe from the First Phase of KamLAND-Zen and Comparison with the Positive Claim in ^{76}Ge". In: *Phys. Rev. Lett.* 110.6 (2013), p. 062502. DOI: 10.1103/PhysRevLett.110.062502. arXiv: 1211.3863 [hep-ex].

[33] A. Gando et al. "Search for Majorana Neutrinos near the Inverted Mass Hierarchy Region with KamLAND-Zen". In: *Phys. Rev. Lett.* 117.8 (2016). [Addendum: Phys. Rev. Lett.117,no.10,109903(2016)], p. 082503. DOI: 10.1103/PhysRevLett.117.109903, 10.1103/PhysRevLett.117.082503. arXiv: 1605.02889 [hep-ex].

[34] N. Aghanim et al. "Planck 2018 results. VI. Cosmological parameters". In: (2018). arXiv: 1807.06209 [astro-ph.CO].

[35] A. D. Sakharov. "Violation of CP Invariance, C asymmetry, and baryon asymmetry of the universe". In: *Pisma Zh. Eksp. Teor. Fiz.* 5 (1967). [Usp. Fiz. Nauk161,no.5,61(1991)], pp. 32–35. DOI: 10.1070/PU1991v034n05ABEH002497.

[36] Peter Minkowski. "$\mu \to e\gamma$ at a Rate of One Out of 10^9 Muon Decays?" In: *Phys. Lett.* 67B (1977), pp. 421–428. DOI: 10.1016/0370-2693(77)90435-X.

[37] Rabindra N. Mohapatra and Goran Senjanovic. "Neutrino Mass and Spontaneous Parity Violation". In: *Phys. Rev. Lett.* 44 (1980). [,231(1979)], p. 912. DOI: 10.1103/PhysRevLett.44.912.

[38] Tsutomu Yanagida. "Horizontal Symmetry and Masses of Neutrinos". In: *Prog. Theor. Phys.* 64 (1980), p. 1103. DOI: 10.1143/PTP.64.1103.

[39] Murray Gell-Mann, Pierre Ramond, and Richard Slansky. "Complex Spinors and Unified Theories". In: *Conf. Proc.* C790927 (1979), pp. 315–321. arXiv: 1306.4669 [hep-th].

[40] Ernest Ma. "Pathways to naturally small neutrino masses". In: *Phys. Rev. Lett.* 81 (1998), pp. 1171–1174. DOI: 10.1103/PhysRevLett.81.1171. arXiv: hep-ph/9805219 [hep-ph].

[41] F. Maltoni, J. M. Niczyporuk, and S. Willenbrock. "Upper bound on the scale of Majorana neutrino mass generation". In: *Phys. Rev. Lett.* 86 (2001), pp. 212–215. DOI: 10.1103/PhysRevLett.86.212. arXiv: hep-ph/0006358 [hep-ph].

[42] A. Zee. "A Theory of Lepton Number Violation, Neutrino Majorana Mass, and Oscillation". In: *Phys. Lett.* 93B (1980). [Erratum: Phys. Lett.95B,461(1980)], p. 389. DOI: 10.1016/0370-2693(80)90349-4, 10.1016/0370-2693(80)90193-8.

[43] Lincoln Wolfenstein. "A Theoretical Pattern for Neutrino Oscillations". In: *Nucl. Phys.* B175 (1980), pp. 93–96. DOI: 10.1016/0550-3213(80)90004-8.

[44] A. Zee. "Quantum Numbers of Majorana Neutrino Masses". In: *Nucl. Phys.* B264 (1986), pp. 99–110. DOI: 10.1016/0550-3213(86)90475-X.

[45] K. S. Babu. "Model of 'Calculable' Majorana Neutrino Masses". In: *Phys. Lett.* B203 (1988), pp. 132–136. DOI: 10.1016/0370-2693(88)91584-5.

[46] Ernest Ma. "Verifiable radiative seesaw mechanism of neutrino mass and dark matter". In: *Phys. Rev.* D73 (2006), p. 077301. DOI: 10.1103/PhysRevD.73.077301. arXiv: hep-ph/0601225 [hep-ph].

[47] P. F. Harrison, D. H. Perkins, and W. G. Scott. "Tri-bimaximal mixing and the neutrino oscillation data". In: *Phys. Lett.* B530 (2002), p. 167. DOI: 10.1016/S0370-2693(02)01336-9. arXiv: hep-ph/0202074 [hep-ph].

[48] Guido Altarelli and Ferruccio Feruglio. "Discrete Flavor Symmetries and Models of Neutrino Mixing". In: *Rev. Mod. Phys.* 82 (2010), pp. 2701–2729. DOI: 10.1103/RevModPhys.82.2701. arXiv: 1002.0211 [hep-ph].

[49] A. Aguilar-Arevalo et al. "Evidence for neutrino oscillations from the observation of anti-neutrino(electron) appearance in a anti-neutrino(muon) beam". In: *Phys. Rev.* D64 (2001), p. 112007. DOI: 10.1103/PhysRevD.64.112007. arXiv: hep-ex/0104049 [hep-ex].

[50] A. A. Aguilar-Arevalo et al. “Observation of a Significant Excess of Electron-Like Events in the MiniBooNE Short-Baseline Neutrino Experiment”. In: (2018). arXiv: 1805.12028 [hep-ex].

[51] Carlo Giunti and Marco Laveder. “Statistical Significance of the Gallium Anomaly”. In: *Phys. Rev.* C83 (2011), p. 065504. DOI: 10.1103/PhysRevC.83.065504. arXiv: 1006.3244 [hep-ph].

[52] P. Anselmann et al. “First results from the Cr-51 neutrino source experiment with the GALLEX detector”. In: *Phys. Lett.* B342 (1995), pp. 440–450. DOI: 10.1016/0370-2693(94)01586-2.

[53] W. Hampel et al. “Final results of the Cr-51 neutrino source experiments in GALLEX”. In: *Phys. Lett.* B420 (1998), pp. 114–126. DOI: 10.1016/S0370-2693(97)01562-1.

[54] F. Kaether et al. “Reanalysis of the GALLEX solar neutrino flux and source experiments”. In: *Phys. Lett.* B685 (2010), pp. 47–54. DOI: 10.1016/j.physletb.2010.01.030. arXiv: 1001.2731 [hep-ex].

[55] Dzh.N. Abdurashitov et al. “The Russian-American gallium experiment (SAGE) Cr neutrino source measurement”. In: *Phys. Rev. Lett.* 77 (1996), pp. 4708–4711. DOI: 10.1103/PhysRevLett.77.4708.

[56] J. N. Abdurashitov et al. “Measurement of the response of the Russian-American gallium experiment to neutrinos from a Cr-51 source”. In: *Phys. Rev.* C59 (1999), pp. 2246–2263. DOI: 10.1103/PhysRevC.59.2246. arXiv: hep-ph/9803418 [hep-ph].

[57] J. N. Abdurashitov et al. “Measurement of the response of a Ga solar neutrino experiment to neutrinos from an Ar-37 source”. In: *Phys. Rev.* C73 (2006), p. 045805. DOI: 10.1103/PhysRevC.73.045805. arXiv: nucl-ex/0512041 [nucl-ex].

[58] J. N. Abdurashitov et al. “Measurement of the solar neutrino capture rate with gallium metal. III: Results for the 2002–2007 data-taking period”. In: *Phys. Rev.* C80 (2009), p. 015807. DOI: 10.1103/PhysRevC.80.015807. arXiv: 0901.2200 [nucl-ex].

[59] G. Mention et al. “The Reactor Antineutrino Anomaly”. In: *Phys. Rev.* D83 (2011), p. 073006. DOI: 10.1103/PhysRevD.83.073006. arXiv: 1101.2755 [hep-ex].

[60] F. P. An et al. “Evolution of the Reactor Antineutrino Flux and Spectrum at Daya Bay”. In: *Phys. Rev. Lett.* 118.25 (2017), p. 251801. DOI: 10.1103/PhysRevLett.118.251801. arXiv: 1704.01082 [hep-ex].

[61] Mona Dentler et al. “Sterile neutrinos or flux uncertainties? — Status of the reactor antineutrino anomaly”. In: *JHEP* 11 (2017), p. 099. DOI: 10.1007/JHEP11(2017)099. arXiv: 1709.04294 [hep-ph].

[62] S. Schael et al. "Precision electroweak measurements on the Z resonance". In: *Phys. Rept.* 427 (2006), pp. 257–454. DOI: 10.1016/j.physrep.2005.12.006. arXiv: hep-ex/0509008 [hep-ex].

[63] K. Abe et al. "Combined Analysis of Neutrino and Antineutrino Oscillations at T2K". In: *Phys. Rev. Lett.* 118.15 (2017), p. 151801. DOI: 10.1103/PhysRevLett.118.151801. arXiv: 1701.00432 [hep-ex].

[64] Srubabati Goswami and Toshihiko Ota. "Testing non-unitarity of neutrino mixing matrices at neutrino factories". In: *Phys. Rev.* D78 (2008), p. 033012. DOI: 10.1103/PhysRevD.78.033012. arXiv: 0802.1434 [hep-ph].

[65] O. G. Miranda, M. Tortola, and J. W. F. Valle. "New ambiguity in probing CP violation in neutrino oscillations". In: *Phys. Rev. Lett.* 117.6 (2016), p. 061804. DOI: 10.1103/PhysRevLett.117.061804. arXiv: 1604.05690 [hep-ph].

[66] Shao-Feng Ge et al. "Measuring the Leptonic CP Phase in Neutrino Oscillations with Non-Unitary Mixing". In: (2016). arXiv: 1605.01670 [hep-ph].

[67] André de Gouvêa and Kevin J. Kelly. "False Signals of CP-Invariance Violation at DUNE". In: (2016). arXiv: 1605.09376 [hep-ph].

[68] Debajyoti Dutta and Pomita Ghoshal. "Probing CP violation with T2K, NOνA and DUNE in the presence of non-unitarity". In: *JHEP* 09 (2016), p. 110. DOI: 10.1007/JHEP09(2016)110. arXiv: 1607.02500 [hep-ph].

[69] Thomas J. Weiler and D. J. Wagner. "Invariant box parameterization of neutrino oscillations". In: *AIP Conf. Proc.* 444 (1998), pp. 46–58. DOI: 10.1063/1.56585. arXiv: hep-ph/9806490 [hep-ph].

[70] D. J. Wagner and Thomas J. Weiler. "Boxing with neutrino oscillations". In: *Phys. Rev.* D59 (1999), p. 113007. DOI: 10.1103/PhysRevD.59.113007. arXiv: hep-ph/9801327 [hep-ph].

[71] C. Jarlskog. "Commutator of the Quark Mass Matrices in the Standard Electroweak Model and a Measure of Maximal CP Violation". In: *Phys. Rev. Lett.* 55 (1985), p. 1039. DOI: 10.1103/PhysRevLett.55.1039.

[72] Y. Farzan and A. Yu. Smirnov. "Leptonic unitarity triangle and CP violation". In: *Phys. Rev.* D65 (2002), p. 113001. DOI: 10.1103/PhysRevD.65.113001. arXiv: hep-ph/0201105 [hep-ph].

[73] Zhi-zhong Xing and He Zhang. "Reconstruction of the neutrino mixing matrix and leptonic unitarity triangles from long-baseline neutrino oscillations". In: *Phys. Lett.* B618 (2005), pp. 131–140. DOI: 10.1016/j.physletb.2005.05.016. arXiv: hep-ph/0503118 [hep-ph].

[74] James D. Bjorken, P. F. Harrison, and W. G. Scott. "Simplified unitarity triangles for the lepton sector". In: *Phys. Rev.* D74 (2006), p. 073012. DOI: 10.1103/PhysRevD.74.073012. arXiv: hep-ph/0511201 [hep-ph].

[75] Zhi-Zhong Xing. "Implications of the Daya Bay observation of θ_{13} on the leptonic flavor mixing structure and CP violation". In: *Chin. Phys.* C36 (2012), pp. 281–297. DOI: 10.1088/1674-1137/36/4/L01. arXiv: 1203.1672 [hep-ph].

[76] Hong-Jian He and Xun-Jie Xu. "Connecting Leptonic Unitarity Triangle to Neutrino Oscillation". In: *Phys. Rev.* D89.7 (2014), p. 073002. DOI: 10.1103/PhysRevD.89.073002. arXiv: 1311.4496 [hep-ph].

[77] Hong-Jian He and Xun-Jie Xu. "Connecting Leptonic Unitarity Triangle to Neutrino Oscillation with CP Violation in Vacuum and in Matter". In: (2016). arXiv: 1606.04054 [hep-ph].

[78] T. Suzuki. "Some formulas for invariant phases of unitary matrices by Jarlskog". In: *Journal of Mathematical Physics* 50.12 (Dec. 2009), pp. 123526–123526. DOI: 10.1063/1.3272544. arXiv: 0907.2353 [math-ph].

[79] F. J. Escrihuela et al. "On the description of nonunitary neutrino mixing". In: *Phys. Rev.* D92.5 (2015). [Erratum: Phys. Rev.D93,no.11,119905(2016)], p. 053009. DOI: 10.1103/PhysRevD.93.119905, 10.1103/PhysRevD.92.053009. arXiv: 1503.08879 [hep-ph].

[80] E. Fernandez-Martinez et al. "CP-violation from non-unitary leptonic mixing". In: *Phys. Lett.* B649 (2007), pp. 427–435. DOI: 10.1016/j.physletb.2007.03.069. arXiv: hep-ph/0703098 [hep-ph].

[81] S. Antusch et al. "Unitarity of the Leptonic Mixing Matrix". In: *JHEP* 10 (2006), p. 084. DOI: 10.1088/1126-6708/2006/10/084. arXiv: hep-ph/0607020 [hep-ph].

[82] K. Abe et al. "Search for CP Violation in Neutrino and Antineutrino Oscillations by the T2K Experiment with 2.2×10^{21} Protons on Target". In: *Phys. Rev. Lett.* 121.17 (2018), p. 171802. DOI: 10.1103/PhysRevLett.121.171802. arXiv: 1807.07891 [hep-ex].

[83] Stephen Parke and Mark Ross-Lonergan. "Unitarity and the three flavor neutrino mixing matrix". In: *Phys. Rev.* D93.11 (2016), p. 113009. DOI: 10.1103/PhysRevD.93.113009. arXiv: 1508.05095 [hep-ph].

[84] S. Gariazzo et al. "Model-independent $\bar{\nu}_e$ short-baseline oscillations from reactor spectral ratios". In: *Phys. Lett.* B782 (2018), pp. 13–21. DOI: 10.1016/j.physletb.2018.04.057. arXiv: 1801.06467 [hep-ph].

[85] Mattias Blennow et al. "Non-Unitarity, sterile neutrinos, and Non-Standard neutrino Interactions". In: (2016). arXiv: 1609.08637 [hep-ph].

[86] Patrick Huber et al. "New features in the simulation of neutrino oscillation experiments with GLoBES 3.0: General Long Baseline Experiment Simulator". In: *Comput. Phys. Commun.* 177 (2007), pp. 432–438. DOI: 10.1016/j.cpc.2007.05.004. arXiv: hep-ph/0701187 [hep-ph].

[87] Patrick Huber, M. Lindner, and W. Winter. "Simulation of long-baseline neutrino oscillation experiments with GLoBES (General Long Baseline Experiment Simulator)". In: *Comput. Phys. Commun.* 167 (2005), p. 195. DOI: 10.1016/j.cpc.2005.01.003. arXiv: hep-ph/0407333 [hep-ph].

[88] Patrick Huber, Manfred Lindner, and Walter Winter. "Superbeams versus neutrino factories". In: *Nucl. Phys.* B645 (2002), pp. 3–48. eprint: hep-ph/0204352.

[89] Mark D. Messier. "Evidence for neutrino mass from observations of atmospheric neutrinos with Super-Kamiokande". In: (). UMI-99-23965.

[90] E. A. Paschos and J. Y. Yu. "Neutrino interactions in oscillation experiments". In: *Phys. Rev.* D65 (2002), p. 033002. eprint: hep-ph/0107261.

[91] Y. Itow et al. "The JHF-Kamioka neutrino project". In: (2001). eprint: hep-ex/0106019.

[92] Masaki Ishitsuka et al. "Resolving neutrino mass hierarchy and CP degeneracy by two identical detectors with different baselines". In: *Phys. Rev.* D72 (2005), p. 033003. eprint: hep-ph/0504026.

[93] I. Ambats et al. "NOvA proposal to build a 30-kiloton off-axis detector to study neutrino oscillations in the Fermilab NuMI beamline". In: (2004). eprint: hep-ex/0503053.

[94] T. Yang and S. Woijcicki. "Study of physics sensitivity of $\nu_m u$ disappearance in a totally active version of NoVA detector". In: (2004). eprint: Off-Axis-Note-SIM-30.

[95] K. Abe et al. "T2K neutrino flux prediction". In: *Phys. Rev.* D87.1 (2013). [Addendum: Phys. Rev.D87,no.1,019902(2013)], p. 012001. DOI: 10.1103/PhysRevD.87.012001, 10.1103/PhysRevD.87.019902. arXiv: 1211.0469 [hep-ex].

[96] M. D. Messier. "First neutrino oscillation measurements in NOvA". In: *Nucl. Phys.* B908 (2016), pp. 151–160. DOI: 10.1016/j.nuclphysb.2016.04.027.

[97] F. J. Escrihuela et al. "Probing CP violation with non-unitary mixing in long-baseline neutrino oscillation experiments: DUNE as a case study". In: *New J. Phys.* 19.9 (2017), p. 093005. DOI: 10.1088/1367-2630/aa79ec. arXiv: 1612.07377 [hep-ph].

[98] O. G. Miranda and H. Nunokawa. "Non standard neutrino interactions: current status and future prospects". In: *New J. Phys.* 17.9 (2015), p. 095002. DOI: 10.1088/1367-2630/17/9/095002. arXiv: 1505.06254 [hep-ph].

[99] C. Jarlskog. "A Basis Independent Formulation of the Connection Between Quark Mass Matrices, CP Violation and Experiment". In: *Z. Phys.* C29 (1985), pp. 491–497. DOI: 10.1007/BF01565198.

[100] P. F. Harrison and W. G. Scott. "CP and T violation in neutrino oscillations and invariance of Jarlskog's determinant to matter effects". In: *Phys. Lett.* B476 (2000), pp. 349–355. DOI: 10.1016/S0370-2693(00)00153-2. arXiv: hep-ph/9912435 [hep-ph].

[101] Zhi-zhong Xing. "Commutators of lepton mass matrices, CP violation, and matter effects in-medium baseline neutrino experiments". In: *Phys. Rev.* D63 (2001), p. 073012. DOI: 10.1103/PhysRevD.63.073012. arXiv: hep-ph/0009294 [hep-ph].

[102] C. Jarlskog. "Invariants of lepton mass matrices and CP and T violation in neutrino oscillations". In: *Phys. Lett.* B609 (2005), pp. 323–329. DOI: 10.1016/j.physletb.2005.01.057. arXiv: hep-ph/0412288 [hep-ph].

[103] Vadim A. Naumov. "Three neutrino oscillations in matter, CP violation and topological phases". In: *Int. J. Mod. Phys.* D1 (1992), pp. 379–399. DOI: 10.1142/S0218271892000203.

[104] Mona Dentler et al. "Updated Global Analysis of Neutrino Oscillations in the Presence of eV-Scale Sterile Neutrinos". In: *JHEP* 08 (2018), p. 010. DOI: 10.1007/JHEP08(2018)010. arXiv: 1803.10661 [hep-ph].

[105] S. N. Gninenko. "The MiniBooNE anomaly and heavy neutrino decay". In: *Phys. Rev. Lett.* 103 (2009), p. 241802. DOI: 10.1103/PhysRevLett.103.241802. arXiv: 0902.3802 [hep-ph].

[106] Peter Ballett, Silvia Pascoli, and Mark Ross-Lonergan. "U(1)' mediated decays of heavy sterile neutrinos in MiniBooNE". In: (2018). arXiv: 1808.02915 [hep-ph].

[107] Enrico Bertuzzo et al. "Neutrino Masses and Mixings Dynamically Generated by a Light Dark Sector". In: (2018). arXiv: 1808.02500 [hep-ph].

[108] Enrico Bertuzzo et al. "Dark Neutrino Portal to Explain MiniBooNE excess". In: *Phys. Rev. Lett.* 121.24 (2018), p. 241801. DOI: 10.1103/PhysRevLett.121.241801. arXiv: 1807.09877 [hep-ph].

[109] Gabriel Magill et al. "Dipole portal to heavy neutral leptons". In: *Phys. Rev.* D98.11 (2018), p. 115015. DOI: 10.1103/PhysRevD.98.115015. arXiv: 1803.03262 [hep-ph].

[110] Jiajun Liao, Danny Marfatia, and Kerry Whisnant. "MiniBooNE, MINOS+ and IceCube data imply a baroque neutrino sector". In: (2018). arXiv: 1810.01000 [hep-ph].

[111] M. G. Aartsen et al. "Searches for Sterile Neutrinos with the IceCube Detector". In: *Phys. Rev. Lett.* 117.7 (2016), p. 071801. DOI: 10.1103/PhysRevLett.117.071801. arXiv: 1605.01990 [hep-ex].

[112] K. Abe et al. "Limits on sterile neutrino mixing using atmospheric neutrinos in Super-Kamiokande". In: *Phys. Rev.* D91 (2015), p. 052019. DOI: 10.1103/PhysRevD.91.052019. arXiv: 1410.2008 [hep-ex].

[113] K. Abe et al. "Search for short baseline ν_e disappearance with the T2K near detector". In: *Phys. Rev.* D91 (2015), p. 051102. DOI: 10.1103/PhysRevD.91.051102. arXiv: 1410.8811 [hep-ex].

[114] P. Adamson et al. "Search for sterile neutrinos in MINOS and MINOS+ using a two-detector fit". In: *Submitted to: Phys. Rev. Lett.* (2017). arXiv: 1710.06488 [hep-ex].

[115] P. Adamson et al. "Search for active-sterile neutrino mixing using neutral-current interactions in NOvA". In: *Phys. Rev.* D96.7 (2017), p. 072006. DOI: 10.1103/PhysRevD.96.072006. arXiv: 1706.04592 [hep-ex].

[116] C. Giunti and E. M. Zavanin. "Appearance–disappearance relation in $3 + N_s$ short-baseline neutrino oscillations". In: *Mod. Phys. Lett.* A31.01 (2015), p. 1650003. DOI: 10.1142/S0217732316500036. arXiv: 1508.03172 [hep-ph].

[117] Heinrich Päs, Sandip Pakvasa, and Thomas J. Weiler. "Sterile-active neutrino oscillations and shortcuts in the extra dimension". In: *Phys. Rev.* D72 (2005), p. 095017. DOI: 10.1103/PhysRevD.72.095017. arXiv: hep-ph/0504096 [hep-ph].

[118] D. Marfatia et al. "A model of superluminal neutrinos". In: *Phys. Lett.* B707 (2012), pp. 553–557. DOI: 10.1016/j.physletb.2012.01.028. arXiv: 1112.0527 [hep-ph].

[119] Daniel J. H. Chung and Katherine Freese. "Cosmological challenges in theories with extra dimensions and remarks on the horizon problem". In: *Phys. Rev.* D61 (2000), p. 023511. DOI: 10.1103/PhysRevD.61.023511. arXiv: hep-ph/9906542 [hep-ph].

[120] Daniel J. H. Chung and Katherine Freese. "Can geodesics in extra dimensions solve the cosmological horizon problem?" In: *Phys. Rev.* D62 (2000), p. 063513. DOI: 10.1103/PhysRevD.62.063513. arXiv: hep-ph/9910235 [hep-ph].

[121] Csaba Csaki, Joshua Erlich, and Christophe Grojean. "Gravitational Lorentz violations and adjustment of the cosmological constant in asymmetrically warped space-times". In: *Nucl. Phys.* B604 (2001), pp. 312–342. DOI: 10.1016/S0550-3213(01)00175-4. arXiv: hep-th/0012143 [hep-th].

[122] Sebastian Hollenberg and Heinrich Päs. "Resonant active-sterile neutrino mixing in the presence of matter potentials and altered dispersion relations". In: (2009). arXiv: 0904.2167 [hep-ph].

[123] Sebastian Hollenberg et al. "Baseline-dependent neutrino oscillations with extra-dimensional shortcuts". In: *Phys. Rev.* D80 (2009), p. 093005. DOI: 10.1103/PhysRevD.80.093005. arXiv: 0906.0150 [hep-ph].

[124] Elke Aeikens et al. "Flavor ratios of extragalactic neutrinos and neutrino shortcuts in extra dimensions". In: *JCAP* 1510.10 (2015), p. 005. DOI: 10.1088/1475-7516/2015/10/005. arXiv: 1410.0408 [hep-ph].

[125] Elke Aeikens et al. "Suppression of cosmological sterile neutrino production by altered dispersion relations". In: *Phys. Rev.* D94.11 (2016), p. 113010. DOI: 10.1103/PhysRevD.94.113010. arXiv: 1606.06695 [hep-ph].

[126] Dominik Döring and Heinrich Päs. "Sterile Neutrino Shortcuts in Asymmetrically Warped Extra Dimensions". In: (2018). arXiv: 1808.07734 [hep-ph].

[127] Dukjae Jang, Motohiko Kusakabe, and Myung-Ki Cheoun. "Effects of sterile neutrinos and an extra dimension on big bang nucleosynthesis". In: *Phys. Rev.* D97.4 (2018), p. 043005. DOI: 10.1103/PhysRevD.97.043005. arXiv: 1611.04472 [nucl-th].

[128] Fengpeng An et al. "Neutrino Physics with JUNO". In: *J. Phys.* G43.3 (2016), p. 030401. DOI: 10.1088/0954-3899/43/3/030401. arXiv: 1507.05613 [physics.ins-det].

Eidesstattliche Versicherung

Ich versichere hiermit an Eides statt, dass ich die vorliegende Masterarbeit mit dem Titel „Searches for New Physics with Neutrino Oscillations in the High Precision Era" selbständig und ohne unzulässige fremde Hilfe erbracht habe. Ich habe keine anderen als die angegebenen Quellen und Hilfsmittel benutzt sowie wörtliche und sinngemäße Zitate kenntlich gemacht. Die Arbeit hat in gleicher oder ähnlicher Form noch keiner Prüfungsbehörde vorgelegen.

Ort, Datum	Unterschrift

Belehrung

Wer vorsätzlich gegen eine die Täuschung über Prüfungsleistungen betreffende Regelung einer Hochschulprüfungsordnung verstößt handelt ordnungswidrig. Die Ordnungswidrigkeit kann mit einer Geldbuße von bis zu 50000.00 € geahndet werden. Zuständige Verwaltungsbehörde für die Verfolgung und Ahndung von Ordnungswidrigkeiten ist der Kanzler/die Kanzlerin der Technischen Universität Dortmund. Im Falle eines mehrfachen oder sonstigen schwerwiegenden Täuschungsversuches kann der Prüfling zudem exmatrikuliert werden (§ 63 Abs. 5 Hochschulgesetz – HG –).

Die Abgabe einer falschen Versicherung an Eides statt wird mit Freiheitsstrafe bis zu 3 Jahren oder mit Geldstrafe bestraft.

Die Technische Universität Dortmund wird ggf. elektronische Vergleichswerkzeuge (wie z.B. die Software „turnitin") zur Überprüfung von Ordnungswidrigkeiten in Prüfungsverfahren nutzen.

Die oben stehende Belehrung habe ich zur Kenntnis genommen.

Ort, Datum	Unterschrift